

This is the peer reviewed version of the following article:

The Late Pleistocene Po River lowstand wedge in the Adriatic Sea: Controls on architecture variability and sediment partitioning / Pellegrini, C., Asioli, A., Bohacs, K.m., Drexler, T.m., Feldman, H.r., Sweet, M.I., Maselli, V., Rovere, M., Gamberi, F., Dalla Valle, G., Trincardi, F.. - In: MARINE AND PETROLEUM GEOLOGY. - ISSN 0264-8172. - 96:(2018), pp. 16-50. [10.1016/j.marpetgeo.2018.03.002]

*Terms of use:*

The terms and conditions for the reuse of this version of the manuscript are specified in the publishing policy. For all terms of use and more information see the publisher's website.

10/06/2026 23:23

(Article begins on next page)

**THE LATE PLEISTOCENE PO RIVER LOWSTAND WEDGE IN THE ADRIATIC SEA:  
CONTROLS ON ARCHITECTURE VARIABILITY AND SEDIMENT PARTITIONING**

**Claudio Pellegrini<sup>1</sup>, Alessandra Asioli<sup>1</sup>, Kevin M. Bohacs<sup>2</sup>, Tina M. Drexler<sup>3</sup>, Michael L. Sweet<sup>2</sup>, Vittorio Maselli<sup>4</sup>, Marzia Rovere<sup>1</sup>, Fabiano Gamberi<sup>1</sup>, Giacomo Dalla Valle<sup>1</sup>, Fabio Trincardi<sup>1</sup>**

- (<sup>1</sup>) Istituto di Scienze Marine (ISMAR-CNR), Via Gobetti 101, 40129, Bologna, Italia
- (<sup>2</sup>) ExxonMobil Upstream Research Company, 22777 Springwoods Village Parkway, Spring, TX 77389, U.S.A
- (<sup>3</sup>) ExxonMobil Exploration Company, 22777 Springwoods Village Parkway, Spring, TX 77389, U.S.A
- (<sup>4</sup>) Department of Geology and Petroleum Geology, University of Aberdeen, King's College, Aberdeen, UK

**ABSTRACT**

Although the facies and stratal geometries of continental margin successions can be defined in detail based on subsurface and outcrop studies, most documentations lack the high-resolution age control needed to constrain their timing and infer their external forcing mechanisms. The 350-m-thick Po River Lowstand Wedge (PRLW) preserves a high-resolution record of stacked deltaic clinothems deposited during the Last Glacial Maximum (LGM) in the Adriatic basin (Mediterranean Sea). We investigated clinothem internal geometry, stacking patterns, and facies distributions to infer the main controls on their growth by integrating seismic reflection data with seismic facies attributes. The stratigraphic framework of the clinothems was then related to major paleoenvironmental shifts driven by the last glacial cycle and associated eustatic and climatic changes. This framework is well constrained by geochronological dates based on <sup>14</sup>C and tephra recognition.

Within the PRLW, three distinctive types of clinothems, Type A, Type B and Type C, each with diagnostic topset geometries, shelf-edge trajectories, and associated basinal deposits: Type A clinothems display moderate topset aggradation, ascending shelf-edge trajectories, and Mass-

1 Transport Complexes (MTCs) in the slope-basin; Type B clinothem have eroded topsets,  
2 descending shelf-edge trajectories, and Distributary Channel-Lobe Complexes (DLCs) in the slope-  
3 basin; and Type C clinothem show pronounced topset aggradation, ascending shelf-edge  
4 trajectories and fine-grained concordant strata in the slope-basin. The clinothem types also show  
5 systematic variations in sediment accumulation rates as well as in their individual areal distribution  
6 and extent. In particular during the last glacial maximum, clinothem accumulation rates were as  
7 much as 200 km<sup>3</sup>/ky (in some of the Type B clinothem). Changes in sediment export to the basin  
8 correlate with the distance of the clinothem shorelines from the shelf-edge: when the distance is less  
9 than 5 km, topset degradation coupled with direct sediment bypass to the basin promoted the  
10 formation of DLCs (Type B clinothem), and when that distance was more than 10 km, no direct  
11 conduit linked the shelf to the slope and no significant volume of coarser-grained sediment reached  
12 the basin floor (Type C clinothem).

13 The elementary clinothem types stack into two Clinothem Sets. Clinothem Set 1, with  
14 essentially flat to slightly descending shelf-edge trajectory, is composed of stacked A and B  
15 clinothem, and records the direct influence of river flux (maximum during the deposition of Type  
16 B clinothem) leading to dysoxic conditions on the bottom of the basin. Clinothem Set 2, showing  
17 ascending shelf-edge trajectory, records an aggradational stacking coupled with a retreat of the  
18 river-entry points with benthic fauna assemblages that reflect the influence of peaks in fresh water  
19 discharge. Whereas Clinothem Set 1 developed under perturbations of river supply linked to the  
20 multi-scale waxing-waning of glaciers during an interval dominated by eustatic fall, Clinothem Set  
21 2 reflects the main thawing of glaciers during the first phase of the eustatic rise.

22 Borehole calibration of the grid of seismic profiles indicates that the entire PRLW  
23 accumulated in 17 ky, with individual clinothem representing intervals that range from 400 to  
24 4,700 years. The high-resolution age control enabled us to relate stratal character to independently  
25 constrained environmental parameters; this revealed how the evolution of a margin-scale system

1 intricately convolves the influences of both global (eustasy) and regional (climate-driven supply  
2 fluctuations) controls. Finally, the thickness, geometry, and stacking patterns of the PRLW  
3  
4 clinothems vary in systematic ways resulting in geometries that closely resemble those of ancient  
5 shelf-edge systems, and offering the PRLW as a modern analogue. By recognizing the very short-  
6  
7 time interval associated with the deposition of each type of clinothem we question if, in ancient  
8  
9 records, clinothems with a putative duration of hundreds of thousands of years might record instead  
10  
11 much shorter intervals with most of the geological time condensed in hiatuses and stratigraphic  
12  
13 surfaces. We suggest that the PRLW provides valuable insight into the lower end of the possible  
14  
15 range of time spans recorded by such ancient margin-scale clinothems. Our observations also  
16  
17 reinforce the focus of the classic sequence-stratigraphic approach on analyzing surfaces and their  
18  
19 geometric relations and not on time duration or formation mechanisms.  
20  
21  
22  
23  
24  
25  
26  
27  
28

## 29 **1. INTRODUCTION**

30  
31 Shelf-margin wedges and associated clinothems are the critical link between continental and  
32  
33 deep-water realms and a distinctive record of the growth of continental margins. Although  
34  
35 localized, on a global scale they have an outsized importance and their strata have been estimated to  
36  
37 sequester > 40% of the biogenic carbon in the modern ocean and to host > 40% of global oil  
38  
39 reserves, including many important recent discoveries (e.g., Suter and Berryhill, 1985; Walsh, 1991;  
40  
41 Sydow et al., 2003; Muller-Karger et al., 2005; IEA, 2013). Detailed analyses of the stratigraphic  
42  
43 record in shelf-margin settings can provide useful insights on their response to external and internal  
44  
45 forcing mechanisms on time scales longer than available in weather- and oceanographic-instrument  
46  
47 records. Therefore the characterization of clinothem evolution within high-resolution  
48  
49 chronostratigraphic contexts is a fundamental aid in the prediction of hydrocarbon reservoir  
50  
51 potential and in the reconstruction of continental-margin history and controls (e.g. eustasy and  
52  
53 climate). In this view, sequence stratigraphy is a method through which a systematic analysis of the  
54  
55  
56  
57  
58  
59  
60  
61  
62  
63  
64  
65

1 stratigraphic record can help in reconstructing the evolution of continental margins in time and  
2 space (Boyd et al., 1989; Plink-Björklund et al., 2001; Johannessen and Steel, 2005; Zecchin et al.,  
3 2008; Fatoke and Bhattacharya, 2010; Bhattacharya et al., 2016) and their response to cyclic  
4 autogenic and allogenic controls (e.g. Muto and Steel et al., 1997; Jerolmack and Paola, 2010;  
5 Madof et al., 2016). Focused initially on million-years time scales (Mitchum et al., 1977), sequence  
6 stratigraphy has long since been applied to the study of Quaternary continental margins at  
7 Milankovitch-band time scales (mostly at 100,000 year scale). At all scales, accommodation and  
8 sediment supply are recognized as the main factors that govern changes in stratal architecture and  
9 sediment partitioning across continental margins (e.g. Trincardi and Field, 1991; Pillans et al., 1998;  
10 Roberts et al., 2004; Jouet et al., 2006; Ridente et al., 2009; Fatoke and Bhattacharya, 2010;  
11 Anderson et al., 2016; Amorosi et al., 2016).

12 In the study of continental margins, clinothems have been documented as one of the  
13 fundamental building blocks of the stratigraphic record (Asquit, 1970; Helland-Hansen and  
14 Martinsen, 1996; Pirmez et al., 1998; Steel et al., 2000; Pellegrini et al., 2017). Clinothems have  
15 been recognized over several spatial and temporal scales ranging from shoreline accretion to  
16 continental-margin progradation (Vail et al., 1991; Steckler et al., 1999; Swenson et al., 2005;  
17 Carvajal et al., 2009; Helland-Hansen and Hampson, 2009; Patruno et al., 2015; Pellegrini et al.,  
18 2015) and are sensitive archives of climate and oceanographic regime (e.g. Cattaneo et al., 2003;  
19 Swenson et al., 2005; Fanget et al., 2014; Pellegrini et al., 2015; Tesi et al., 2017).

20 By studying the anatomy of a 350-m-thick shelf-margin wedge deposited during a single  
21 short-lived lowstand of sea level, we document, in a chronologically well-constrained framework  
22 (Pellegrini et al., 2017), a composite succession of late-Pleistocene clinothems recording short-term  
23 (sub-Milankovitch-scale) environmental and climatic change during the Last Glacial Maximum  
24 (LGM). Particular attention has been paid to the characterization of 1) the 3D shape of individual  
25 margin-scale clinothems (100s m thick; up to 5 km of progradation) and their thickness distribution

1  
2 as a function of the Sediment Accumulation Rate (SAR) and accommodation; 2) the vertical and  
3 lateral distribution of sedimentary facies; 3) the timing of and controls on the activity of deep-water  
4 channel-lobe complexes.  
5

6  
7 These results have been combined with a well-constrained suite of paleo-environmental  
8 proxies with the aim of testing some of the key concepts typically adopted in the reconstructions of  
9 recent and ancient progradational margins. We thus are able to correlate our observations on  
10 clinothem development with a suite of environmental parameters to assign stratigraphic variations  
11 to their possible causes. The main goal of this paper is to illustrate how the growth of this sediment  
12 wedge was controlled by the intricate interactions of climatic variations and eustatic oscillations  
13 that largely impact on sediment-supply fluctuations and the character of sedimentation in the  
14 different sectors of a prograding margin. Finally, we highlight the role of sub-Milankovitch  
15 cyclicity in controlling the stacking pattern of clinothems and clinothem sets even down to  
16 centennial- to millennial-scale variations in the rates of sediment supply and fresh-water discharge  
17 and accompanying environmental changes.  
18  
19  
20  
21  
22  
23  
24  
25  
26  
27  
28  
29  
30  
31  
32  
33  
34  
35

## 36 **2. SETTING**

### 37 *2.1 Geological evolution of the Adriatic foredeep*

38  
39 Following the early Alpine compression that led to the closure of the Tethys in the late  
40 Cretaceous (Doglioni, 1994), the Mediterranean region was characterized by a compressive regime  
41 affecting the Apennine mountain chain starting in the Oligocene. During the lower Pliocene, the  
42 eastward migration of the Apennine front induced the tilting of the Adriatic foreland toward the  
43 orogenic front, causing the formation of foredeep depocenters of variable-thickness and their  
44 subsequent infill through Quaternary prograding sequences along the axis of the basin (Royden et  
45 al., 1987; Dalla Valle et al., 2013a, 2013b; Ghielmi et al., 2013; Rossi et al., 2015).  
46  
47  
48  
49  
50  
51  
52  
53  
54  
55  
56  
57  
58  
59  
60  
61  
62  
63  
64  
65

1  
2 In the north-central Adriatic basin, the most recent southeastward prograding sequence (Fig.  
3 1), is of late Pleistocene age (Trincardi et al., 1994). The late Pleistocene succession encompasses  
4 the eustatic lowstand of the Last Glacial Maximum (LGM; Fig. 2), when the Po River Lowstand  
5 Wedge (PRLW) recorded a 40 km shelf-edge progradation (Pellegrini et al., 2017; Fig. 3) partially  
6 filling the Mid Adriatic Dip (MAD), a remnant slope basin that was few hundred meters deep.  
7 During the deposition of the PRLW, most of the underlying tectonic structures became inactive  
8 (Fig. 4); however, localized active geological structures, possibly related to halo-kinetic  
9 deformation of Triassic evaporates, punctuate the eastern sector of the MAD (Geletti et al., 2008).  
10  
11  
12  
13  
14  
15  
16  
17  
18  
19  
20  
21

## 22 *2.2 Adriatic basin physiography from the Last Interglacial to Last Glacial Maximum times*

23

24 During the last previous interglacial (Marine Isotope Stage 5e, ~132-116 ky BP, Bazin et al.,  
25 2013) the physiography of the Adriatic basin was similar to the modern one, with a shoreline  
26 somewhat landward of the modern position (Amorosi et al., 2004). The ensuing step-wise lowering  
27 of sea level between oxygen-isotope Substage 5e and 2 (ca. 11.7 ky BP, Walker et al., 2009; Fig. 2),  
28 promoted a marked basinward shift of the shoreline and the formation of a regionally-extensive  
29 unconformity associated with alluvial-plain sedimentation in the northern, shallower reaches of the  
30 basin (Amorosi et al., 2016). From land to basin, the succession of MIS 3 and MIS 2 is identified  
31 as: 1) paleosols and associated channel-belt deposits in the northern and southern Adriatic coastal  
32 plain (Amorosi et al., 2017; Campo et al., 2017); 2) an extensive hiatal surface across a significant  
33 portion of the area presently occupied by the modern shelf (Amorosi et al., 2016); and 3) a thick  
34 sedimentary succession that fills in the MAD (Fig. 3), recording glacio-eustatic oscillations at  
35 Milankovitch and sub-Milankovitch scales (Piva et al., 2008a; Pellegrini et al., 2017). In essence,  
36 the interval between the MIS 5e and the onset of the LGM (at ca. 26 ky BP) spanned a substantial  
37 shrinking of the Adriatic basin and the concurrent broadening of the Po plain drainage area with a  
38 stepwise displacement of the shoreline up to ca. 250 km southeastward (Amorosi et al., 2016), and a  
39  
40  
41  
42  
43  
44  
45  
46  
47  
48  
49  
50  
51  
52  
53  
54  
55  
56  
57  
58  
59  
60  
61  
62  
63  
64  
65

1 relative sea level position at ca. 130 m lower than present day (e.g. Lambeck et al., 2014; Benjamin  
2 et al., 2017). During that time interval, extensive glaciers capped the Alpine chain (Florineth and  
3 Schluchter, 1998; Monegato et al., 2007, 2017) nourishing the ancestral Po River system which  
4 debouched into the central Adriatic slope basin promoting the formation of the PRLW during  
5 overall cold climatic conditions (Fig. 2; Pellegrini et al., 2017).  
6  
7  
8  
9  
10

### 11 12 13 14 *2.3 Sediment supply: modern and inferred for the Last Glacial Maximum* 15

16 The modern Adriatic basin is fed mainly by Alpine and Apennine Rivers, while the sediment  
17 yield from the Dinarides is negligible because of the intensely fractured and karstic nature of the  
18 catchments that trap water and sediment influx in basins close to the coastal area (Simeoni et al.,  
19 1997; Milliman and Farnsworth, 2013; Del Bianco et al., 2014). Fluvial sediment sources along the  
20 western side of the Adriatic Basin form a “line source”, with combined modern delivery of  $51.7 \times$   
21  $10^6$  tons  $\text{yr}^{-1}$  of mean suspended load and an average freshwater discharges of  $1500 \text{ m}^3 \text{ s}^{-1}$  (Frignani  
22 et al., 2005; Cattaneo et al., 2003; Milliman et al., 2016). In contrast, during the LGM the drainage  
23 system of the ancestral Po River was more than double its current size, reaching about  $190,000 \text{ km}^2$ ,  
24 compared to the modern catchment of  $94,000 \text{ km}^2$  (Kettner and Syvitski, 2008). The estimated  
25 average suspended sediment flux into the Northern Adriatic Sea during the Pleistocene is estimated  
26 to have been  $46.6 \times 10^6$  tons  $\text{yr}^{-1}$ , with an average freshwater discharge of  $3000 \text{ m}^3 \text{ s}^{-1}$ , from the Po  
27 River alone (Kettner and Syvitski, 2008).  
28  
29  
30  
31  
32  
33  
34  
35  
36  
37  
38  
39  
40  
41  
42  
43  
44  
45  
46  
47  
48

## 49 **3. DATA, METHODS, AND STRATEGY**

### 50 *3.1 Seismic data, borehole and sediment cores* 51

52 The main set of reflection-seismic profiles used for this work was acquired during the  
53 LowStand Delta (LSD) 2014 cruise and was shot using a mini water-gun source (Sercel S15-02 of  
54  $15 \text{ inc}^3$ ) and recorded through a multichannel streamer (Teledyne mini-streamer with 24 channels;  
55  
56  
57  
58  
59  
60  
61  
62  
63  
64  
65

1 80-500 Hz frequency band width) complemented by single-channel profiles shot with a 300-J  
2 Sparker electro-mechanic source and by a dense grid of CHIRP sub-bottom lines with a 2-7 kHz  
3 outgoing signal. All data were digitally recorded after band-pass filtering and gain adjustment. The  
4 seismic grid comprises high-resolution seismic profiles with a total length of 1500 km and covers  
5 an area of 5000 km<sup>2</sup> centered in the MAD (Fig. 1). In addition, a multibeam bathymetry of the  
6 MAD was acquired using a Kongsberg EM710 hull-mounted multibeam and gridded at 20 m  
7 resolution.  
8

9  
10  
11  
12  
13  
14  
15  
16  
17 The seismic grid has been tied to the PRAD1-2 borehole (Pellegrini et al., 2017), a 71.2 m  
18 long borehole with a total recovery of 99.6% sampled in 185.5 m water depth (Fig. 1). Seismic-  
19 stratigraphic correlation from the expanded stratigraphic clinoform succession to the distal borehole  
20 is straightforward, and was corroborated for the upper ca. 80 m of the succession by correlation  
21 through a network of CHIRP sonar profiles. Key stratigraphic surfaces of regional extent are tied to  
22 PRAD1-2 borehole with a vertical resolution of 0.3-0.5 m (Fig. 5).  
23  
24  
25  
26  
27  
28  
29  
30

31  
32 The PRAD1-2 borehole and two other sediment cores were analyzed in detail for  
33 micropaleontological analyses to form a composite biostratigraphic section. Sediment core CM92-  
34 43 is located at 252 m water depth at the bottom of the slope basin, and sediment core PAL94-8 is  
35 at 150 m water depth close to the shelf-edge (Trincardi et al., 1996). The chronology of these two  
36 cores, already published by Asioli (1996) and Asioli et al. (2001), is here partially revised for the  
37 interval older than 15 ky BP (Tab. 1; see supplemental material).  
38  
39  
40  
41  
42  
43  
44  
45  
46  
47

### 48 *3.2 Seismic Interpretation and Analysis*

49

50  
51 We conducted seismic-stratigraphic interpretation and then seismic-facies analyses with that  
52 stratigraphic framework to delineate genetically related strata and infer depositional conditions. The  
53 interpretation of seismic profiles was based on the principles of seismic stratigraphy (Mitchum et  
54 al., 1977; Mitchum et al., 1991), and the accommodation-succession method (Neal and Abreu,  
55  
56  
57  
58  
59  
60  
61  
62  
63  
64  
65

1  
2  
3  
4  
5  
6  
7  
8  
9  
10  
11  
12  
13  
14  
15  
16  
17  
18  
19  
20  
2009; Neal et al., 2016). Following these approaches, which use reflection terminations as the principal criteria for the recognition of seismic sequence boundaries, the sequence boundary (SB) at the base of the PRLW was identified on the shelf by toplap and onlap terminations of respectively the underlying and overlying reflections (angular unconformity of Mitchum et al., 1977), and traced basinward to a correlative conformity with onlap and downlap terminations of the overlying reflections (Figs. 6 and 7; Pellegrini et al., in press). The maximum regression surfaces (MRS), atop the PRLW, separates progradational-aggradational stacking from retrogradational stacking of coastal transgressive strata on the shelf (see Pellegrini et al., 2017) and corresponds with a marine onlap surface of limited extent on the slope (according to the definition by Catuneanu et al., 2009).

21  
22  
23  
24  
25  
26  
27  
28  
29  
30  
31  
32  
33  
34  
35  
36  
37  
38  
39  
40  
41  
42  
43  
44  
45  
46  
47  
48  
49  
50  
51  
52  
53  
54  
55  
56  
57  
58  
59  
60  
61  
62  
63  
64  
65  
Within the PRLW, we recognized three types of clinothems based on topset geometry, shelf-edge- and onlap-point-trajectory, and internal seismic facies (Pellegrini et al., 2017). Seismic-facies analysis is the description, mapping, and geologic interpretation of seismic-reflection parameters within a chronostratigraphic framework of sequence boundaries (after Mitchum et al., 1977). We delineated the external form, internal reflection characteristics, and 3-D associations of the stratal units within the larger seismic-stratigraphic framework to assure the identification and correlation of genetically related strata. Reflection configuration reveals gross stratification patterns from which depositional processes and erosion can be interpreted. Reflection continuity is closely associated with continuity of strata; continuous reflections suggest widespread, uniformly stratified deposits. Reflection amplitude contains information on the velocity and density contrasts of individual bedding interfaces and their spacing. It is used to predict lateral bedding changes. Reflection spacing ('frequency'), although mainly a characteristic of the seismic pulse, is also related to geologic factors such as the spacing of reflectors and lateral changes in interval velocity (due to lithofacies and pore-fluid changes). Grouping these seismic parameters into mappable seismic-facies facilitates their interpretation in terms of lithotype, depositional processes and environment, possible sediment entry-point locations, and geological setting. Within the PRLW

1 distinctive seismic facies are grouped into 11 generic subclasses (Table 2). The criteria we used to  
2 distinguish different facies included seismic-reflection amplitude, continuity, and dip (where  
3 dipping reflections are  $>0.8^\circ$ ), internal reflection character, and the nature of their boundaries, as  
4 well as their position in the depositional system (Table 2 and Fig. 6).  
5  
6  
7

8  
9 Trajectory analysis considers lateral and vertical migration of geomorphological features and  
10 associated sedimentary environments, with emphasis on the paths and direction of migration of the  
11 coastal onlap and correlative shelf-edge (Steel et al., 2000; Henriksen et al., 2009 and reference  
12 there in). We conducted shelf-edge trajectory analysis in due consideration of the fact that the  
13 rollover point (offlap break of Vail et al., 1977 and Jervey, 1988) at the topset–foreset transition of a  
14 clinothem can occur in shelfal marine environments and thus might not necessarily represent the  
15 shoreline (i.e., the shelf-edge rollover point, at best, only approximates the shoreline position: see  
16 Pellegrini et al., 2015 and discussion therein). Key stratigraphic surfaces of regional extent and  
17 seismic facies (Table 2) were recognized, correlated, loop-tied, and mapped using Petrel® software.  
18  
19 The maps of these key stratigraphic surfaces were constructed by using a “convergent interpolation”  
20 method. A seismic velocity of 1600 m/s, as suggested by the sonic-log analyses (Maselli et al.,  
21 2010), was adopted to convert two-way travel times (TWTT) into depth units and to calculate the  
22 volume of seismic units.  
23  
24  
25  
26  
27  
28  
29  
30  
31  
32  
33  
34  
35  
36  
37  
38  
39  
40

41 The nature of the key surfaces and the reflection configurations of the clinothems were then  
42 combined with the timing of their formation to examine the relative roles of controlling factors on  
43 deposition and sediment distribution such as eustasy and sediment supply. For each clinothem, the  
44 progradation and the Sediment Accumulation Rate (SAR) are given as horizontal migration and  
45 vertical thickness, respectively, at the corresponding shelf-edge divided by their time-duration.  
46  
47  
48  
49  
50  
51  
52  
53  
54  
55

### 56 *3.3 Analyses of micropaleontology*

57  
58  
59  
60  
61  
62  
63  
64  
65

1 Planktic and benthic foraminifera concentrations are expressed as number of specimens per  
2 gram of dry sediment, whereas the species are expressed as percentages. *Globigerinoides sacculifer*  
3 includes *Globigerinoides trilobus*, *Globigerinoides quadrilobatus* and *Globigerinoides sacculifer*  
4 according to Hemleben et al. (1989). The category “warm planktic species” in [figure 8](#) includes  
5 species that preferred warm waters, such as *Globigerinoides ruber*, *Globoturborotalita rubescens*,  
6 *Globigerinoides tenellus*, *G. sacculifer*, *Globigerinella praecalida*, *Orbulina universa* (Pujol and  
7 Vergnaud-Grazzini, 1995).  
8  
9

10  
11  
12 Among the benthic foraminifera, the “deep-infaunal” group mainly comprises the benthic  
13 species *Glandulina laevigata* and, occasionally, by *Fursenkoina*, a taxon adapted to a deep infaunal  
14 microhabitat and especially resistant to low-oxygen conditions (Jorissen, 1993, 1999). *Glandulina*  
15 *laevigata* is reported as very rare in biocenosis restricted to Arctic (Knudsen, 1971, Murray, 2013),  
16 Atlantic and Indian oceans with highest abundances in slightly hypersaline Arabian Gulf shelf  
17 (Murray, 2013). Here we tentatively include this taxon in the deep-infaunal community on the basis  
18 of its great morphological affinity with the taxa, including *Glandulonodosariidae*, that went extinct  
19 during the Last Global Extinction (Pliocene-Mid Pleistocene Transition, see Hayward et al., 2012  
20 for more details), whose habitat was infaunal with enhanced food supply and consequent low  
21 oxygen concentrations, as suggested by geochemical analyses ( $\delta^{13}\text{C}$ ).  
22  
23  
24  
25  
26  
27  
28  
29  
30  
31  
32  
33  
34  
35  
36  
37  
38  
39  
40  
41  
42  
43

### 44 3.4 Age control

45  
46 The timing of the clinotherms of the PRLW was derived from the chronology of the borehole  
47 PRAD1-2 analyzed in detail by Pellegrini et al. (2017) for the time interval MIS 3-MIS 2, with 106  
48 samples counted for foraminiferal content through a ca. 16.5 m thick succession (regarding the  
49 sample preparation and the counting method the reader is referred to Piva et al., 2008a). The age-  
50 model relies on a quantitative assessment of the variations in relative abundance of the diverse  
51 foraminifera species, stable isotope records,  $^{14}\text{C}$  AMS dates, and tephrochronology on macro and  
52  
53  
54  
55  
56  
57  
58  
59  
60  
61  
62  
63  
64  
65

1  
2 cryptotephra (Bourne et al., 2010), as well as on bioevents and event-stratigraphy (Fig. 5 and Table  
3 1).

## 4. RESULTS

### 4.1 Chronology of the PRLW

4  
5  
6  
7  
8  
9  
10  
11  
12 The base (SB) and the top (MRS) of the PRLW cross the PRAD1-2 borehole at 14.6 m (bmsl)  
13 and 2.5 m (bmsl), respectively, bracketing the entire PRLW between 31.8 cal. ky BP and 14.4 cal.  
14 ky BP (Fig. 5; Pellegrini et al., 2017). The chronological data indicate therefore that the PRLW  
15 represents an expanded stratigraphic succession that developed in solely ca. 17 ky (achieving up to  
16 350 m of thickness) during the latest phase of sea level fall, the LGM sea level lowstand, and the  
17 early phase of sea level rise (Figs. 2 and 5).  
18  
19  
20  
21  
22  
23  
24  
25  
26  
27  
28  
29  
30

### 4.2 Micropaleontology 31.8-14.6 ky

31  
32 Due to favorable conditions of accommodation and sediment supply, middle Pleistocene  
33 regressive successions are exceptionally expanded in the Central Adriatic (Trincardi and  
34 Correggiari, 2000; Ridente and Trincardi, 2005; Ridente et al., 2009), and the MIS 5e-MIS 2  
35 interval (late Pleistocene), in particular, preserves a nearly continuous record of a fourth-order (100  
36 kyr) stepwise sea level fall (Amorosi et al., 2016). Starting from the SB at 31.8 ky BP the PRLW  
37 succession shows four intervals that are characterized by distinct foraminifera assemblages (Fig. 8):  
38  
39  
40  
41  
42  
43  
44  
45  
46  
47

48 **Interval 1** (31.8 to 24.7 ky BP: Type A<sub>1</sub>-A<sub>2</sub>; Fig. 8). Both planktic and benthic foraminifera  
49 are present, although planktic foraminifera are more scarce (even one order of magnitude in some  
50 intervals). The planktic assemblage is largely dominated by *Turborotalita quinqueloba* and  
51 occasionally by *Globigerina bulloides*. At 28.2 ky BP (corresponding ca. to e1 surface), the  
52 concentration of planktic foraminifera shows an abrupt decrease. The benthic assemblage is largely  
53  
54  
55  
56  
57  
58  
59  
60  
61  
62  
63  
64  
65

1 dominated by *Cassidulina carinata*, except during the pronounced inflection between 30.2-28.2 ky  
2 BP, where *C. carinata* is replaced by miliolids and later by *Hyalinea balthica*. Deep infaunal taxa  
3 are rare and below 10% of abundance.  
4  
5

6  
7 **Interval 2** (24.7 to 19.2 ky BP: B<sub>2</sub>-A<sub>5</sub>; Fig. 8). Planktic-foraminifera abundance and benthic  
8 concentration show an upward decreasing trend, starting from 21 ky (close to A<sub>3</sub>-B<sub>3</sub> clinotherm  
9 boundary). This interval is characterized by closely spaced fluctuations in the abundance of *C.*  
10 *carinata* and includes the continuous occurrence of *Nonion depressulus* and *Nonion pauciloculum*,  
11 whereas deep infaunal taxa peak only at the base of the interval. The planktic assemblage is similar  
12 to the previous Interval 1.  
13  
14  
15  
16  
17  
18  
19  
20

21  
22 **Interval 3** (19.2 to 18.0 ky BP: B<sub>5</sub>-A<sub>6</sub>; Fig. 8). The concentration of both planktic and  
23 benthic foraminifera decrease further and the *C. carinata* abundance drops to zero. *N. pauciloculum*  
24 and *N. depressulus* show abundances similar to the previous interval, as well as deep infaunal taxa,  
25 always present although with low frequency.  
26  
27  
28  
29  
30

31  
32 **Interval 4** (18.0 to 14.6 ky BP: C<sub>1</sub>-C<sub>2</sub>; Fig. 8). During this interval the concentration of  
33 planktic and benthic foraminifera reaches a minimum compared to the rest of the PRLW, and  
34 especially the planktic component drops close to zero (2 specimens per gram on average, mainly  
35 belonging to *T. quinqueloba*). *N. pauciloculum* and *N. depressulus* makes up to the 80% of the  
36 foraminifera assemblage. This turnover of the benthic assemblage is accompanied by a marked  
37 increase of deep infaunal taxa.  
38  
39  
40  
41  
42  
43  
44  
45  
46  
47

### 48 **4.3 Seismic facies description and inferred depositional environments**

49

50  
51 The most striking feature seen on dip-oriented seismic lines (Figs. 3 and 6) are the  
52 southward dipping and hundred-meter thick clinotherms. The internal architecture of these  
53 clinotherms changes in a repeated way that consists of a common suite of seismic facies that have  
54 been interpreted as clues to the sedimentary processes that shaped the clinotherms.  
55  
56  
57  
58  
59  
60

1  
2 *Topset seismic facies (HAC, HACH, HAD)*  
3  
4

5 The topsets of all three types of clinothems are characterized by High Amplitude Continuous  
6 reflectors (HAC) that change laterally to High Amplitude Chaotic reflectors (HACH). The latter are  
7 discontinuous, irregular reflections (Table 2). At the modern seafloor, High Amplitude  
8 Discontinuous reflections (HAD) characterize deposits with irregular spatial distribution.  
9  
10  
11  
12  
13

14  
15  
16  
17 *Topset inferred depositional environment*  
18  
19

20 The topset seismic facies are interpreted as coastal-plain deposits: HAC are interpreted as  
21 delta plain sandy-silty deposits that change laterally to HACH reflections interpreted as  
22 amalgamated fluvial channel belts with sandy-muddy fill (Table 2). At the modern seafloor, HAD  
23 reflections characterize lagoon deposits formed behind highly discontinuous and reworked barrier  
24 features with sparse distribution as documented by earlier publications (Trincardi et al., 1994;  
25 Storms et al., 2008).  
26  
27  
28  
29  
30  
31  
32  
33  
34  
35  
36

37 *Upper foreset seismic facies (HACHDip-HACDip-HACWDip-LACDip)*  
38  
39

40 Foresets are characterized by a variety of seismic facies: High Amplitude Chaotic Dipping  
41 reflections (HACHDip), High Amplitude Continuous Dipping reflections (HACDip) and Low  
42 Amplitude Continuous Dipping reflections (LACDip) are present in the topset-foreset transition  
43 sector of clinothems. Locally, parallel to wedge-shaped high-amplitude reflection packages pass  
44 laterally to low-amplitude reflections that characterize sediment strata up to several ten of meters  
45 thick (Fig. 9). In addition, packages up to 10-m-thick composed of High Amplitude Continuous  
46 Wavy and Dipping reflections (HACWDip; Table 2), characterize the clinothems developed in the  
47 western sector of the MAD.  
48  
49  
50  
51  
52  
53  
54  
55  
56  
57  
58  
59  
60  
61  
62  
63  
64  
65

1  
2 *Upper foreset inferred depositional environment*  
3

4  
5 Located seaward from the coastal-plain and channel-belt deposits, HAChDip reflections  
6  
7 suggest the presence of distributary channels that extended over the shelf-edge and in the upper  
8  
9 slope (Table 2). The HACDip and LACDip reflections are interpreted as heterolithic foreset  
10  
11 deposits, related to the delta front and prodeltaic zone. Locally, wedge-shaped reflections indicate  
12  
13 the presence of channel-levee systems several tens of meters thick acting as a major conduits of  
14  
15 sediment bypass from the shelf to the basin (Fig. 9). Finally, the HACWDip reflections include 10-  
16  
17 m-scale crenulated features resembling those documented on several late-Holocene prodelta  
18  
19 deposits (see Urgeles et al., 2011 and references therein).  
20  
21  
22  
23  
24  
25

26 *Lower foreset-bottomset seismic facies (SHAM-DLAH-HLAC)*  
27

28  
29 Three characteristic seismic facies developed in the transitional area between foreset and  
30  
31 bottomset. Semi-Continuous High Amplitude Mounded reflections (SHAM), Discontinuous Low  
32  
33 Amplitude reflections with internal Hyperbolic diffractions (DLAH), and High- and Low-  
34  
35 Amplitude Continuous reflections (HLAC). The first two seismic facies characterize clinothem  
36  
37 developed during the first phases of PRLW progradation and highlight up to 45 ms thick basin  
38  
39 deposits (Tab. 2 and Fig. 6). The latter seismic facies is associated with clinothem developed in the  
40  
41 late phase of the PRLW progradation (Fig. 6).  
42  
43  
44  
45  
46  
47  
48

49 *Lower foreset-bottomset inferred depositional environment*  
50

51  
52 The SHAM, DLAH, and HLAC seismic facies are interpreted as prodeltaic-deep-marine  
53  
54 facies. In particular, SHAM and DLAH are interpreted, based on their close resemblance to core-  
55  
56 calibrated seismic facies found in basin-floor fan deposits in the Gulf of Mexico (Beaubouef and  
57  
58  
59  
60  
61  
62  
63  
64  
65

1 Friedmann, 2000), as Distributary channel-Lobe Complexes (DLCs), and as Mass Transport  
2 Complexes (MTCs), respectively. HLAC seismic facies suggest the presence of concordant  
3 heterolithic strata in the younger clinothems (Fig. 6).  
4  
5  
6  
7  
8

#### 9 *Bottomset seismic facies (HLAC)*

10  
11  
12 At the basinward end of clinothems High- and Low-Amplitude Continuous reflections  
13 (HAC and LAC) characterize the sedimentary packages (Fig. 6).  
14  
15  
16  
17  
18  
19

#### 20 *Bottomset inferred depositional environment*

21  
22  
23 This facies has been calibrated by extensive coring results as representing muddy basinal  
24 facies with black fine-grained intercalations (Trincardi et al., 1996; Piva et al., 2008a, b). Fairly  
25 continuous (but variable rate) sedimentation promoted continuous bottomset aggradation also in the  
26 easternmost portion of the PRLW (Gallignani-Pelagosa sector; Fig. 4).  
27  
28  
29  
30  
31  
32  
33  
34

## 35 **4.4 Evolution of the PRLW**

### 36 **4.4.1 The Mid Adriatic Deep 31.8 cal. ky BP (SB surface) and the PRLW total thickness**

37  
38  
39  
40 At 31.8 ky BP, the MAD was a semi-elliptical slope basin about 45 km by 40 km wide with  
41 a maximum paleo-depth of ca. 450 m (Pellegrini et al., in press; Fig. 10). The gently dipping shelf  
42 passed into a slope dipping about 1°, and to a pronounced bowl-shaped topography in the central  
43 sector of the basin, which hosted a central NNE-SSW anticline structure named in the following  
44 MAD anticline (Fig. 10). The PRLW accumulated in the MAD reaching 350 m in thickness (>400  
45 ms; Fig. 10) for a total accumulation of 504 km<sup>3</sup>.  
46  
47  
48  
49  
50  
51  
52  
53  
54  
55  
56

### 57 **4.4.2 Clinothem characterization**

1  
2  
3  
4  
5  
6  
7  
8  
9  
10  
11  
12  
13  
14  
15  
16  
17  
18  
19  
20  
21  
22  
23  
24  
25  
26  
27  
28  
29  
30  
31  
32  
33  
34  
35  
36  
37  
38  
39  
40  
41  
42  
43  
44  
45  
46  
47  
48  
49  
50  
51  
52  
53  
54  
55  
56  
57  
58  
59  
60  
61  
62  
63  
64  
65

Within the PRLW we recognize three types of elemental clinothems based on their geometry and seismic facies. The elemental clinothems are separated by key regional surfaces named “e” and “s” surfaces whose character, significance, and dating are described in detail in Pellegrini et al. (2017). Type A clinothems show topset aggradation, typically 10 m at the shelf-edge, over an average distance of 10 km; Type B clinothems, in contrast, do not display topset aggradation and show a maximum distance of less than 5 km between the shelf-edge and correlative onlap point where the “e” surface merges with the underlying “s” surface; Type C clinothems show maximum topset aggradation of up to 20 m thickness over an average distance of 20 km and the maximum horizontal distance between the shelf-edge and the time-equivalent shoreline. The 3 clinothem types are 64 to 160 m thick and have basinward dips of up to 2.1° (Fig. 6). The character of each type of clinothem is reported in the following paragraphs and summarized in [Table 3](#), where average shelf-edge progradation and foreset inclination for each clinothem is also provided.

The types of clinothems are systematically stacked with Type A and B clinothems that constitute Clinothem Set 1, characterized by a flat/slightly falling shelf-edge trajectory and a shelf-edge progradation of ca. 30 km; Type C clinothems constitute Clinothem Set 2, showing an ascending shelf-edge trajectory and a shelf-edge progradation of ca. 10 km (Fig. 6). Altogether, the shelf-edge through Clinothem Set 1 and 2 prograded a total of 40 km.

The following paragraphs describe the key features of each clinothem in the PRLW, highlighting their bounding surfaces and ages, paleobathymetry at their base (inferred from its basal structure map), map pattern of sediment accumulation, and lateral distribution of seismic facies and inferred depositional environments. These factors, along with sediment accumulation rates and environmental changes are summarized in [Table 4a, b](#). A detailed description of the older Clinothem A<sub>1</sub> is followed by shorter descriptions of the succeeding clinothems, highlighting the main changes through time.

*Clinothem A<sub>1</sub> (SB-s1 surfaces: 31.8-29.4 ky BP)*

1  
2 The structural map of the base of Clinothem A<sub>1</sub> (Fig. 11a) shows the MAD antiform striking  
3 NNW-SSE, extending from the shelf edge to the base of the slope and separating the MAD in two  
4 sub-basins. The thickness map shows the main depocenter reaching the maximum thickness, of 110  
5 m, on upper slope, just westward of the MAD antiform. Clinothem A<sub>1</sub> extends distally over ca. 40  
6 km pinching out at the southern edge of the MAD basin (Fig. 11b). The seismic facies map (Fig.  
7 11c) shows the extent of the HACH topset facies that corresponds with amalgamated channels on a  
8 large coastal plain located landward of the shelf-edge both NW of the MAD (Po plain channel belt)  
9 and WSW of it (Apennine Rivers channel belt). The foreset is dominantly characterised by  
10 HACHDip corresponding with a channelized prodelta. The bottomset is characterised by DLAH  
11 reflections indicating the presence of Mass Transport Complexes (MTCs). The MTCs are confined  
12 east of the MAD antiform and lap onto the southern margin of the basin. The distal seismic facies in  
13 the toe of the foreset is characterised by HAC reflections that are the evidence of fine-grained  
14 deposition.

*Clinothem B<sub>1</sub> (s1-e1 surfaces: 29.4-28.4 ky BP)*

15  
16  
17  
18  
19  
20  
21  
22  
23  
24  
25  
26  
27  
28  
29  
30  
31  
32  
33  
34  
35  
36 The structural map of surface s1 (Fig. 12a) indicates that the MAD antiform still maintained a  
37 morphological expression at the sea floor in the basin and at the shelf-edge. The main depocenter of  
38 Clinothem B<sub>1</sub> is located just east of the MAD antiform. In addition, the B<sub>1</sub> depocenter (Fig. 12b),  
39 being restricted to the northern edge of the MAD basin, has a smaller areal extent than that of the  
40 underlying Clinothem A<sub>1</sub>; the lack of B<sub>1</sub> clinothem on the shelf shows that no aggradation occurred  
41 during its deposition. The proximal bottomset is characterized by SHAM reflections ascribed to  
42 Distributary Channel-Lobe Complexes (DLCs; Fig. 12c).

*Clinothem A<sub>2</sub> (e1-s2 surfaces: 28.4-24.7 ky BP)*

1 The structural map of surface e1 (Fig. 13a) shows an area of minimum depth corresponding to  
2 the NNE-SSW MAD antiform. The thickness map (Fig. 13b) shows a main depocenter located on  
3 the eastern slope and extensive aggradation on the shelf resulting in an overall linear progradation  
4 of the eastern sector of the MAD. The seismic facies distribution of Clinothem A<sub>2</sub> (Fig. 13c) shows  
5 the occurrence of DLAH reflections of MTCs in the eastern reaches of the MAD, as in the previous  
6 A<sub>1</sub> clinothem.  
7  
8  
9  
10  
11  
12  
13  
14  
15  
16

17 *Clinothem B<sub>2</sub> (s2-e2 surfaces: 24.7 and 24.2 ky BP)*

18  
19 Structural map of s2 surface (Fig. 14a) suggests that the underlying MAD antiform was not  
20 completely buried after the deposition of previous clinothems. The sediment-thickness map (Fig.  
21 14b) shows a main depocenter striking WSW-ENE on the upper slope with Clinothem B<sub>2</sub> thicker  
22 and more extensive along the shelf-edge compared to the underlying Clinothem A<sub>2</sub>. The seismic  
23 facies map (Fig. 14c) denotes SHAM reflections of DLCs as in the preceding Type B<sub>1</sub> clinothem.  
24  
25  
26  
27  
28  
29  
30  
31  
32  
33

34 *Clinothem A<sub>3</sub> (e2-s3 surfaces: 24.2-21.1 ky BP)*

35  
36 The structural map of the e2 surface (Fig. 15a) shows a deeper sub-basin in the western sector  
37 compared to the eastern sector. The thickness map of Clinothem A<sub>3</sub> (Fig. 15b) shows two main  
38 coalescing depocenters developed on the upper slope. In the distal sector, Clinothem A<sub>3</sub> is  
39 characterized by digitate external geometries. Distally, Clinothem A<sub>3</sub> reflects the structural  
40 confinement exerted by structure on southern rim. The seismic facies map (Fig. 15c) shows  
41 LACDip and DLAH reflections of muddy prodelta and MTCs respectively, down in the bottomset  
42 sector whereas the distal area is characterized by LAC reflections of fine-grained deposits—a  
43 distinct change from the HAC reflections in the underlying clinothems.  
44  
45  
46  
47  
48  
49  
50  
51  
52  
53  
54  
55  
56  
57

58 *Clinothem B<sub>3</sub> (s3-e3 surfaces: 21.1-20.6 ky BP)*

1 The structural map of surface s2 (Fig. 16a) shows a deeper sub-basin in the western compared  
2 to the eastern sector. The thickness map (Fig. 16b) reveals coalescing individual depocenters that  
3 define an external geometry elongated along the E-W axis of the basin. In the toset sector,  
4 Clinothem B<sub>3</sub> shows a digitate external geometry and reflects the structural confinement exerted by  
5 the southern flank of the basin. The seismic facies map (Fig. 16c) is characterized by SHAM  
6 reflections ascribed to DLCs.  
7  
8  
9  
10  
11  
12  
13

14  
15  
16  
17 *Clinothem A<sub>4</sub> (e3-s4 surfaces: 20.6-19.4 ky BP)*  
18

19 The structural map of e3 surface (Fig. 17a) shows the presence of a deeper sub-basin in the  
20 western sector. The thickness map (Fig. 17b) shows a main depocenter on the slope that extends  
21 mainly in the western sub-basin reflecting the structural confinement at the toe of clinothem. The  
22 seismic facies map of Clinothem A<sub>4</sub> (Fig. 17c) shows a bottomset characterised by DLAH  
23 reflections ascribed to the presence of MTCs with an erratic distribution.  
24  
25  
26  
27  
28  
29  
30  
31  
32  
33

34 *Clinothem B<sub>4</sub> (s4-e4 surfaces: 19.4-19.3 ky BP)*  
35

36 The structural map of Clinothem B<sub>4</sub> (Fig. 18a) shows a linear shelf-edge and a quasi-buried  
37 MAD antiform in the slope sector. The thickness map (Fig. 18b) highlights an elongated depocenter  
38 in the central part of the slope characterized by a digitate external geometry in the distal sector.  
39 Clinothem B<sub>4</sub> contains HACH and HACHDip reflections that are the evidence of amalgamated  
40 channels on the northern foreset which pass laterally to SHAM reflections (DLCs) in the foreset and  
41 bottomset.  
42  
43  
44  
45  
46  
47  
48  
49  
50  
51  
52

53 *Clinothem A<sub>5</sub> (e4-s5 surfaces: 19.3-19.0 ky BP)*  
54

55 The structural map of surface e4 (Fig. 19a) indicates that the NNW-SSE MAD antiform still  
56 had a morphological expression in the bottomset sector. The thickness map (Fig. 19b) shows a  
57  
58  
59  
60  
61  
62  
63  
64  
65

1 maximum thickness at the foreset/bottomset transition represented by coalescent depocenters with  
2 no digitate pattern. The seismic facies map (Fig. 19c) reveals HAC reflections that indicate, for the  
3 first time during the PRLW progradation, the presence of delta-plain deposits in the western sector,  
4 along with HACH reflections with locally isolated incised valleys containing internal oblique  
5 reflections (Fig. 9). The foreset sector in the western sub-basin is characterized by HACDip  
6 reflections of heterolithic prodelta. Basinward the presence of DLAH reflections are the evidence of  
7 MTCs; these distribution of MTCs appears to have been confined structurally.  
8  
9  
10  
11  
12  
13  
14  
15  
16  
17  
18

#### 19 *Clinothem B<sub>5</sub> (s5-e5 surfaces: 19.0-18.6 ky BP)*

20  
21 The structural map of surface s5 at the base of the unit (Fig. 20a) shows an irregular shelf-  
22 edge with a prominent bulge in the centre of the study area. The thickness map (Fig. 20b) highlights  
23 two main coalescing depocenters extending to the upper slope in the western sub-basin. The map of  
24 the seismic facies (Fig. 20c) highlights the replacement of MTDs (LACH) with DLCs (SHAM) and  
25 of HAC with LAC reflections in the proximal and distal bottomset, respectively, compared to the  
26 underlying A<sub>5</sub> clinothem.  
27  
28  
29  
30  
31  
32  
33  
34  
35  
36  
37  
38

#### 39 *Clinothem A<sub>6</sub> (e5-s6 surfaces: 18.6-18.0 ky BP)*

40  
41 The structural map of the basal surface e5 (Fig. 21a), shows a bulge at shelf-edge with an  
42 indentation in the eastern sub-basin, possibly suggesting a sector of slope instability. The thickness  
43 map (Fig. 21b) highlights elliptical depocenter in western sub-basin and an elongated depocenter in  
44 the eastern one. The seismic facies map (Fig. 21c) shows LACDip reflections of muddy prodelta  
45 characterize the foreset/bottomset sector. In the eastern sub-basin and at the toe of the clinothem,  
46 DLAH reflections indicate the presence of MTCs.  
47  
48  
49  
50  
51  
52  
53  
54  
55  
56  
57

#### 58 *Clinothem C<sub>1</sub> (s6-s7 surfaces: 18.0 and 15.8 ky BP)*

1  
2 The structural map (Fig. 22a) indicates an irregular shelf-edge and shows the presence of a  
3 deeper sub-basin in the western sector. The thickness map (Fig. 22b) shows aggradation in the  
4 topset sector and a depocenter elongated in an E-W direction on the upper slope. In the western sub-  
5 basin, where Clinothem A<sub>6</sub> reaches the maximum thickness, the deposit tends to adapt to the  
6 structural confinement. The seismic facies map (Fig. 22c) shows HACH reflections that pass to  
7 HAC reflections suggesting the confinement of amalgamated channels in the western topset. On the  
8 foreset, Clinothem C<sub>1</sub> shows a variety of seismic facies from LACDip to HACWDip reflections  
9 reminiscent of muddy to sandy prodelta deposits that locally are characterized by crenulation  
10 features (*sensu* Urgeles et al., 2011).  
11  
12  
13  
14  
15  
16  
17  
18  
19  
20  
21  
22  
23

#### 24 *Clinothem C<sub>2</sub> (s7-MRS surfaces: 15.8-14.4 ky BP)*

25  
26 The structural map (Fig. 23a) is characterized by the presence of a quasi-linear shelf-edge and  
27 two sub-basins with similar depth in the eastern and western sector of the MAD. The main sub-  
28 rounded depocenter is in the foreset/bottomset sector of the western sub-basin (Fig. 23b) and a  
29 widespread area of topset aggradation on the north-western shelf. The seismic facies map (Fig. 23c)  
30 highlights the presence of HAC reflections of delta-plain and distal deposits that occupy a broad  
31 sector of the depositional area.  
32  
33  
34  
35  
36  
37  
38  
39  
40  
41  
42

#### 43 **4.4.3 The Mid Adriatic Deep: modern configuration**

44  
45 The modern bathymetry is characterized by a straight 35-km shelf edge in the north, a western  
46 slope sector characterized by slope-parallel bedforms, and a narrow 254-m deep slope-basin  
47 bounded to the east and to the south by the complex Gallignani-Pelagosa relief of tectonic origin.  
48 The multibeam data (Fig. 10) document a widespread field of pockmarks (Fig. 24), confirming the  
49 escape of fluids through the underlying units (Hovland and Curzi, 1989; Trincardi et al., 2004;  
50 Geletti et al., 2008).  
51  
52  
53  
54  
55  
56  
57  
58  
59  
60  
61  
62  
63  
64  
65

1 A comparison of the modern bathymetry with the paleobathymetry of the MAD at 31.8 ky  
2 BP, reveals the macro changes of the basin configuration that occurred mainly through the  
3  
4 progressive southward shift of the northern rim of the basin, reflecting 40 km progradation of the  
5 shelf-edge (Fig. 24). Conversely, the configuration of the southern boundary of the basin remained  
6  
7 substantially fixed, reflecting an area of fine-grained sediment aggradation. As a consequence, the  
8  
9 basin size shrunk from ca. 3500 to 1600 km<sup>2</sup> (this measure is taken comparing the areas surrounded  
10  
11 by the 200 m bathymetric contour at 31.8 ky BP and today).  
12  
13  
14  
15  
16  
17  
18  
19  
20  
21

## 22 **5. DISCUSSION**

### 23 **5.1 History of the PRLW: patterns, influences, and controls**

24 The development of the PRLW occurred in four main phases recorded by integrated changes  
25  
26 in stratal-stacking patterns, shelf-edge trajectory, map-pattern distribution of sediment  
27  
28 accumulation, character of the strata within the clinothems, and basin environmental conditions.  
29  
30 These phases appear to be closely related to changes in both accommodation and sediment supply,  
31  
32 as influenced by pre-existing bathymetry, eustasy, oceanographic conditions, and global and  
33  
34 regional climate. Oceanographic conditions of importance to stratal character included salinity,  
35  
36 temperature, turbidity, nutrient availability, and dominant energy mode (waves, river, or tides).  
37  
38 Integration of the broad range of controls and influences reveals the genesis of the stratal patterns  
39  
40 and enables appropriate use of the PRLW as an analog for prediction of rock properties in ancient  
41  
42 systems. The following section discusses the main patterns, influences, and controls of each phase  
43  
44 of development of the PRLW. Table 4a and b presents details of each clinothem and associated  
45  
46 paleoenvironment regime, respectively. The following section combines, for each phase,  
47  
48 information on the stratal patterns with environmental information.  
49  
50  
51  
52  
53  
54  
55  
56  
57  
58  
59  
60  
61  
62  
63  
64  
65

1 For completeness, we briefly describe the strata that occur below the basal sequence  
2 boundary (SB): The stratigraphic unit below SB has been interpreted as a regressive succession of  
3  
4 subaqueous muddy clinothems that accumulated on the shelf under the influence of along-shore  
5  
6 sediment transport during the last phase of the Pleistocene eustatic fall (Trincardi and Correggiari,  
7  
8 2000; Ridente and Trincardi, 2005; Ridente et al., 2009). These subaqueous muddy clinothems were  
9  
10 probably genetically related to subaerial progradation nourished by the ancestral Po River  
11  
12 (Pellegrini et al., in press). This interpretation is supported by the overall external geometry of this  
13  
14 unit, its seismic facies, and the location of the shoreline during its deposition (> 15 km from the  
15  
16 shelf-edge). Reflections in the uppermost part of this unit show truncation and toplap terminations  
17  
18 at the overlying SB. The microfaunal assemblages recorded in the PRAD1-2 borehole below SB  
19  
20 confirm an outer shelf paleoenvironment with bottom waters relatively well oxygenated and warm  
21  
22 surface waters characterized by winter mixing during the early phase of MIS 3 (59-40 ky BP; Piva  
23  
24 et al., 2008b). This condition evolves after 40 ky BP into a shallower (mid-shelf) environment with  
25  
26 progressively colder, more productive and stratified surface waters (Piva et al., 2008b). The  
27  
28 overlying strata of the Phase 1 interval lap onto the SB (Pellegrini et al., in press).  
29  
30  
31  
32  
33  
34  
35  
36  
37  
38

### 39 **5.1.1 Phase 1: basal Sequence Boundary (SB) to s2 (clinothems A<sub>1</sub> to A<sub>2</sub>), 31.8 to 24.7 ky BP**

40  
41 **Patterns:** The strata between surfaces SB and s2 comprise two Type A and one Type B  
42  
43 clinothems that stack in an overall progradational pattern. The shelf-edge trajectory evolves from  
44  
45 flat to slightly ascending to slightly descending. In plan view, sediment accumulation evolves from  
46  
47 a radial pattern restricted to the central outer shelf with compensational stacking of clinothems A<sub>1</sub>  
48  
49 and B<sub>1</sub>, to linear progradation in the eastern slope area in Clinothem A<sub>2</sub> (Figs. 11-13; Tab. 4a). The  
50  
51 upstream (topset) region is interpreted to have been a broad coastal plain with amalgamated channel  
52  
53 belts of the Po River (more preserved from the NW) and the Apennine rivers (less preserved from  
54  
55 the WSW) converging to the Mid-Adriatic Dip (MAD). The foreset region was a channelized sandy  
56  
57  
58  
59  
60  
61  
62  
63  
64  
65

1 prodelta environment. The proximal bottomset region includes stacks of Mass-Transport  
2 Complexes (MTCs in A<sub>1</sub> and A<sub>2</sub>) and Distributary Channel-Lobe Complexes (DLCs in B<sub>1</sub>), while  
3  
4 the distal bottomset area accumulated conformable fine-grained strata.  
5  
6

7 ***Influences and controls:*** At the onset of the deposition of Phase 1 clinothems the basin  
8  
9 morphology was influenced by the presence of the MAD antiform that extended SSE from the  
10 shelf-edge to the base of the slope. This antiform separated the MAD into two sub-basins that are  
11  
12 prominent at the base of the interval, but progressively more subdued upward. Eustasy fell by 45 m  
13  
14 to 125 m below present-day sea level quite rapidly at the beginning of this phase (A<sub>1</sub>), and  
15  
16 continued to fall, but more slowly during the upper two-thirds of this phase (A<sub>2</sub>; Lambeck et al.,  
17  
18 2014). This fall corresponds globally to the end of Dansgaard-Oeschger Interstadial 5 (based on  
19  
20 lighter  $\delta^{18}\text{O}$  values and an abundance peak of warm planktic species at this level in the PRAD1-2  
21  
22 borehole), followed by a phase of rapid and continued growth of the Laurentide and European ice  
23  
24 sheets (Dyke et al., 2002; Boulton et al., 2001). Sediment supply rates to the basin increased  
25  
26 significantly at the base of the interval, and decreased towards the top by a factor of 5; sediment  
27  
28 accumulation rates vary from 27.5 to 44 to 9 km<sup>3</sup>/ky upward in the three A<sub>1</sub>, B<sub>1</sub>, and A<sub>2</sub> clinothems,  
29  
30 respectively (Tab. 4b). Regionally, the Apennine glaciers were advancing throughout Phase 1, with  
31  
32 Alpine glaciers starting their advance slightly later, during A<sub>2</sub> time (Fig. 8; Tab. 4b; Giraudi, 2017;  
33  
34 Monegato et al., 2017).  
35  
36  
37  
38  
39  
40  
41  
42

43 The planktic assemblage, not abundant, indicates that surface waters were cold and  
44  
45 biogenically productive; (Hemleben et al., 1989; Pujol and Vergnaud-Grazzini, 1995), at least far  
46  
47 from direct riverine influence, as suggested by the dominance of the opportunistic benthic  
48  
49 foraminifera species *C. carinata* (Fig. 8; Tab. 4b; Van der Zwaan and Jorissen, 1991, Mojthaid et  
50  
51 al., 2009, Goineau et al., 2011). Bottom waters appear to have been relatively well oxygenated, with  
52  
53 organic matter being decreasingly well preserved upward (Fig. 8). This interpretation is based on  
54  
55 the peaks of the epifaunal/shallow infaunal foraminifer *H. balthica* that suggest relatively well-  
56  
57  
58  
59  
60  
61  
62  
63  
64  
65

1 oxygenated bottom water and/or a lowering of the quality of the organic matter (Schmiedl et al.,  
2 2000, Hess and Jorissen, 2009, Murray, 2006, Sweetman et al., 2009). Starting abruptly from 28.2  
3 ky BP (corresponding ca. to the e1 surface, Fig. 8) conditions became less favorable, in particular  
4 for the intermediate-water dweller *G. bulloides* (much less abundant from this level upward) driven  
5 by a progressive decrease of the water depth (Fig. 8). This shift matches the beginning of the Global  
6 LGM, coeval with Greenland Stadial 3 (27.540-23.340 ka) and encompasses the global sea-level  
7 lowstand (Hughes and Gibbard, 2015).  
8  
9  
10  
11  
12  
13  
14  
15  
16  
17  
18

### 19 **5.1.2 Phase 2: s2-s5 (clinothems B<sub>2</sub> to A<sub>5</sub>), 24.7 to 19.0 ky BP**

21 *Patterns:* The strata between surfaces s2 and s5 comprise three Type A as well as three  
22 Type B clinothems that stack in an overall progradational pattern. The shelf-edge trajectory  
23 alternated between descending in Type B clinothems to slightly ascending in Type A clinothems. In  
24 plan view, sediment accumulation evolves from three main radial depocenters on the slope of B<sub>2</sub>  
25 clinothem to elliptical depocenters slightly elongated W-E and with a digitate map pattern. For the  
26 first time since the PRLW progradation began, clinothems depocenter started to reflect a structural  
27 confinement against the distal limit of the basin (southern rim). In addition, A<sub>4</sub>-B<sub>4</sub>-A<sub>5</sub> clinothems  
28 are reduced in thickness and extent compared to the previous couplets, and show clear  
29 compensational patterns (Figs. 17-19; Tab. 4a). The topset region is interpreted to have been a  
30 broad coastal plain with amalgamated channel belts of the Po River (to the NW) and the Apennine  
31 rivers with occasionally-preserved delta plain sandy-silt deposits converging to the MAD. In the  
32 topset and upward, clinothems deposits evolve from amalgamated channel-belt deposits (A<sub>3</sub>  
33 clinothem; Fig. 25), to isolated incised valleys with internal point-bar migration that suggest a  
34 switch of the fluvial systems to more sinuous, meandering patterns (A<sub>5</sub> clinothem; Fig. 25). In the  
35 foreset area, large-scale turbidite slope channel-levee complexes covered by mud wedges (B<sub>2</sub>  
36 clinothem; Fig. 25) record the closest linkage of the shelf to the basin during the entire PRLW  
37  
38  
39  
40  
41  
42  
43  
44  
45  
46  
47  
48  
49  
50  
51  
52  
53  
54  
55  
56  
57  
58  
59  
60  
61  
62  
63  
64  
65

1 progradation. The proximal bottomset alternated between Mass-Transport Complexes (MTCs in A<sub>3</sub>,  
2 A<sub>4</sub>, and A<sub>5</sub>) and Distributary Channel-Lobe Complexes (DLCs in B<sub>2</sub>, B<sub>3</sub>, and B<sub>4</sub>). The distal area  
3 shows a change in seismic facies character of the conformable fine-grained strata from HAC to  
4 LAC reflections for most of this phase.  
5  
6  
7

8  
9 ***Influences and controls:*** Pre-existing bathymetry is subtly influenced by the sea-floor  
10 expression of the MAD antiform with the western sub-basin deeper than the eastern sub-basin up to  
11 the progradation of B<sub>4</sub> clinothem after which the MAD antiform is expressed mainly in the  
12 bottomset sector (Figs. 14-19). Eustasy continued to fall slowly down to 135 m below present-day  
13 sea level (Lambeck et al., 2014) during the first half of this phase (B<sub>2</sub>-B<sub>3</sub>) until reaching stillstand  
14 during accumulation of clinothems A<sub>4</sub> to A<sub>5</sub> (Fig. 8). This eustatic phase reflects an interval of  
15 further increase in ice volume of the Laurentide and Scandinavian ice sheets (Dyke et al., 2002;  
16 Boulton et al., 2001, respectively). Sediment composition changed at the beginning of Phase 2  
17 (surface s<sub>2</sub>, 24.7; Fig. 8) when Ca/Ti and K/Ti ratios increased abruptly. We interpret these shifts to  
18 reflect a change of the weathering intensity and a major change of sediment provenance probably  
19 driven by the maximum advance of Alpine glaciers documented at 25 ky BP by Monegato et al.  
20 (2017). In turn, this evidence suggests a very small buffering time (i.e. delay) between catchment  
21 and sink areas. Sediment supply rates in Phase 2 changed as well, showing alternating increases and  
22 decreases that were one order of magnitude larger in Type B clinothems than in Type A clinothems.  
23 In particular, Clinothem B<sub>4</sub> attained the maximum SAR of 200 km<sup>3</sup>/ky for the entire PRLW (Tab.  
24 4b). Regionally, during Phase 2 the Alpine and Apennine glaciers were waxing and waning (Fig. 8;  
25 Tab. 4b; Giraudi, 2017; Monegato et al., 2017).  
26  
27  
28  
29  
30  
31  
32  
33  
34  
35  
36  
37  
38  
39  
40  
41  
42  
43  
44  
45  
46  
47  
48  
49  
50

51 The microfaunal assemblages indicate that surface waters were still cold and productive  
52 (Fig. 8; Tab. 4b). In contrast to the Phase 1, however, bottom waters during Phase 2 were affected  
53 by reduced ventilation (as indicated by the concurrent abundance peaks of the deep-infaunal  
54 species; Fig. 8), reflecting the onset of millennial-scale (from B<sub>2</sub> upward) up to centennial-scale  
55  
56  
57  
58  
59  
60  
61  
62  
63  
64  
65

1 (from B<sub>4</sub> upward) fluctuations of riverine input, witnessing a marked environment variability. This  
2 interpretation is based on a decreasing concentration of planktic foraminifera coupled with the  
3  
4 minima in abundance of *C. carinata* and concurrent peaks of *N. depressulus* and *N. pauciloculum*,  
5  
6 indicative of inner shelf to estuaries/lagoons environments (Fig. 8; Hohenneger et al., 1989, Murray,  
7  
8 2006). Moreover, foraminifera *N. depressulus* and *N. pauciloculum* are more common (at intervals  
9  
10 even abundant) and continuously distributed compared to the Phase 1, indicating that riverine  
11  
12 discharge was closer to the borehole site.  
13  
14  
15  
16  
17  
18

### 19 **5.1.3 Phase 3: s5 to s6 (clinothems B<sub>5</sub> to A<sub>6</sub>), 19.0 to 18.0 ky BP**

20  
21 *Patterns:* The strata between surfaces s5 and s6 comprise one Type B and one Type A  
22  
23 clinothems stacked in an overall progradational to aggradational pattern. The shelf-edge trajectory  
24  
25 evolves from slightly descending to ascending. In plan view, sediment accumulation occurs mainly  
26  
27 in elliptical, coalescing depocenters that extended to the upper slope and were restricted to the  
28  
29 western sub-basin (Figs. 20-21; Tab. 4a). The topset region is interpreted as a local coastal plain  
30  
31 with amalgamated channel belts of the Po River (more preserved to the NW) coupled with delta  
32  
33 plains of the Apennine rivers (more preserved to the WSW) converging to the MAD. The foreset  
34  
35 region appears to have evolved from sandy to muddy prodelta and the proximal bottomset region  
36  
37 shifts from Distributary Channel-Lobe Complexes (DLCs in B<sub>5</sub>) to Mass-Transport Complexes  
38  
39 (MTCs in A<sub>6</sub>). The distal bottomset area accumulated LAC reflections interpreted as conformable  
40  
41 fine-grained strata.  
42  
43  
44  
45  
46  
47

48 *Influences and controls:* Pre-existing bathymetry is subtly influenced by the sea-floor  
49  
50 expression of the MAD antiform in the bottomset area with the western sub-basin being still deeper  
51  
52 than the eastern one. Eustasy began to rise with a jump of 15 m at the onset of Clinothem B<sub>5</sub> (19 ky  
53  
54 BP). The beginning of eustatic rise corresponds globally to the first melt-water pulse (MWP-1),  
55  
56 ascribed to the partial collapse of the Northern Hemisphere ice sheets (Yokoyama et al., 2001;  
57  
58  
59  
60  
61  
62  
63  
64  
65

1 Tarasov and Peltier, 2004; Bard et al., 1996; Carlson and Clark, 2012), followed by a phase of  
2 eustatic rise with rates of ca. 12 m/ky (Lea et al., 2002; Mitrovica et al., 2003; Siddal et al., 2003;  
3  
4 Peltier and Fairbanks, 2006; Bard et al., 2010; Lambeck et al., 2014; Benjamin et al., 2017).  
5  
6 Sediment-supply rates to the basin remained substantially constant with sediment-accumulation  
7  
8 rates of 57.5 and 56 km<sup>3</sup>/ky in B<sub>5</sub> and A<sub>6</sub>, respectively (Tab. 4b). Regionally, glaciers were  
9  
10 retreating in the Alps and the extent of Apennine glaciers was approaching zero (Fig. 8; Tab. 4b;  
11  
12 Giraudi, 2017).  
13  
14

15  
16 The microfaunal assemblage indicates that surface waters continued to be cold and  
17  
18 productive (Fig. 8; Tab. 4). Bottom waters were still affected by minor ventilation (as indicated by  
19  
20 the concurrent abundance peaks of the deep-infaunal species; Fig. 8). Fresh-water supply condition  
21  
22 were similar to the preceding Phase 2, whereas the abrupt drop in abundance of *C. carinata*  
23  
24 suggests variations in water environmental parameters such as salinity and water turbidity.  
25  
26  
27  
28  
29  
30

#### 31 **5.1.4 Phase 4: s<sub>6</sub> to MRS (clinothems C<sub>1</sub> to C<sub>2</sub>), 18.0 to 14.4 ky BP**

32  
33 **Patterns:** The strata between surfaces s<sub>6</sub> and MRS comprise two Type C clinothems stacked  
34  
35 in an overall aggradational pattern. The shelf-edge trajectory is markedly ascending. In plan view,  
36  
37 sediment accumulation evolves from an E-W elongated depocenter to a more elliptical depocenter  
38  
39 on the slope, coupled with aggradation of the topsets of both clinothems on a broad area of the  
40  
41 northwestern shelf (Figs. 22-23; Tab. 4a). During the progradation of Type C clinothems their  
42  
43 topsets aggraded up to 45 m —the thickest and most extensive aggradation of the entire PRLW. The  
44  
45 topset is interpreted has a coastal and delta plain where the Po and Apennine channels tended to  
46  
47 become isolated, narrower, and thinner with subdued levees compared to the underlying clinothems  
48  
49 (Fig. 25). The foreset region comprises heterolithic prodelta deposits characterized by crenulation  
50  
51 features possibly reflecting density flows (Fig. 24, and Mulder and Syvitzky, 1995). The proximal  
52  
53 bottomset region evolved to strata that are conformable with the underlying clinothems (where  
54  
55  
56  
57  
58  
59  
60  
61  
62  
63  
64  
65

1  
2 DLCs in B clinothems and MTCs in A clinothems are preserved). The distal bottomset area is  
3 characterized by LAC reflections interpreted as conformable fine-grained strata, similar to  
4 preceding Phase-3 strata.  
5

6  
7 ***Influences and controls:*** During this phase, the pre-existing bathymetry evolved to a  
8 surface where the MAD antiform is almost buried. Eustasy continued to rise with rates of up to 12  
9 m/ky (e.g. Lambeck et al., 2014) followed by an event of accelerated eustatic rise to a rate of  
10 several m per century (Clark et al., 2004), at ca. 14.5 ky BP. This accelerated rise has been  
11 attributed to meltwater pulse (MWP-1A; Fairbanks, 1989; Lambeck et al., 2014) after the onset of  
12 the Bølling-Allerød warm period and coincided with the formation of the MRS atop Clinothem C<sub>2</sub>  
13 (Fig. 8; Tab. 4b). Sediment-supply rates to the basin decreased towards the top of this interval by a  
14 factor of 5 relative to the preceding Phase-3 SAR; sediment-accumulation rates vary from 30.5 to a  
15 minimum of 21.5 km<sup>3</sup>/ky upward in the two C<sub>2</sub> clinothems (Tab. 4b), and to about zero at the MRS.  
16 Regionally, glaciers were drastically retreating: Alpine glaciers to within their catchment outlets  
17 (Monegato et al., 2017) and Apennine glacial extent was close to zero (Giraudi, 2017; Fig. 8; Tab.  
18 4b).  
19  
20  
21  
22  
23  
24  
25  
26  
27  
28  
29  
30  
31  
32  
33  
34  
35

36 The microfaunal assemblage indicates that surface waters was still influenced by high  
37 riverine influence. Increased fresh-water discharge during Phase 4 was probably also the main  
38 factor affecting the planktic foraminifera, which responded with 1) a markedly oligotypic  
39 assemblage dominated by the small subarctic surface dweller *T. quinqueloba* (ca. 90% on average),  
40 and 2) the absolute minima in concentration for the entire PRLW (Fig. 8; Tab. 4b). Bottom waters  
41 were affected by low ventilation (as indicated by the concurrent abundance peaks of the deep  
42 infaunal species; Fig. 8), reflecting centennial oscillations of riverine input. The centennial-scale  
43 oscillations in fresh-water input to the basin increased in magnitude that culminated between 18 and  
44 16 ky BP. This trend is recorded by rapid shifts in the abundance of *Nonion* spp (Fig. 8), and very  
45 large oscillations of the  $\delta^{18}\text{O}$  composition of planktic foraminifera (up to 2 per mil towards lighter  
46  
47  
48  
49  
50  
51  
52  
53  
54  
55  
56  
57  
58  
59  
60  
61  
62  
63  
64  
65

1 values) that reflect salinity drops during phases of enhanced fresh-water discharge. Increased fresh-  
2 water input in Phase 4 is also indicated, in the shallowest coring sites, by a frequency peak of the  
3 benthic species *Ammonia perlucida* (Fig. 8) a taxon with a modern distribution restricted to very  
4 shallow shelf areas in the Adriatic Sea (< 20m, Jorissen, 1987, 1988) and neighboring lagoon  
5 environments (Donnici et al., 1997). At ca. 14.6 ky BP an abrupt increase of the abundance and a  
6 substantial turnover of the assemblages of planktic and benthic foraminifera in all three coring sites  
7 records the drowning and abandonment of the PRLW (MRS at 14.4 ky BP; Fig. 8; Tab. 4a, b).  
8  
9  
10  
11  
12  
13  
14  
15  
16  
17  
18

## 19 **5.2 Variations between the distance of shoreline and its time-equivalent shelf-edge**

21 Earlier publications dealing with delta systems have tried to predict the nature of basinal  
22 deposits by analyzing specific indicators such as coastal-onlap or shelf-edge trajectory (e.g. Helland  
23 Hansen and Martinsen, 1996; Plink-Björklund et al., 2001; Johannessen and Steel, 2005; Carvajal  
24 and Steel, 2006; Porebski and Steel, 2006; Ryan et al., 2009; Patruno et al., 2015; Poyatos-Moré et  
25 al., 2016; Gong et al., 2016 for a review). Stratigraphic concepts interpret stratal architecture and  
26 sediment distribution as results of the interaction of accommodation and sediment supply. Yet,  
27 sediment supply to a basin can vary over time in response to autogenic and allogenic processes (e.g  
28 Muto and Steel, 1997; Jerolmack and Paola, 2010; Calves et al., 2013). Additionally, the supply to a  
29 basin may be out of phase with eustatic changes promoting geometrical variations at local scale  
30 (Madof et al., 2016). The PRLW represents an ideal site for deciphering the relations among topset  
31 geometry, shelf-edge trajectory, and basinal deposits, and to extrapolate scaling factors related to  
32 the different type of clinothems (Pellegrini et al., 2017). During much of the PRLW progradation,  
33 the shoreline was docked close to the shelf-edge and a significant amount of sediment was delivered  
34 to the basin floor (Pellegrini et al., 2017). Our work suggests that even when the shoreline was in  
35 that area, subtle changes in the distance to the shelf-edge result in distinctive topset geometries  
36 associated with specific basinal deposits. We conclude that when the shoreline was within 10 km  
37  
38  
39  
40  
41  
42  
43  
44  
45  
46  
47  
48  
49  
50  
51  
52  
53  
54  
55  
56  
57  
58  
59  
60  
61  
62  
63  
64  
65

1 from the shelf-edge, margin destabilization and MTCs were likely promoted (Fig. 26; Type A  
2 clinothem). In physiographic settings where the shoreline was closer to the shelf-edge (< 5 km)  
3  
4 topset degradation coupled with high sediment bypass to the basin promote the formation of DLCs  
5  
6 (Figs. 26 Type B clinothemes). Finally, when the shoreline was more than 10 km from the shelf-  
7  
8 edge, and no direct conduit linked the shelf to the slope, no significant volume of coarse sediment  
9  
10 reached the basin floor (Figs. 26). These values are in agreement with the independently constrained  
11  
12 values of connection between shoreline and canyon head documented by Sweet and Blum (2016).  
13  
14 Our finding suggests that subtle and systematic changes in the distance between shoreline and the  
15  
16 shelf-edge result in systematically stacked basinal deposits. In this view, we show the importance of  
17  
18 carefully analyzing both the topset geometry and the shelf-edge trajectory. Our work demonstrates  
19  
20 the potential of Quaternary successions as high-resolution frameworks from which to extrapolate  
21  
22 scaling-factor parameters that enhance the predictability of sand-prone deposits in the basin.  
23  
24 Whereas previous studies have focused on 100,000 year-scale cycles of glaciation-deglaciation as  
25  
26 the temporal scale that determines the balance between shelf aggradation and sediment export to the  
27  
28 deep basin, data from the PRLW show that sediment export to the basin can be episodic, even over  
29  
30 centennial to millennial time-scales. In this view, our documentation demonstrates, for the first  
31  
32 time, the minimum time interval (centennial) in which DLCs can develop with volumes on the order  
33  
34 of 60 km<sup>3</sup> bypassing the shelf-edge (Tab. 3).  
35  
36  
37  
38  
39  
40  
41  
42  
43  
44  
45

### 46 **5.3 The record of composite cyclicity in the PRLW -Sequence Stratigraphic Interpretation-**

47

48 We conclude this discussion section with a consideration of how the strata of the PRLW  
49  
50 would be interpreted on the basis of sequence stratigraphy alone, in the absence of such detailed  
51  
52 chronological and paleontology data. This exercise can reveal how transportable are the lessons  
53  
54 from the PRLW and what is essential to predicting the character and distribution of basinal deposits  
55  
56 based on shelfal observations. It reinforces the fundamental focus of classic sequence stratigraphy  
57  
58  
59  
60  
61  
62  
63  
64  
65

1  
2  
3  
4  
5  
6  
7  
8  
9  
10  
11  
12  
13  
14  
15  
16  
17  
18  
19  
20  
21  
22  
23  
24  
25  
26  
27  
28  
29  
30  
31  
32  
33  
34  
35  
36  
37  
38  
39  
40  
41  
42  
43  
44  
45  
46  
47  
48  
49  
50  
51  
52  
53  
54  
55  
56  
57  
58  
59  
60  
61  
62  
63  
64  
65

(*sensu* Vail et al., 1977; Neal et al., 2016) on the recognition of various types of stratal surfaces as foundational to stratigraphic interpretation, correlation, and mapping.

The PRLW represents a succession constrained by robust physical, bio- and chrono-stratigraphic data of high resolution. It thus represents an excellent natural laboratory wherein to apply the classic sequence-stratigraphic approach to decipher the complex strata of the PRLW in terms of composite cyclicity of forcing mechanisms. Upon initial inspection, the data allowed three alternative hypotheses for the interpretation of the PRLW stratal patterns in a sequence-stratigraphic context; each hypothesis had its pluses and minuses (Fig. 27). The following paragraphs discuss these alternative hypotheses and how we chose our lead hypothesis based on the preponderance of evidence (Fig. 27).

The first hypothesis interprets each A-B clinothem couplet, as well as each Type C clinothem as a parasequence (Fig. 27A). This view is driven by the most obvious and easily traceable surfaces in the PRLW being below the landward shifts that occur at the base of every A+B couplet (except A<sub>1</sub>+B<sub>1</sub>), A<sub>6</sub>, and the two Type C clinothems. The basinward shift below A<sub>1</sub>+B<sub>1</sub> couplet is explained by the location of that couplet just above the basal sequence boundary. For the A+B parasequences, Type A clinothems would record the aggradation to progradation characteristic of parasequences (e.g, Van Wagoner et al., 1990). Type B clinothems would record the continuation of progradation, with the truncation at their tops recording in-facies erosion at base of distributary channels (or, alternatively, ravinement during the transgression at the base of the overlying Type A clinothem). Following Neal and Abreu (2009) and Neal et al. (2016), Clinothem Set 1, formed by A-B couplets, represents the Progradational component of a Progradational-Aggradational Set (PA Set) and Clinothem Set 2, with stacked type C clinothems, the Aggradational element of the same PA Set (Pellegrini et al., 2017). On the plus side, this interpretation has the charm of simplicity, it is consistent with the observations of Pellegrini et al. (2017) that the truncation at top of Type B clinothems does not exceed the ca. 10-m distributary-channel depth seen in this system (Amorosi et

1 al., 2016), and it explains the lack of well-developed parasequence sets inside the Type A or Type B  
2 clinothem that would be expected if these clinothem represent higher-frequency depositional  
3 sequences. On the minus side, this interpretation would reveal an internal complexity of  
4 parasequences not widely reported—although Gerber et al. (2008) and Plint et al. (2009) suggest  
5 some internal complexity, there are no reports of full bypass of the foreset and development of  
6 basinally restricted strata of two types (DLCs and MTCs) at the parasequence scale.  
7  
8  
9  
10  
11  
12  
13

14 The second hypothesis interprets each A-B couplet to represent a complete high-frequency  
15 depositional sequence *sensu* Mitchum and Van Wagoner (1991), but with sequence boundaries  
16 defined in the sense of Van Wagoner (1995): each sequence boundary is represented by the  
17 erosional surface at the base of a Type A clinothem in the topset zone connected to the erosional  
18 surface at the top of a Type B clinothem, to the conformable surface between the Type A and Type  
19 B clinothem in the slope zone, to the base of the Type A clinothem beneath the MTC deposits in  
20 the basinal zone (Fig. 27; ‘Correlation Method 2’ of Martin et al., 2009). In this view, all Type A  
21 clinothem (except A<sub>1</sub>) would record aggradational (A) stacking, and all Type B clinothem would  
22 record progradational (P) stacking (Fig. 27). All the A-B couplets together (A<sub>1</sub> to A<sub>6</sub>) form a  
23 lowstand/PA sequence set (Fig. 27). Following the same approach, the two Type C clinothem  
24 delimited by regional flooding surfaces form a high-frequency transgressive sequence set (Mitchum  
25 and Van Wagoner, 1991). On the plus side, this interpretation explains the two types of basinally  
26 restricted strata as related to progradation at or near the shelf-edge, and the high-frequency  
27 depositional-sequence boundaries (at base of A<sub>2</sub> through A<sub>6</sub>) correlate to mass-transport deposits in  
28 the basin as normally observed (e.g., Haq, 1993; Maslin et al., 1998; Beauboeuf and Friedmann,  
29 2000; Posamentier and Kolla, 2003). On the minus side, this interpretation has the sequence  
30 boundary at the base of Type A clinothem, where there are landward shifts of facies and not the  
31 basinward shifts in facies expected (Fig. 27). This hypothesis leads to the interpretation that the  
32 High Amplitude and Chaotic (HACH) seismic facies observed in the most proximal part of Type B  
33  
34  
35  
36  
37  
38  
39  
40  
41  
42  
43  
44  
45  
46  
47  
48  
49  
50  
51  
52  
53  
54  
55  
56  
57  
58  
59  
60  
61  
62  
63  
64  
65

1  
2  
3  
4  
5  
6  
7  
8  
9  
10  
11  
12  
13  
14  
15  
16  
17  
18  
19  
20  
21  
22  
23  
24  
25  
26  
27  
28  
29  
30  
31  
32  
33  
34  
35  
36  
37  
38  
39  
40  
41  
42  
43  
44  
45  
46  
47  
48  
49  
50  
51  
52  
53  
54  
55  
56  
57  
58  
59  
60  
61  
62  
63  
64  
65

clinothem are shelf-edge gullies, relatively far from shore, but this is inconsistent with the observation of DLCs on the basal surface of Type B clinothem which imply that the shoreline was less than 5 km from shelf edge (as discussed in a previous section). In addition, this alternative has two different interpretations of the stacking patterns for Type A (AP for A<sub>1</sub>, PA for A<sub>2</sub> to A<sub>6</sub>). It also has an APD succession sitting directly upon the basal, lower-order sequence boundary, which is the most likely place to find, instead, a PA succession (Neal and Abreu, 2009). This hypothesis implies that all transgressive systems tracts (R stacking) and practically all the AP stacked parts of the APD systems tract are not developed at a scale resolvable by seismic data, perhaps due to the very rapid progradation of the shelf edge.

The third hypothesis bundles the clinothem into high-frequency sequences differently, and mostly associates each Type B with its overlying Type A clinothem (B<sub>1</sub>-A<sub>2</sub>, B<sub>2</sub>-A<sub>3</sub>, B<sub>3</sub>-A<sub>4</sub>, B<sub>4</sub>-A<sub>5</sub>, B<sub>5</sub>-A<sub>6</sub>; Fig. 27). Following strictly the usage of Mitchum et al. (1977), each sequence boundary is represented by the erosional surface at the base of a Type A clinothem in the topset zone connected to the base of the immediately underlying Type B clinothem at the point where the Type B clinothem laps onto the underlying stratal unit, to the surface at the base of that Type B clinothem in the slope and basinal zones onto which the DLC deposits lap on in the lower-slope zone and lap down in the basinal zone ('Correlation Method 1' of Martin et al., 2009). Each B-A couplet would represent PA stacking (A<sub>1</sub> is missing its P component because it directly overlies the lower-order depositional sequence boundary), wherein the upper surface of each Type B clinothem records the change from progradation to aggradation. The topset aggradation observed in Type A clinothem reflects periods of decreased sediment supply to the slope (Tab. 3), as observed in model simulations from Burgess and Prince (2015). The two Type C clinothem would represent parasequences bounded by flooding surfaces developed during the first phase of eustatic rise when sediment supply still keeps pace with the increase in accommodation (as discussed in the previous section). Overall, the interval from A<sub>1</sub> to A<sub>6</sub> (Clinothem Set 1) would be a progradational sequence

1 set, and the interval from  $C_1$  to  $C_2$  would be an aggradational parasequence set. This interpretation  
2 was informed by the close geometric similarity of the PRLW strata to those seen in the XES02  
3 experiment of Martin et al. (2009), which is illustrated in figure 27 and the strict application of the  
4 sequence-boundary criteria of Mitchum et al. (1977). On the plus side, this hypothesis explains the  
5 basinally restricted stratal units. The sequence boundaries are marked by coastal onlap of Type B  
6 clinothems below the pre-existing shelf-break (as expected). This hypothesis implies that the High  
7 Amplitude and Chaotic (HACH) seismic facies at the most proximal part of Type B clinothems are  
8 amalgamated distributary channels, albeit potentially their subaqueous extensions (*sensu* Olariu and  
9 Bhattacharya, 2006). These strata would still be near shore, because the development of DLCs on  
10 the basal surfaces of Type B clinothems means that the shoreline was less than 5 km from the shelf-  
11 edge (as discussed in a previous section). Thus, the onlap of Type B clinothems is effectively  
12 coastal onlap. The erosion across the tops of Type B clinothems would represent continuing  
13 extension of the fluvial system (the 'Ef' surface of Martin et al., 2009) within the PA/Lowstand  
14 Systems Tract, and the strata within Type B clinothems is the basal record of the diachroneity of  
15 that erosional surface (Martin et al., 2009). The surface identified in hypothesis 2 (correlation  
16 method 2 of Martin et al., 2009), although not a sequence boundary (*sensu* Mitchum et al., 1977), is  
17 still useful because it marks the change from progradation to aggradation within the high-frequency  
18 lowstand/PA systems tracts (we propose naming it the "P-A surface"). In addition, the landward  
19 shifts at the base of Type A clinothems are consistent with their aggradational stacking (Fig. 27).  
20 On the minus side, this hypothesis implies that all high-frequency transgressive and highstand  
21 systems tracts (R and APD sets) were not developed at a seismically resolvable scale. This is  
22 potentially not a fatal flaw, as discussed above, because those are the stacking patterns and systems  
23 tracts that are least likely to be well developed under falling to low accommodation (e.g., Jervey,  
24 1988; Van Wagoner et al., 1990; Martin et al., 2009).  
25  
26  
27  
28  
29  
30  
31  
32  
33  
34  
35  
36  
37  
38  
39  
40  
41  
42  
43  
44  
45  
46  
47  
48  
49  
50  
51  
52  
53  
54  
55  
56  
57  
58  
59  
60  
61  
62  
63  
64  
65

1 The balance of evidence, plus versus minus, as well as the use of the original criteria for  
2 sequence-boundary identification (i.e., Mitchum et al., 1977) and the close match of the PRLW  
3 systems to both the stratal geometries and base-level curve of the XES02 experiment, suggest the  
4 third option as our lead hypothesis. Ultimate confirmation probably requires a grid of long cores  
5 and wells through the entire PRLW. This would enable detailed facies definition and correlation  
6 supported by refined chronological control.  
7  
8  
9  
10  
11  
12  
13  
14  
15  
16

## 17 **6. CONCLUSIONS**

18 The stratal geometry within the Po River Lowstand Wedge, formed in 17 ky encompassing the  
19 Last Glacial Maximum, documents repeated short-term changes in accommodation and sediment  
20 supply controlling the formation of “elementary” margin-scale clinothems. This revealed how the  
21 evolution of a margin-scale system intricately convolves the influences of both global (eustacy) and  
22 regional (climate-driven supply fluctuations) controls. In particular:  
23  
24  
25  
26  
27  
28  
29  
30  
31  
32  
33

- 34 1. based on the available chronological control, the architectural motif of the elementary  
35 clinothems and clinothems sets record sub-Milankovitch cyclicity driven by changes in  
36 hydrological balance (fresh-water discharge) and oceanographic regime in the receiving  
37 slope basin;  
38  
39  
40  
41  
42
- 43 2. distinctive configurations are associated with different timing and quantity of sediment  
44 delivered to the basin: respectively, i) centennial-scale, descending shelf-edge trajectory and  
45 Channel-Lobe Complexes: Type B clinothem up to 200 km<sup>3</sup>/yr; ii) millennial-scale,  
46 ascending shelf-edge trajectory and Mass Transport Complexes: Type A clinothem up to  
47 100 km<sup>3</sup>/yr; iii) millennial-scale markedly ascending shelf-edge trajectory and mud wedges:  
48 Type C clinothem up to 30 km<sup>3</sup>/yr;  
49  
50  
51  
52  
53  
54  
55  
56  
57  
58  
59  
60  
61  
62  
63  
64  
65

3. distinctive topset geometries (Type B degradational, Type A moderately aggradational and Type C markedly aggradational), associated with distinctive basal deposits (respectively Channel-Lobe Complexes, Mass Transport Complexes or mud wedges), reflect subtle changes in the relative distance between the shoreline and the time-correlative shelf-edge that ranges from virtually zero (Type B) to 10s of km (Type C);
4. the activation and time span of channel-lobe complexes, such as within the Type B clinothems can occur at century scale;
5. the progradation of Clinothem Set 1 during eustatic fall and stillstand led to an essentially flat shelf-edge trajectory accompanied by significant sediment bypass to the basin and low-oxygen conditions at the seafloor, whereas Clinothem Set 2 records the first phases of sea level rise through ascending shelf-edge trajectory and sediment increasingly sequestered in the topset during increasing accommodation on a broadening shelf sector, along with intermittent increases in benthic-oxygen levels;
6. the main linkage between shelf and basin occurs throughout the falling limb of sea level (Clinothem Set 1), but the major sediment export to the basin coincides with lowstand sea level through a more extensive fluvial system;
7. a substantial decoupling between eustatic rise and enduring river influence on a mid-latitude continental margin impacted by post-glacial melt-water injections.

By recognizing the very short-time interval associated to the deposition of each “elementary” clinothem (few hundreds to a few thousand years) we question if, in ancient records, clinothems with a putative duration of hundreds of thousands of years might, at least in some cases, record instead much shorter intervals with most of the geological time condensed in hiatuses and stratigraphic surfaces. We suggest that the PRLW provides valuable insight into the lower end of the range of time spans recorded by such ancient margin-scale clinothems. All of these

1 considerations reinforce the focus of classic sequence stratigraphy on surface recognition for  
2 interpretation, correlation, mapping, and prediction of rock properties. Finally, we highlighted the  
3 importance of integrating paleoenvironment data with the sequence stratigraphic method in the  
4 reconstruction of the history of a continental margin.  
5  
6  
7  
8  
9

## 10 11 **ACKNOWLEDGMENTS**

12 The authors dedicate this study to their colleague Giovanni Bortoluzzi, who passed away in 2015. A  
13 special tank is due to Marco Ligi and Nevio Zitellini for geophysical data acquisition and  
14 processing; Marco Pastore and Filippo D’Oriano for their support during the cruise LSD2014 and  
15 processing of geophysical data. Elisabetta Campiani provided additional support for processing the  
16 multibeam bathymetry. A particular thank goes to Cpt. Emanuele Gentile and the crew of the R/V  
17 Urania during cruise LSD2014. This project was funded by ExxonMobil Upstream Research  
18 Company and by the Flagship Project RITMARE–The Italian Research for the Sea. We  
19 acknowledge the European Union Project PROMESS-1 (contract EVR1-2001-41) for borehole  
20 PRAD 1-2. This is ISMAR-CNR contribution number XXXX.  
21  
22  
23  
24  
25  
26  
27  
28  
29  
30  
31  
32  
33  
34  
35  
36  
37  
38  
39  
40  
41  
42  
43  
44  
45  
46  
47  
48  
49  
50  
51  
52  
53  
54  
55  
56  
57  
58  
59  
60  
61  
62  
63  
64  
65

## REFERENCES CITED

- 1  
2 Amorosi, A., Colalongo, M. L., Fiorini, F., Fusco, F., Pasini, G., Vaiani, S. C., and Sarti, G., 2004,  
3  
4 Palaeogeographic and palaeoclimatic evolution of the Po Plain from 150-ky core records:  
5  
6 Global and Planetary Change, v. 40(1), p. 55-78.  
7  
8  
9 Amorosi, A., Maselli, V., and Trincardi, F., 2016, Onshore to offshore anatomy of a late Quaternary  
10  
11 source-to-sink system (Po Plain–Adriatic Sea, Italy). *Earth-Science Reviews*, 153, 212-237.  
12  
13  
14 Amorosi, A., Bruno, L., Campo, B., Morelli, A., Rossi, V., Scarponi, D., Hong, W., Bohacs, M. K.,  
15  
16 and Drexler, T. M., 2017, Global sea-level control on local parasequence architecture from  
17  
18 the Holocene record of the Po Plain, Italy. *Marine and Petroleum Geology*.  
19  
20  
21 Anderson, J. B., A. Rodriguez, K. C. Abdulah, R. H. Fillon, L. A. Banfield, H. A. McKeown, and J.  
22  
23 S. Wellner, 2004, Late Quaternary stratigraphic evolution of the northern Gulf of Mexico  
24  
25 margin: A synthesis, in J. B. Anderson and R. H. Fillon, eds., *Late Quaternary stratigraphic*  
26  
27 *evolution of the northern Gulf of Mexico margin: SEPM Special Publication 79*, p. 1–23.  
28  
29  
30 Anderson, J. B., Wallace, D. J., Simms, A. R., Rodriguez, A. B., Weight, R. W., and Taha, Z. P.,  
31  
32 2016, Recycling sediments between source and sink during a eustatic cycle: Systems of late  
33  
34 Quaternary northwestern Gulf of Mexico Basin. *Earth-Science Reviews*, 153, 111-138.  
35  
36  
37  
38 Asioli, A., 1996, High resolution foraminifera biostratigraphy in the Central Adriatic basin during  
39  
40 the last deglaciation: a contribution to the PALICLAS Project. *Memorie-Istituto Italiano di*  
41  
42 *Idrobiologia*, v. 55, p. 197-218.  
43  
44  
45 Asioli, A., Trincardi, F., Lowe, J.J., Ariztegui, D., Langone, L., and Oldfield, F., 2001, Sub-  
46  
47 millennial scale climatic oscillations in the central Adriatic during the Late glacial:  
48  
49 palaeoceanographic implications: *Quaternary Science Reviews*, v. 20(11), p. 1201-1221.  
50  
51  
52 Asquith, D. O., 1970, Depositional topography and major marine environments, Late Cretaceous,  
53  
54 Wyoming. *AAPG Bulletin*, 54(7), 1184-1224.  
55  
56  
57  
58  
59  
60  
61  
62  
63  
64  
65

- 1 Bard, E., Hamelin, B., Arnold, M., and Montaggioni, L., 1996, Deglacial sea-level record from  
2 Tahiti corals and the timing of global meltwater discharge. *Nature*, 382(6588), 241.  
3  
4 Bard, E., Hamelin, B., and Delanghe-Sabatier, D., 2010, Deglacial meltwater pulse 1B and Younger  
5 Dryas sea levels revisited with boreholes at Tahiti. *Science*, 327(5970), 1235-1237.  
6  
7 Bazin, L., Landais, A., Lemieux-Dudon, B., Toy'e Mahamadou Kele, H., Veres, D., Parrenin, F.,  
8  
9 Martinerie, P., Ritz, C., Capron, E., Lipenkov, V., Loutre, M.-F., Raynaud, D., Vinther, B.,  
10  
11 Svensson, A., Rasmussen, S.O., Severi, M., Blunier, T., Leuenberger, M., Fischer, H.,  
12  
13 Masson-Delmotte, V., Chappellaz, J., and Wolff, E., 2013, An optimized multi-proxy, multi-  
14  
15 site Antarctic ice and gas orbital chronology (AICC2012): 120–800 ka, *Climate of the Past*, v.  
16  
17 9, p. 1715–1731.  
18  
19  
20  
21  
22  
23  
24 Beaubouef, R. T., and S. J. Friedmann, 2000, High resolution seismic/sequence-stratigraphic  
25  
26 framework for the evolution of Pleistocene intraslope basins, western Gulf of Mexico:  
27  
28 Depositional models and reservoir analogs, in P. Weimer, R. M. Slatt, J. Coleman, N. C.  
29  
30 Rosen, H. Nelson, A. H. Bouma, M. J. Styzen, and D. T. Lawrence, eds., *Deep-water*  
31  
32 *reservoirs of the world: Gulf Coast Section SEPM 20th Annual Research Conference*, p. 40–  
33  
34 60.  
35  
36  
37  
38  
39 Benjamin, J., Rovere, A., Fontana, A., Furlani, S., Vacchi, M., Inglis, R. H., Galili, E., Antonioli,  
40  
41 F., Sivan, D., Miko, S., Mourtzas, N., Felja, I., Meredith-Williams, M., Goodman-Tchernov,  
42  
43 B., Kolaiti, E., Anzidei, M., Gehrels, R., 2017, Late Quaternary sea-level changes and early  
44  
45 human societies in the central and eastern Mediterranean Basin: An interdisciplinary review.  
46  
47 *Quaternary International*.  
48  
49  
50  
51 Bhattacharya, J. P., Copeland, P., Lawton, T. F., and Holbrook, J., 2016, Estimation of source area,  
52  
53 river paleo-discharge, paleoslope, and sediment budgets of linked deep-time depositional  
54  
55 systems and implications for hydrocarbon potential. *Earth-Science Reviews*, 153, 77-110.  
56  
57  
58  
59  
60  
61  
62  
63  
64  
65

- 1  
2  
3  
4  
5  
6  
7  
8  
9  
10  
11  
12  
13  
14  
15  
16  
17  
18  
19  
20  
21  
22  
23  
24  
25  
26  
27  
28  
29  
30  
31  
32  
33  
34  
35  
36  
37  
38  
39  
40  
41  
42  
43  
44  
45  
46  
47  
48  
49  
50  
51  
52  
53  
54  
55  
56  
57  
58  
59  
60  
61  
62  
63  
64  
65
- Boulton, G. S., Dongelmans, P., Punkari, M., and Broadgate, M., 2001, Palaeoglaciology of an ice sheet through a glacial cycle: the European ice sheet through the Weichselian. *Quaternary Science Reviews*, v. 20(4), p. 591-625.
- Bourne, A.J., Lowe, J.J., Trincardi, F., Asioli, A., Blockley, S.P.E., Wulf, S. Matthews, I.P. Piva, A., and Vigliotti, L., 2010, Distal tephra record for the last ca 105,000 years from core PRAD 1-2 in the central Adriatic Sea: implications for marine tephrostratigraphy: *Quaternary Science Reviews* v. 29, p. 3079-3094.
- Boyd, R., Suter, J., and Penland, S., 1989, Relation of sequence stratigraphy to modern sedimentary environments. *Geology*, 17(10), 926-929.
- Bruno, L., Amorosi, A., Severi, P., & Costagli, B., 2017, Late Quaternary aggradation rates and stratigraphic architecture of the southern Po Plain, Italy: *Basin Research*, 29(2), 234-248.
- Burgess, P. M., and Prince, G. D., 2015, Non-unique stratal geometries: implications for sequence stratigraphic interpretations. *Basin Research*, 27(3), 351-365.
- Campo, B., Amorosi, A., and Vaiani, S. C., 2017, Sequence stratigraphy and late Quaternary paleoenvironmental evolution of the Northern Adriatic coastal plain (Italy). *Palaeogeography, Palaeoclimatology, Palaeoecology*, 466, 265-278.
- Calves, G., Toucanne, S., Jouet, G., Charrier, S., Thereau, E., Etoubleau, J., Marsset, T., Droz, L., Bez, M., Abreu, V., Jorry, S., Mulder, T., and Lericolais, G., 2013, Inferring denudation variations from the sediment record; an example of the last glacial cycle record of the Golo Basin and watershed, East Corsica, western Mediterranean sea. *Basin Research*, 25(2), 197-218.
- Carlson, A. E., and Clark, P. U., 2012, Ice sheet sources of sea level rise and freshwater discharge during the last deglaciation. *Reviews of Geophysics*, 50(4), p. 1-72.
- Carvajal, C. R., Steel, R. J., 2006, Thick turbidite successions from supply-dominated shelves during sea-level highstand. *Geology*, 34(8), 665-668.

- 1 Carvajal, C., Steel, R., and Petter, A., 2009, Sediment supply: the main driver of shelf-margin  
2 growth: *Earth-Science Reviews*, v. 96(4), p. 221-248.  
3
- 4 Cattaneo, A., Correggiari, A., Langone, L., Trincardi, F., 2003, The late-Holocene Gargano  
5 subaqueous delta, Adriatic shelf: sediment pathways and supply fluctuations. *Marine*  
6  
7 *Geology*, 193(1), 61-91.  
8  
9
- 10  
11 Catuneanu, O., Abreu, V., Bhattacharya, J. P., Blum, M. D., Dalrymple, R. W., Eriksson, P. G.,  
12  
13 Winker, C., 2009, Towards the standardization of sequence stratigraphy. *Earth-Science*  
14  
15 *Reviews*, 92(1), 1-33.  
16  
17
- 18  
19 Clark, P. U., McCabe, A. M., Mix, A. C., and Weaver, A. J., 2004, Rapid rise of sea level 19,000  
20  
21 years ago and its global implications. *Science*, 304 (5674), 1141-1144.  
22  
23
- 24 Dyke, A. S., Andrews, J. T., Clark, P. U., England, J. H., Miller, G. H., Shaw, J., and Veillette, J. J.  
25  
26 2002, The Laurentide and Innuitian ice sheets during the last glacial maximum. *Quaternary*  
27  
28 *Science Reviews*, v. 21(1), p. 9-31.  
29  
30
- 31 Dalla Valle, G., Gamberi, F., Rocchini, P., Minisini, D., Errera, A., Baglioni, L., Trincardi, F.,  
32  
33 2013a, 3D seismic geomorphology of mass transport complexes in a foredeep basin:  
34  
35 Examples from the Pleistocene of the Central Adriatic Basin (Mediterranean Sea).  
36  
37 *Sedimentary Geology*, 294, 127-141.  
38  
39  
40
- 41 Dalla Valle, G., Gamberi, F., Trincardi, F., Baglioni, L., Errera, A., Rocchini, P., 2013b,  
42  
43 Contrasting slope channel styles on a prograding mud-prone margin. *Marine and Petroleum*  
44  
45 *Geology*, 41, 72-82.  
46  
47
- 48 Del Bianco, F., Gasperini, L., Giglio, F., Bortoluzzi, G., Kljajic, Z., Ravaioli, M., 2014, Seafloor  
49  
50 morphology of the Montenegro/N. Albania Continental Margin (Adriatic Sea—Central  
51  
52 Mediterranean). *Geomorphology*, 226, 202-216.  
53  
54  
55  
56  
57  
58  
59  
60  
61  
62  
63  
64  
65

- 1  
2  
3  
4  
5  
6  
7  
8  
9  
10  
11  
12  
13  
14  
15  
16  
17  
18  
19  
20  
21  
22  
23  
24  
25  
26  
27  
28  
29  
30  
31  
32  
33  
34  
35  
36  
37  
38  
39  
40  
41  
42  
43  
44  
45  
46  
47  
48  
49  
50  
51  
52  
53  
54  
55  
56  
57  
58  
59  
60  
61  
62  
63  
64  
65
- Dogliani, C., Mongelli, F., and Pieri, P., 1994, The Puglia uplift (SE Italy): An anomaly in the foreland of the Apenninic subduction due to buckling of a thick continental lithosphere: *Tectonics*, v. 13, p. 1309–1321, doi:10.1029/94TC01501.
- Donnici, S., Serandrei Barbero, R., Taroni, G., 1997. Living benthic foraminifera in the lagoon of Venice (Italy): population dynamics and its significance. *Micropaleontology* 43, 440-
- Fairbanks, R. G., 1989, A 17, 000-year glacio-eustatic sea level record: influence of glacial melting rates on the Younger Dryas event and deep-ocean circulation. *Nature*, 342(6250), 637-642.
- Fanget, A. S., Berné, S., Jouet, G., Bassetti, M. A., Dennielou, B., Maillet, G. M., and Tondut, M., 2014, Impact of relative sea level and rapid climate changes on the architecture and lithofacies of the Holocene Rhone subaqueous delta (Western Mediterranean Sea): *Sedimentary Geology*, 305, 35-53.
- Fatoke, O. A., and Bhattacharya, J. P., 2010. Controls on Depositional Systems and Sequence Stratigraphy of the Pliocene-Pleistocene Strata of Eastern Niger Delta, Nigeria. *Search and Discovery Article*, 10220.
- Florineth, D., and Schlüchter, C., 1998, Reconstructing the Last Glacial Maximum (LGM) ice surface geometry and flowlines in the Central Swiss Alps. *Eclogae Geologicae Helvetiae*, 91, 391-407.
- Frignani, M., Langone, L., Ravaioli, M., Sorgente, D., Alvisi, F., Albertazzi, S., 2005, Fine-sediment mass balance in the western Adriatic continental shelf over a century time scale. *Marine Geology*, 222, 113-133.
- Geletti, R., Del Ben, A., Busetti, M., Ramella, R., and Volpi, V., 2008, Gas seeps linked to salt structures in the Central Adriatic Sea: *Basin Research*, 20(4), 473-487.
- Gerber, T., Pratson, L., Wolinsky, M., Steel, R., Mohr, J., Swenson, J. and Paola, C. 2008, Cliniform progradation by turbidity currents: modeling and experiments. *Journal of Sedimentary Research*, 78, 220 – 238454.

- 1  
2  
3  
4  
5  
6  
7  
8  
9  
10  
11  
12  
13  
14  
15  
16  
17  
18  
19  
20  
21  
22  
23  
24  
25  
26  
27  
28  
29  
30  
31  
32  
33  
34  
35  
36  
37  
38  
39  
40  
41  
42  
43  
44  
45  
46  
47  
48  
49  
50  
51  
52  
53  
54  
55  
56  
57  
58  
59  
60  
61  
62  
63  
64  
65
- Ghielmi, M., Minervini, M., Nini, C., Rogledi, S., and Rossi, M., 2013, Late Miocene–Middle Pleistocene sequences in the Po Plain–Northern Adriatic Sea (Italy): the stratigraphic record of modification phases affecting a complex foreland basin: *Marine and Petroleum Geology*, 42, 50-81.
- Giraudi, C., 2017, Climate evolution and forcing during the last 40 ka from the oscillations in Apennine glaciers and high mountain lakes, Italy. *Journal of Quaternary Science*.
- Goineau, A., Fontanier, C., Jorissen, F.J., Lansard, B., Buscail, R., Mouret, A., Kerhervé, P., Zaragosi, S., Ernoult, E., Artéro, C., Anschutz, P., Metzger, E., Rabouill, C. 2011. Live (stained) benthic foraminifera from the Rhône prodelta (Gulf of Lion, NW Mediterranean): environmental controls on a river-dominated shelf. *Journal Sea Research*, 65, 58–75.
- Gong, C., Steel, R. J., Wang, Y., Lin, C., and Olariu, C., 2016, Shelf-margin architecture variability and its role in sediment-budget partitioning into deep-water areas. *Earth-Science Reviews*, 154, 72-101.
- Hayward, W., S. Kawagata, A. Sabaa, H. Grenfell, L. Van Kerckhoven, K. Johnson, and E. Thomas. 2012. The Last Global Extinction (Mid-Pleistocene) of Deep-sea Benthic Foraminifera (Chrysalogoniidae, Ellipsoidinidae, Glandulonodosariidae, Plectofrondiculariidae, Pleurostomellidae, Stilostomellidae), Their Late Cretaceous-Cenozoic History and Taxonomy. *Cushman Foundation for Foraminiferal Research Special Publication*, 43, p. 408.
- Haq, B.U., 1993, Deep sea response to eustatic changes and significance of gas hydrates for continental margin stratigraphy, in Posamentier, H.W., Summerhayes, C.P., Haq, B.U., and Allen, G.P., eds., *Sequence Stratigraphy and Facies Associations: International Association of Sedimentologists, Special Publication 18*, p. 93–106.
- Helland-Hansen, W., and Martinsen, O. J., 1996, Shoreline trajectories and sequences: description of variable depositional-dip scenarios: *Journal of Sedimentary Research*, v. 66(4), p. 670-688.

- 1 Helland-Hansen, W., and Hampson, G.J., 2009, Trajectory analysis: concepts and applications:  
2 Basin Research, v. 21(5), p. 454-483.  
3
- 4 Hemleben, C., Spindler, M., Anderson, O.R., 1989, Modern Planktonic foraminifera. Springer-  
5 Verlag, New York. p. 1–363.  
6
- 7 Henriksen, S., Hampson, G.J., Helland-Hansen, W., Johannessen, E.P., and Steel, R.J., 2009, Shelf  
8 edge and shoreline trajectories, a dynamic approach to stratigraphic analysis: Basin Research,  
9 v. 21(5), p. 445-453.  
10
- 11 Hess, S., and F. J. Jorissen, 2009, Distribution patterns of living benthic foraminifera from Cap  
12 Breton canyon, Bay of Biscay: Faunal response to sediment instability, Deep Sea Res., Part I,  
13 56, 1555–1578, doi:10.1016/j.dsr.2009.04.003.  
14
- 15 Hohenegger, J., Piller, W. and Ch. Baal, 1989: Reasons for the spatial microdistributions of  
16 foraminifers in an intertidal pool (Northern Adriatic Sea). P.S.Z.N. I. Marine Ecology, 10, 43-  
17 78, Berlin-Hamburg.  
18
- 19 Hovland, M. and Curzi, P., 1989, Gas seepage and assumed mud diapirism in the Italian central  
20 Adriatic Sea. Mar. Petrol. Geol., v. 6, p. 161-169.  
21
- 22 Hughes, P. D., and Gibbard, P. L., 2015, A stratigraphical basis for the Last Glacial Maximum  
23 (LGM). Quaternary International, 383, 174-185.  
24
- 25 IEA, 2013, Resources to reserves 2013; oil, gas, and coal technologies for energy markets of the  
26 future, OECD-IEA, Paris, France, 272 pp. (ISBN 978-92-64-08354-7).  
27
- 28 Jerolmack, D. J., and Paola, C., 2010, Shredding of environmental signals by sediment transport.  
29 Geophysical Research Letters, 37(19).  
30
- 31 Jervey, M. T., 1988, Quantitative geological modeling of siliciclastic rock sequences and their  
32 seismic expression.  
33
- 34 Johannessen, E.P., and Steel, R.J., 2005, Shelf-margin clinoforms and prediction of deepwater  
35 sands. Basin Research, v. 17(4), p. 521-550.  
36

- 1  
2 Jorissen F.J. 1987. The distribution of benthic foraminifera in the Adriatic Sea. *Marine*  
3 *Micropaleontology*, 12, 21-48.
- 4 Jorissen F.J. 1988. Benthic Foraminifera from the Adriatic Sea; principles of phenotypic variation.  
5 *Utrecht Micropaleontology Bulletin*, 37, 176.
- 6  
7 Jorissen, F.J., Asioli, A., Borsetti, A., Capotondi, L., De Visser, J., Hilgen, F., Rohling, E., Van der  
8  
9 Borg, K., Grazzini, C.V., Zachariasse, W., 1993. Late quaternary central Mediterranean  
10  
11 biochronology. *Marine Micropaleontology*, 21, 169-189.
- 12  
13  
14 Jorissen, F.J., 1999. Benthic foraminiferal successions across Late Quaternary Mediterranean  
15  
16 sapropels. *Marine Geology* 153, 91-101.
- 17  
18  
19 Jouet, G., Berne, S., Rabineau, M., Bassetti, M. A., Bernier, P., Dennielou, B., Taviani, M., 2006,  
20  
21 Shoreface migrations at the shelf edge and sea-level changes around the Last Glacial  
22  
23 Maximum (Gulf of Lions, NW Mediterranean). *Marine Geology*, 234(1), 21-42.
- 24  
25  
26 Kettner, A. J., Syvitski, J. P., 2008, *HydroTrend v. 3.0: A climate-driven hydrological transport*  
27  
28 model that simulates discharge and sediment load leaving a river system. *Computers &*  
29  
30 *Geosciences*, 34(10), 1170-1183.
- 31  
32  
33  
34  
35 Kolla, V., Perlmutter, M. A., 1993, Timing of turbidite sedimentation on the Mississippi Fan *AAPG*  
36  
37 *Bull.*, v. 77, p. 1129–1141.
- 38  
39  
40  
41 Knudsen, K.L. (Ed), 1971, Late Quaternary Foraminifera from the Vendsyssel, Denmark and  
42  
43 Sandnes, Norway - systematic part. In: Feyling-Hanssen, Jørgensen, Knudsen and Lykke  
44  
45 Andersen (Eds): Late Quaternary Foraminifera from the Vendsyssel, Denmark and Sandnes,  
46  
47 Norway. *Bulletin of the Geological Society of Denmark*, 21, 185-295.
- 48  
49  
50  
51 Lambeck, K., Rouby, H., Purcell, A., Sun, Y., and Sambridge, M., 2014, Sea level and global ice  
52  
53 volumes from the Last Glacial Maximum to the Holocene. *Proceedings of the National*  
54  
55 *Academy of Sciences*, 111(43), 15296-15303.
- 56  
57  
58  
59  
60  
61  
62  
63  
64  
65

- 1  
2  
3  
4  
5  
6  
7  
8  
9  
10  
11  
12  
13  
14  
15  
16  
17  
18  
19  
20  
21  
22  
23  
24  
25  
26  
27  
28  
29  
30  
31  
32  
33  
34  
35  
36  
37  
38  
39  
40  
41  
42  
43  
44  
45  
46  
47  
48  
49  
50  
51  
52  
53  
54  
55  
56  
57  
58  
59  
60  
61  
62  
63  
64  
65
- Lea, D. W., Martin, P. A., Pak, D. K., and Spero, H. J., 2002, Reconstructing a 350ky history of sea level using planktonic Mg/Ca and oxygen isotope records from a Cocos Ridge core. *Quaternary Science Reviews*, 21(1), 283-293.
- Madof, A. S., Harris, A. D., and Connell, S. D., 2016, Nearshore along-strike variability: Is the concept of the systems tract unhinged?: *Geology*, 44(4), 315-318.
- Martin, J., Paola, C., Abreu, V., Neal, J., and Sheets, B., 2009, Sequence stratigraphy of experimental strata under known conditions of differential subsidence and variable base level. *AAPG bulletin*, 93(4), 503-533.
- Maselli, V., Trincardi, F., Cattaneo, A., Ridente, D., and Asioli, A., 2010, Subsidence patterns in the central Adriatic and its influence on sediment architecture during the last 400 kyr: *Journal of Geophysical Research: Solid Earth*, v. 115, n. B12, doi: 10.1029/2010JB007687.
- Maslin, M., Mikkelsen, N., Vilela, C., and Haq, B.U., 1998, Sea-level and gas-hydrate-controlled catastrophic sediment failures of the Amazon fan: *Geology*, v. 26, p. 1107–1110.
- Milliman, J. D., and Farnsworth, K. L., 2013, River discharge to the coastal ocean: a global synthesis. *Global and planetary change*, v. 39, p. 53-64.
- Milliman, J. D., Bonaldo, D., and Carniel, S., 2016, Flux and fate of river-discharged sediments to the Adriatic Sea. *Advances in Oceanography and Limnology*, 7(2).
- Mitchum Jr, R. M., Vail, P. R., and Sangree, J. B., 1977, Seismic stratigraphy and global changes of sea level: Part 6. Stratigraphic interpretation of seismic reflection patterns in depositional sequences: Section 2. Application of seismic reflection configuration to stratigraphic interpretation.
- Mitchum, R.M.J., Van Wagoner, J.C., 1991. High-frequency sequences and their stacking patterns: sequence-stratigraphic evidence of high-frequency eustatic cycles. *Sedimentary Geology* 70(2-4), 131-160. doi: 10.1016/0037-0738(91)90139-5.

- 1  
2 Mitrovica, J. X., 2003, Recent controversies in predicting post-glacial sea-level change. *Quaternary*  
3 *Science Reviews*, 22(2), 127-133.
- 4  
5 Mojtahid, M., Jorissen, F., Lansard, B., Fontanier, C., Bombled, B., Rabouille, C., 2009. Spatial  
6  
7 distribution of live benthic foraminifera in the Rhône prodelta: faunal response to a  
8  
9 continental-marine organic matter gradient. *Marine Micropaleontology*, 70 (3-4), 177–200.
- 10  
11 Monegato, G., Ravazzi, C., Donegana, M., Pini, R., Calderoni, G., and Wick, L., 2007, Evidence of  
12  
13 a two-fold glacial advance during the last glacial maximum in the Tagliamento end moraine  
14  
15 system (eastern Alps): *Quaternary Research*, v. 68, p. 284–302,  
16  
17 doi:10.1016/j.yqres.2007.07.002.
- 18  
19 Monegato, G., Scardia, G., Hajdas, I., Rizzini, F. and Piccin, A., 2017, The Alpine LGM in the  
20  
21 boreal icesheets game, *Scientific Reports*, vol. 7: 2078, doi:10.1038/s41598-017-02148-7.
- 22  
23  
24 Mulder, T., Syvitski, J.P.M., 1995, Turbidity currents generated at river mouths during exceptional  
25  
26 discharges to the world oceans: *Journal of Geology* 103, 285-299.
- 27  
28  
29 Muller-Karger, F.E., Varela, R., Thunell, R., Luerssen, R., Chuanamin Hu, Walsh, J.J., 2005, The  
30  
31 importance of continental margins in the global carbon cycle: *Geophysical Research Letters* v.  
32  
33 32, L01602.
- 34  
35  
36 Murray, J.W. 2006. *Ecology and Applications of Benthic Foraminifera*. Cambridge University  
37  
38 Press, 426 p.
- 39  
40  
41 Murray, J.W. 2013. Living benthic foraminifera: biogeographical distributions and the significance  
42  
43 of rare morphospecies. *Journal of Micropalaeontology*, 32, 1-58.
- 44  
45  
46 Muto, T., and Steel, R. J., 1997, Principles of regression and transgression: the nature of the  
47  
48 interplay between accommodation and sediment supply: perspectives. *Journal of Sedimentary*  
49  
50 *Research*, 67(6).
- 51  
52  
53 Neal, J., Abreu, V., 2009. Sequence stratigraphy hierarchy and the accommodation succession  
54  
55 method. *Geology*, v. 37(9), p. 779-782.
- 56  
57  
58  
59  
60  
61  
62  
63  
64  
65

- 1  
2  
3  
4  
5  
6  
7  
8  
9  
10  
11  
12  
13  
14  
15  
16  
17  
18  
19  
20  
21  
22  
23  
24  
25  
26  
27  
28  
29  
30  
31  
32  
33  
34  
35  
36  
37  
38  
39  
40  
41  
42  
43  
44  
45  
46  
47  
48  
49  
50  
51  
52  
53  
54  
55  
56  
57  
58  
59  
60  
61  
62  
63  
64  
65
- Neal, J. E., Abreu, V., Bohacs, K. M., Feldman, H. R., and Pederson, K. H., 2016, Accommodation succession ( $\delta A/\delta S$ ) sequence stratigraphy: observational method, utility and insights into sequence boundary formation. *Journal of the Geological Society*, 173(5), 803-816.
- Olariu, C., and Bhattacharya, J. P., 2006, Terminal distributary channels and delta front architecture of river-dominated delta systems. *Journal of sedimentary research*, 76(2), 212-233.
- Patruno, S., Hampson, G. J., Jackson, C. A. L., Whipp, P. S., 2015. Quantitative progradation dynamics and stratigraphic architecture of ancient shallow-marine clinoform sets: a new method and its application to the Upper Jurassic Sognefjord Formation, Troll Field, offshore Norway: *Basin Research*.
- Pellegrini, C., Maselli, V., Cattaneo, A., Piva, A., Ceregato, A., and Trincardi, F., 2015, Anatomy of a compound delta from the post-glacial transgressive record in the Adriatic Sea. *Marine Geology*, 362, 43-59.
- Pellegrini, C., Maselli, V., Gamberi, F., Asioli, A., Bohacs, K. M., Drexler, T. M., and Trincardi, F. 2017, How to make a 350-m-thick lowstand systems tract in 17,000 years: The Late Pleistocene Po River (Italy) lowstand wedge. *Geology*, G38848-1.
- Pellegrini, C., Bohacs, K. M., Drexler, T. M., Gamberi, F., Rovere, M., and Trincardi, F, in press, Identifying the Sequence Boundary in Over- and Under-Supplied Contexts: the Case of the Late Pleistocene Adriatic Continental Margin.
- Peltier, W. R., and Fairbanks, R. G., 2006, Global glacial ice volume and Last Glacial Maximum duration from an extended Barbados sea level record: *Quaternary Science Reviews*, v. 25(23), p. 3322-3337.
- Pillans, B., Chappell, J., and Naish, T. R., 1998, A review of the Milankovitch climatic beat: template for Plio–Pleistocene sea-level changes and sequence stratigraphy. *Sedimentary Geology*, 122(1), 5-21.

- 1  
2  
3  
4  
5  
6  
7  
8  
9  
10  
11  
12  
13  
14  
15  
16  
17  
18  
19  
20  
21  
22  
23  
24  
25  
26  
27  
28  
29  
30  
31  
32  
33  
34  
35  
36  
37  
38  
39  
40  
41  
42  
43  
44  
45  
46  
47  
48  
49  
50  
51  
52  
53  
54  
55  
56  
57  
58  
59  
60  
61  
62  
63  
64  
65
- Pirmez, C., Pratson, L. F., Steckler, M. S., 1998. Clinoform development by advection-diffusion of suspended sediment: Modeling and comparison to natural systems. *Journal of Geophysical Research: Solid Earth* (1978–2012), 103(B10), 24141-24157.
- Piva, A., Asioli, A., Schneider, R. R., Trincardi, F., Andersen, N., Colmenero-Hidalgo, E., Dennielou, B., Flores, J.A., and Vigliotti L., 2008a, Climatic cycles as expressed in sediments of the PROMESS1 borehole PRAD1-2, Central Adriatic, for the last 370 ka, 1: integrated stratigraphy. *Geochemistry, Geophysics, Geosystems*, v. 9 (1), Q01R01, doi: 10.1029/2007GC001713.
- Piva, A., Asioli, A., Andersen, N., Grimalt, J. O., Schneider, R. R., and Trincardi, F., 2008b, Climatic cycles as expressed in sediments of the PROMESS1 borehole PRAD1-2, central Adriatic, for the last 370 ka: 2. Paleoenvironmental evolution. *Geochemistry, Geophysics, Geosystems*, 9(3).
- Plink-Björklund, P., Mellere, D., Steel, R. J., 2001, Turbidite variability and architecture of sand-prone, deep-water slopes: Eocene clinoforms in the Central Basin, Spitsbergen. *Journal of Sedimentary Research*, 71(6), 895-912.
- Plint, A.G., and Kreitner, M.A., 2007, Extensive thin sequences spanning Cretaceous foredeep suggest high-frequency eustatic control: Late Cenomanian, Western Canada foreland basin: *Geology*, v. 35(8), p. 735-738.
- Plint, A. G., 2009, High-frequency Relative Sea-level Oscillations in Upper Cretaceous Shelf Clastics of the Alberta Foreland Basin: Possible Evidence for a Glacio-Eustatic Control? *Sedimentation, Tectonics and Eustasy. Sedimentation, Tectonics and Eustasy, Spec. Publ. Int. Assoc. Sedimentol*, 12, 409-428.
- Porębski, S. J., and Steel, R. J., 2003, Shelf-margin deltas: their stratigraphic significance and relation to deepwater sands. *Earth-Science Reviews*, 62(3), 283-326.

- 1  
2  
3  
4  
5  
6  
7  
8  
9  
10  
11  
12  
13  
14  
15  
16  
17  
18  
19  
20  
21  
22  
23  
24  
25  
26  
27  
28  
29  
30  
31  
32  
33  
34  
35  
36  
37  
38  
39  
40  
41  
42  
43  
44  
45  
46  
47  
48  
49  
50  
51  
52  
53  
54  
55  
56  
57  
58  
59  
60  
61  
62  
63  
64  
65
- Posamentier, H. W., and Kolla, V., 2003, Seismic geomorphology and stratigraphy of depositional elements in deep-water settings. *Journal of sedimentary research*, 73(3), 367-388.
- Poyatos-Moré, M., Jones, G. D., Brunt, R. L., Hodgson, D. M., Wild, R. J., and Flint, S. S., 2016, Mud-Dominated Basin-Margin Progradation: Processes and Implications. *Journal of Sedimentary Research*, 86(8), 863-878.
- Pujol, C., Vergnaud Grazzini, C., 1995, Distribution patterns of live planktic foraminifera as related to regional hydrography and productive systems of the Mediterranean Sea. *Marine Micropaleontology* v. 25, p. 187–217.
- Ridente, D., and Trincardi, F., 2005, Pleistocene “muddy” forced-regression deposits on the Adriatic shelf: a comparison with prodelta deposits of the late Holocene highstand mud wedge. *Marine Geology*, 222, 213-233.
- Ridente, D., Trincardi, F., Piva, A., and Asioli, A. 2009, The combined effect of sea level and supply during Milankovitch cyclicity: Evidence from shallow-marine  $\delta^{18}\text{O}$  records and sequence architecture (Adriatic margin): *Geology*, v. 37, p. 1003-1006.
- Roberts, H. H., Fillon, R. H., Kohl, B., Robalin, J. M., and Sydow, J. C., 2004, Depositional architecture of the Lagniappe Delta: sediment characteristics, timing of depositional events, and temporal relationship with adjacent shelf-edge deltas.
- Rossi, M., Minervini, M., Ghielmi, M., and Rogledi, S., 2015, Messinian and Pliocene erosional surfaces in the Po Plain-Adriatic Basin: Insights from allostratigraphy and sequence stratigraphy in assessing play concepts related to accommodation and gateway turnarounds in tectonically active margins: *Marine and Petroleum Geology*, 66, 192-216.
- Royden, L., Patacca, E., and Scandone, P., 1987, Segmentation and configuration of subducted lithosphere in Italy: an important control on thrust-belt and foredeep-basin evolution. *Geology*, v. 15(8), p. 714-717.

- 1 Ryan, M. C., Helland-Hansen, W., Johannessen, E. P., and Steel, R. J., 2009, Erosional vs.  
2 accretionary shelf margins: the influence of margin type on deepwater sedimentation: an  
3 example from the Porcupine Basin, offshore western Ireland. *Basin Research*, 21(5), 676-703.
- 4  
5  
6  
7 Schmiedl, G., de Bovève, F., Buscail, R., Charrière, B., Hemleben, C., Medernach, L., and Picon, P.  
8  
9  
10 2000. Trophic control of benthic foraminiferal abundance and microhabitat in the bathyal  
11 Gulf of Lions, western Mediterranean Sea, *Marine Micropaleontology*, 40, 167–188.
- 12  
13  
14 Sheets, B.A., Hickson, T.A., and Paola, C., 2002, Assembling the stratigraphic record: Depositional  
15 patterns and time-scales in an experimental alluvial basin: *Basin Research*, v. 14, p. 287–301,  
16  
17 doi:10.1046/j.1365-2117.2002.00185.x.
- 18  
19  
20  
21  
22 Siddall, M., Rohling, E. J., Almogi-Labin, A., Hemleben, C., Meischner, D., Schmelzer, I., and  
23  
24 Smeed, D. A., 2003, Sea-level fluctuations during the last glacial cycle. *Nature*, 423(6942),  
25  
26 853-858.
- 27  
28  
29 Simeoni U, Pano N, Ciavola P, 1997, The coastline of Albania: morphology, evolution and coastal  
30 management issues. *CIESM Publ.* 18: 561-168.
- 31  
32  
33  
34 Steckler, M.S., Mountain, G.S., Miller, K.G., Christie-Blick, N., 1999, Reconstruction of Tertiary  
35 progradation and clinof orm development on the New Jersey passive margin by 2-D  
36 backstripping. *Marine Geology* 154, 399-420.
- 37  
38  
39  
40  
41 Steel, R. J., Crabaugh, J., Schellpeper, M., Mellere, D., Plink-Björklund, P., Deibert, J., and  
42  
43 Loeseth, T. 2000, Deltas vs. rivers on the shelf edge: their relative contributions to the growth  
44 of shelf-margins and basin-floor fans (Barremian and Eocene, Spitsbergen): *Deepwater*  
45  
46  
47  
48  
49  
50  
51  
52  
53  
54  
55  
56  
57  
58  
59  
60  
61  
62  
63  
64  
65  
66  
67  
68  
69  
70  
71  
72  
73  
74  
75  
76  
77  
78  
79  
80  
81  
82  
83  
84  
85  
86  
87  
88  
89  
90  
91  
92  
93  
94  
95  
96  
97  
98  
99  
100  
101  
102  
103  
104  
105  
106  
107  
108  
109  
110  
111  
112  
113  
114  
115  
116  
117  
118  
119  
120  
121  
122  
123  
124  
125  
126  
127  
128  
129  
130  
131  
132  
133  
134  
135  
136  
137  
138  
139  
140  
141  
142  
143  
144  
145  
146  
147  
148  
149  
150  
151  
152  
153  
154  
155  
156  
157  
158  
159  
160  
161  
162  
163  
164  
165  
166  
167  
168  
169  
170  
171  
172  
173  
174  
175  
176  
177  
178  
179  
180  
181  
182  
183  
184  
185  
186  
187  
188  
189  
190  
191  
192  
193  
194  
195  
196  
197  
198  
199  
200  
201  
202  
203  
204  
205  
206  
207  
208  
209  
210  
211  
212  
213  
214  
215  
216  
217  
218  
219  
220  
221  
222  
223  
224  
225  
226  
227  
228  
229  
230  
231  
232  
233  
234  
235  
236  
237  
238  
239  
240  
241  
242  
243  
244  
245  
246  
247  
248  
249  
250  
251  
252  
253  
254  
255  
256  
257  
258  
259  
260  
261  
262  
263  
264  
265  
266  
267  
268  
269  
270  
271  
272  
273  
274  
275  
276  
277  
278  
279  
280  
281  
282  
283  
284  
285  
286  
287  
288  
289  
290  
291  
292  
293  
294  
295  
296  
297  
298  
299  
300  
301  
302  
303  
304  
305  
306  
307  
308  
309  
310  
311  
312  
313  
314  
315  
316  
317  
318  
319  
320  
321  
322  
323  
324  
325  
326  
327  
328  
329  
330  
331  
332  
333  
334  
335  
336  
337  
338  
339  
340  
341  
342  
343  
344  
345  
346  
347  
348  
349  
350  
351  
352  
353  
354  
355  
356  
357  
358  
359  
360  
361  
362  
363  
364  
365  
366  
367  
368  
369  
370  
371  
372  
373  
374  
375  
376  
377  
378  
379  
380  
381  
382  
383  
384  
385  
386  
387  
388  
389  
390  
391  
392  
393  
394  
395  
396  
397  
398  
399  
400  
401  
402  
403  
404  
405  
406  
407  
408  
409  
410  
411  
412  
413  
414  
415  
416  
417  
418  
419  
420  
421  
422  
423  
424  
425  
426  
427  
428  
429  
430  
431  
432  
433  
434  
435  
436  
437  
438  
439  
440  
441  
442  
443  
444  
445  
446  
447  
448  
449  
450  
451  
452  
453  
454  
455  
456  
457  
458  
459  
460  
461  
462  
463  
464  
465  
466  
467  
468  
469  
470  
471  
472  
473  
474  
475  
476  
477  
478  
479  
480  
481  
482  
483  
484  
485  
486  
487  
488  
489  
490  
491  
492  
493  
494  
495  
496  
497  
498  
499  
500  
501  
502  
503  
504  
505  
506  
507  
508  
509  
510  
511  
512  
513  
514  
515  
516  
517  
518  
519  
520  
521  
522  
523  
524  
525  
526  
527  
528  
529  
530  
531  
532  
533  
534  
535  
536  
537  
538  
539  
540  
541  
542  
543  
544  
545  
546  
547  
548  
549  
550  
551  
552  
553  
554  
555  
556  
557  
558  
559  
560  
561  
562  
563  
564  
565  
566  
567  
568  
569  
570  
571  
572  
573  
574  
575  
576  
577  
578  
579  
580  
581  
582  
583  
584  
585  
586  
587  
588  
589  
590  
591  
592  
593  
594  
595  
596  
597  
598  
599  
600  
601  
602  
603  
604  
605  
606  
607  
608  
609  
610  
611  
612  
613  
614  
615  
616  
617  
618  
619  
620  
621  
622  
623  
624  
625  
626  
627  
628  
629  
630  
631  
632  
633  
634  
635  
636  
637  
638  
639  
640  
641  
642  
643  
644  
645  
646  
647  
648  
649  
650  
651  
652  
653  
654  
655  
656  
657  
658  
659  
660  
661  
662  
663  
664  
665  
666  
667  
668  
669  
670  
671  
672  
673  
674  
675  
676  
677  
678  
679  
680  
681  
682  
683  
684  
685  
686  
687  
688  
689  
690  
691  
692  
693  
694  
695  
696  
697  
698  
699  
700  
701  
702  
703  
704  
705  
706  
707  
708  
709  
710  
711  
712  
713  
714  
715  
716  
717  
718  
719  
720  
721  
722  
723  
724  
725  
726  
727  
728  
729  
730  
731  
732  
733  
734  
735  
736  
737  
738  
739  
740  
741  
742  
743  
744  
745  
746  
747  
748  
749  
750  
751  
752  
753  
754  
755  
756  
757  
758  
759  
760  
761  
762  
763  
764  
765  
766  
767  
768  
769  
770  
771  
772  
773  
774  
775  
776  
777  
778  
779  
780  
781  
782  
783  
784  
785  
786  
787  
788  
789  
790  
791  
792  
793  
794  
795  
796  
797  
798  
799  
800  
801  
802  
803  
804  
805  
806  
807  
808  
809  
810  
811  
812  
813  
814  
815  
816  
817  
818  
819  
820  
821  
822  
823  
824  
825  
826  
827  
828  
829  
830  
831  
832  
833  
834  
835  
836  
837  
838  
839  
840  
841  
842  
843  
844  
845  
846  
847  
848  
849  
850  
851  
852  
853  
854  
855  
856  
857  
858  
859  
860  
861  
862  
863  
864  
865  
866  
867  
868  
869  
870  
871  
872  
873  
874  
875  
876  
877  
878  
879  
880  
881  
882  
883  
884  
885  
886  
887  
888  
889  
890  
891  
892  
893  
894  
895  
896  
897  
898  
899  
900  
901  
902  
903  
904  
905  
906  
907  
908  
909  
910  
911  
912  
913  
914  
915  
916  
917  
918  
919  
920  
921  
922  
923  
924  
925  
926  
927  
928  
929  
930  
931  
932  
933  
934  
935  
936  
937  
938  
939  
940  
941  
942  
943  
944  
945  
946  
947  
948  
949  
950  
951  
952  
953  
954  
955  
956  
957  
958  
959  
960  
961  
962  
963  
964  
965  
966  
967  
968  
969  
970  
971  
972  
973  
974  
975  
976  
977  
978  
979  
980  
981  
982  
983  
984  
985  
986  
987  
988  
989  
990  
991  
992  
993  
994  
995  
996  
997  
998  
999  
1000

- 1 Suter, J.R., and Berryhill Jr, H.L., 1985, Late Quaternary shelf-margin deltas, northwest Gulf of  
2 Mexico: AAPG Bulletin, v. 69(1), p. 77-91.  
3
- 4 Sydow, J., Finneran, J., Bowman, A. P., Rosen, H., Fillon, R., and Anderson, J., 2003, Stacked  
5 shelf-edge delta reservoirs of the Columbus Basin, Trinidad, West Indies: Shelf-Margin  
6  
7 Deltas and Linked Downslope Petroleum Systems, p. 441-465.  
8  
9
- 10 Sweet, M. L., and Blum, M. D., 2016, Connections Between Fluvial To Shallow Marine  
11  
12 Environments and Submarine Canyons: Implications For Sediment Transfer To Deep Water.  
13  
14 Journal of Sedimentary Research, 86(10), 1147-1162.  
15  
16
- 17 Sweetman, A.K., S. Sommer, O. Pfannkuche, U. Witte. 2009, Retarded response by macrofauna-  
18  
19 size foraminifera to phytodetritus in a deep Norwegian fjord. Journal of Foraminiferal  
20  
21 Research, 39(1), 15–22.  
22  
23
- 24 Swenson J. B., Paola C., Pratson L., Voller V. R., Murray A. B., 2005. Fluvial and marine controls  
25  
26 on combined subaerial and subaqueous delta progradation: Morphodynamic modeling of  
27  
28 compound-clinoform development. Journal of Geophysical Research: Earth Surface, 110,  
29  
30 0148-0227.  
31  
32
- 33 Tarasov, L., and Peltier, W. R., 2004, A geophysically constrained large ensemble analysis of the  
34  
35 deglacial history of the North American ice-sheet complex. Quaternary Science Reviews,  
36  
37 23(3), 359-388.  
38  
39
- 40 Tesi, T., Asioli, A., Minisini, D., Maselli, V., Dalla Valle, G., Gamberi, F., Langone, L., Cattaneo,  
41  
42 A., Montagna, P., Trincardi, F., 2017, Large-scale response of the Eastern Mediterranean  
43  
44 thermohaline circulation to African monsoon intensification during sapropel S1 formation.  
45  
46 Quaternary Science Reviews, 159, 139-154.  
47  
48
- 49 Trincardi, F., and Field, M. E., 1991, Geometry, lateral variation, and preservation of downlapping  
50  
51 regressive shelf deposits: eastern Tyrrhenian Sea margin, Italy: Journal of Sedimentary  
52  
53 Research, 61(5).  
54  
55  
56  
57  
58  
59  
60  
61  
62  
63  
64  
65

- 1  
2  
3  
4  
5  
6  
7  
8  
9  
10  
11  
12  
13  
14  
15  
16  
17  
18  
19  
20  
21  
22  
23  
24  
25  
26  
27  
28  
29  
30  
31  
32  
33  
34  
35  
36  
37  
38  
39  
40  
41  
42  
43  
44  
45  
46  
47  
48  
49  
50  
51  
52  
53  
54  
55  
56  
57  
58  
59  
60  
61  
62  
63  
64  
65
- Trincardi, F., Correggiari, A., and Roveri, M., 1994, Late Quaternary transgressive erosion and deposition in a modern epicontinental shelf: the Adriatic semienclosed basin. *Geo-Marine Letters*, 14(1), 41-51.
- Trincardi F., Cattaneo, A., Asioli, A., Correggiari, A., and Langone L., 1996, Stratigraphy of the late-Quaternary deposits in the central Adriatic basin and the record of short-term climatic events. In: F. Oldfield and P. Guilizzoni (Editors), *Palaeoenvironmental Analysis of Italian Crater Lake and Adriatic Sediments*, *Memorie dell'Istituto Italiano di Idrobiologia*, v. 55, p. 39-70.
- Trincardi, F., and Correggiari, A., 2000, Quaternary forced regression deposits in the Adriatic basin and the record of composite sea-level cycles. *Geological Society, London, Special Publications*, 172(1), 245-269.
- Trincardi, F., Cattaneo, A., Correggiari, A., and Ridente, D., 2004, Evidence of soft sediment deformation, fluid escape, sediment failure and regional weak layers within the late Quaternary mud deposits of the Adriatic Sea. *Marine Geology*, 213(1), 91-119.
- Urgeles, R., Cattaneo, A., Puig, P., Liqueste, C., De Mol, B., Amblàs, D., and Trincardi, F., 2011, A review of undulated sediment features on Mediterranean prodeltas: distinguishing sediment transport structures from sediment deformation: *Marine Geophysical Research*, v. 32(1-2), p. 49-69.
- Vail, P. R., Mitchum Jr, R. M., Thompson III, S., 1977. *Seismic Stratigraphy and Global Changes of Sea Level: Part 4. Global Cycles of Relative Changes of Sea Level.: Section 2. Application of Seismic Reflection Configuration to Stratigraphic Interpretation.*
- Vail, P.R., Audemard, F., Bowman, S.A., Eisner, P.N. and Perez-Cruz, G., 1991, The stratigraphic signatures of tectonics, eustasy and sedimentation: an overview: A. Seilacher and G. Eisner (Editors), *Cycles and Events in Stratigraphy*, Springer-Verlag, Tiibingen, p. 617-659.

- 1  
2  
3  
4  
5  
6  
7  
8  
9  
10  
11  
12  
13  
14  
15  
16  
17  
18  
19  
20  
21  
22  
23  
24  
25  
26  
27  
28  
29  
30  
31  
32  
33  
34  
35  
36  
37  
38  
39  
40  
41  
42  
43  
44  
45  
46  
47  
48  
49  
50  
51  
52  
53  
54  
55  
56  
57  
58  
59  
60  
61  
62  
63  
64  
65
- Van der Zwaan, G. J., F. J. Jorissen. 1991. Biofacial patterns in river –induced anoxia. In: R. Tyson and Th. Pearson Eds.), Modern and ancient continental shelf anoxia. Geological Society of London Special Publication, 58, 65-82.
- Van Wagoner, J. C., Mitchum, R. M., Campion, K. M., and Rahmanian, V. D., 1990, Siliciclastic sequence stratigraphy in well logs, cores, and outcrops: concepts for high-resolution correlation of time and facies.
- Van Wagoner, J. C., 1995, Sequence stratigraphy and marine to nonmarine facies architecture of foreland basin strata, Book Cliffs, Utah, USA.
- Voelker, A.H.L. and workshop participants, 2002, Global distribution of centennial-scale records for Marine Isotope Stage (MIS) 3: a database. Quaternary Science Reviews 21, 1185–1212.
- Walker, M. J. C., M. Berkelhammer, S. Björck, L. C. Cwynar, D. A. Fisher, A. J. Long, J. J. Lowe, R. M. Newnham, S. O. Rasmussen and H. Weiss, 2009, Formal subdivision of the Holocene Series/Epoch: a Discussion Paper by a Working Group of INTIMATE (Integration of ice-core, marine and terrestrial records) and the Subcommittee on Quaternary Stratigraphy (International Commission on Stratigraphy). Journal of Quaternary Science, 27, 7: 649–659.
- Walsh, J.J., 1991, Importance of continental margins in the marine biogeochemical cycling of carbon and nitrogen, Nature v. 350, p. 53-55 (doi:10.1038/350053a0).
- Yokoyama, Y., Lambeck, K., De Deckker, P., Johnston, P., and Fifield, L. K., 2000, Timing of the Last Glacial Maximum from observed sea-level minima. Nature, 406(6797), 713-716.
- Zecchin, M., Baradello, L., Brancolini, G., Donda, F., Rizzetto, F., and Tosi, L., 2008, Sequence stratigraphy based on high-resolution seismic profiles in the late Pleistocene and Holocene deposits of the Venice area: Marine Geology, v. 253(3), p. 185-198.

# FIGURE CAPTIONS

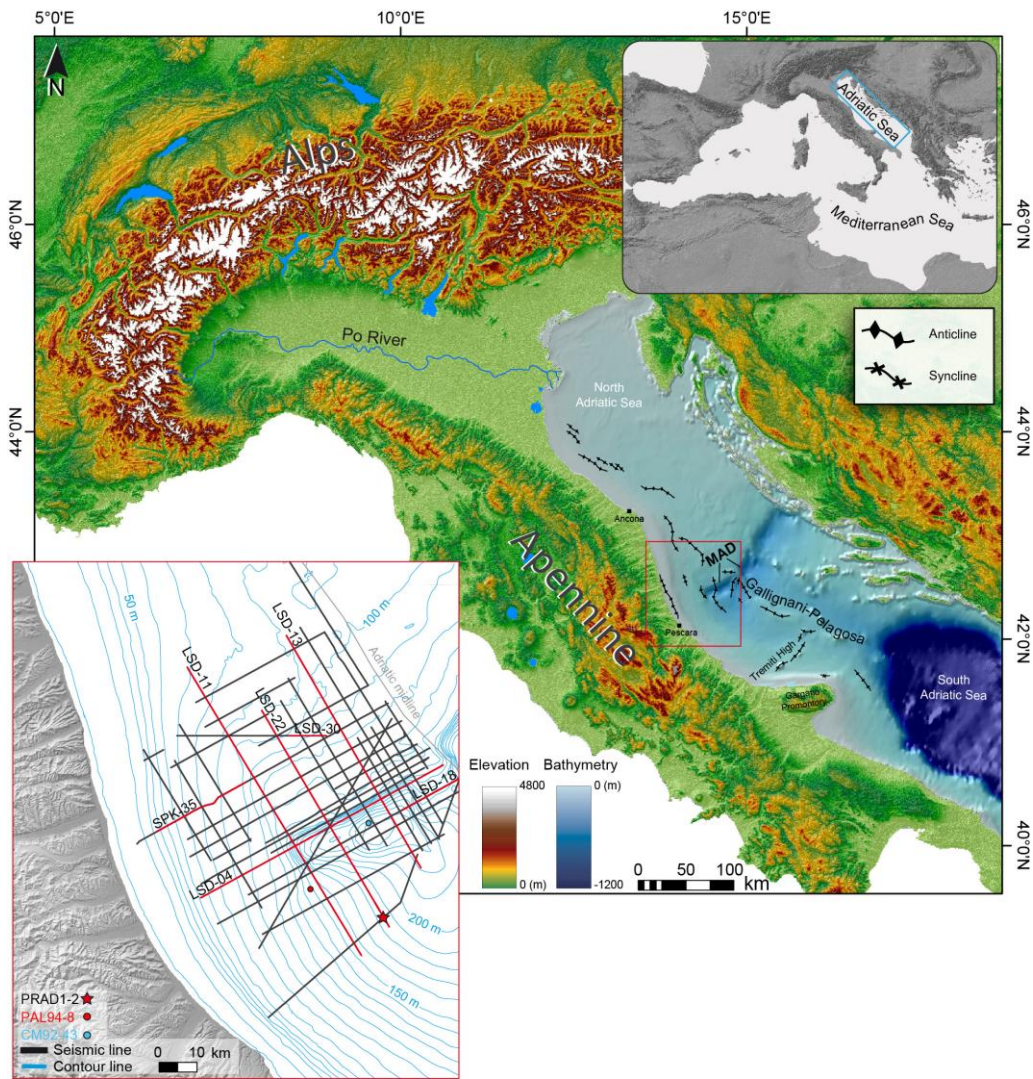


Fig. 1. Digital elevation model for the Adriatic Sea and surrounded area with structural elements. MAD: Mid Adriatic Depression. Top right: Adriatic Sea location in the Mediterranean Sea. Bottom left: detail of the MAD with the orientation of seismic grid, and position of sediment cores and borehole. Seismic profiles showed in this work are highlighted in red.

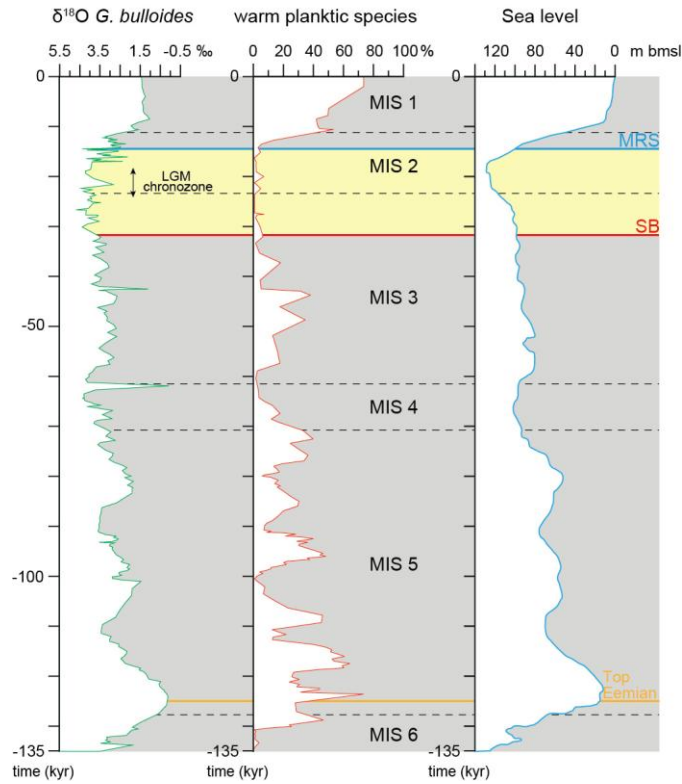


Fig. 2.  $\delta^{18}\text{O}$  (*G. bulloides*), warm planktic species (see Data, Material and Strategy for the species included), and eustatic curves. Vertical scale is in time (ky BP). Horizontal dashed lines mark the boundaries of Marine Isotopic Stages. The PRLW forms between SB and MRS surfaces (yellow interval), during an overall cold climatic interval and encompasses the late phase of sea level fall, the lowstand, and the early phase of sea level rise.

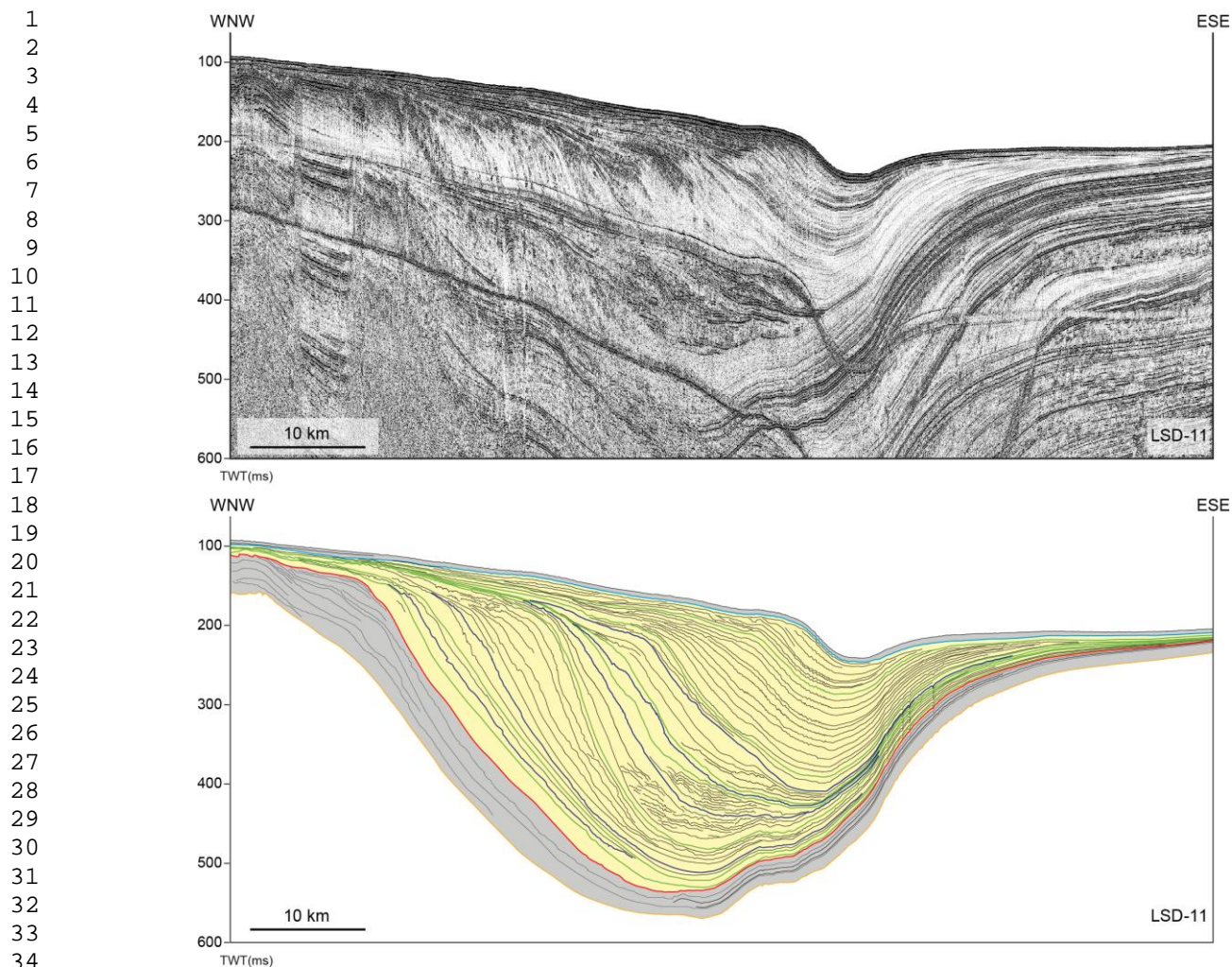


Fig. 3. Line drawing of LSD-11 multichannel profile shows the late Pleistocene Po River lowstand Wedge (PRLW) in yellow. Note that the PRLW is constituted by clinothem with constant bottomset aggradation.

1  
2  
3  
4  
5  
6  
7  
8  
9  
10  
11  
12  
13  
14  
15  
16  
17  
18  
19  
20  
21  
22  
23  
24  
25  
26  
27  
28  
29  
30  
31  
32  
33  
34  
35  
36  
37  
38  
39  
40  
41  
42  
43  
44  
45  
46  
47  
48  
49  
50  
51  
52  
53  
54  
55  
56  
57  
58  
59  
60  
61  
62  
63  
64  
65

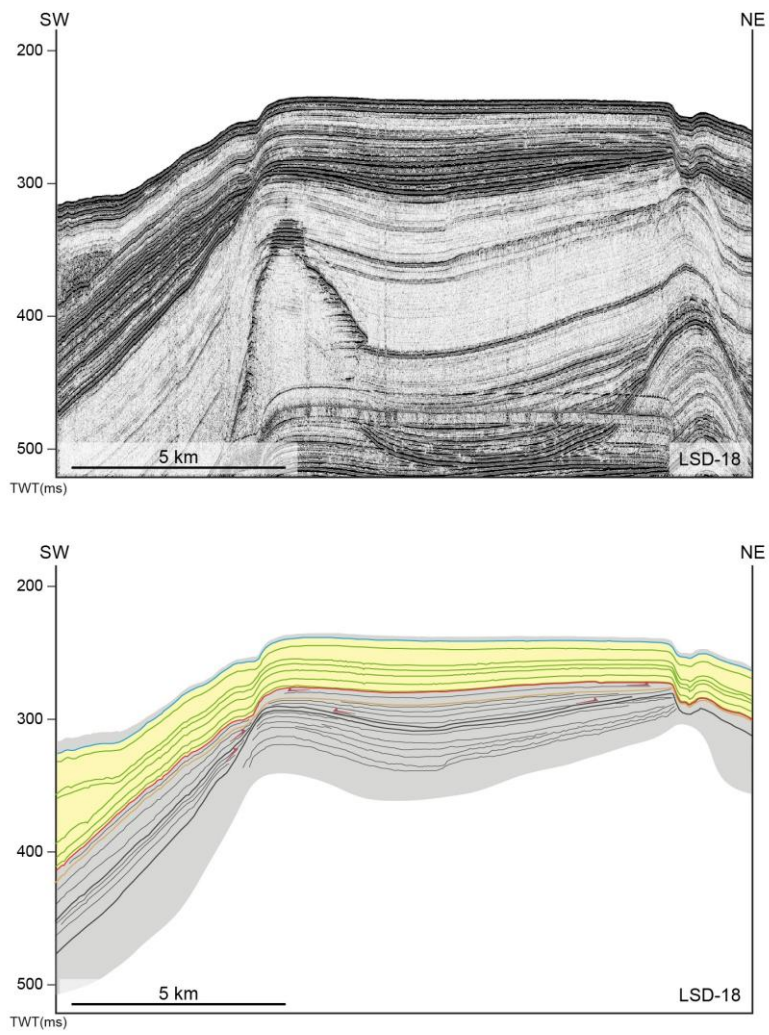


Fig. 4. Multichannel LSD-18 line drawing shows strata terminations suggesting that the tectonic activity is quiescent during the PRLW progradation (yellow interval).

1  
2  
3  
4  
5  
6  
7  
8  
9  
10  
11  
12  
13  
14  
15  
16  
17  
18  
19  
20  
21  
22  
23  
24  
25  
26  
27  
28  
29  
30  
31  
32  
33  
34  
35  
36  
37  
38  
39  
40  
41  
42  
43  
44  
45  
46  
47  
48  
49  
50  
51  
52  
53  
54  
55  
56  
57  
58  
59  
60  
61  
62  
63  
64  
65

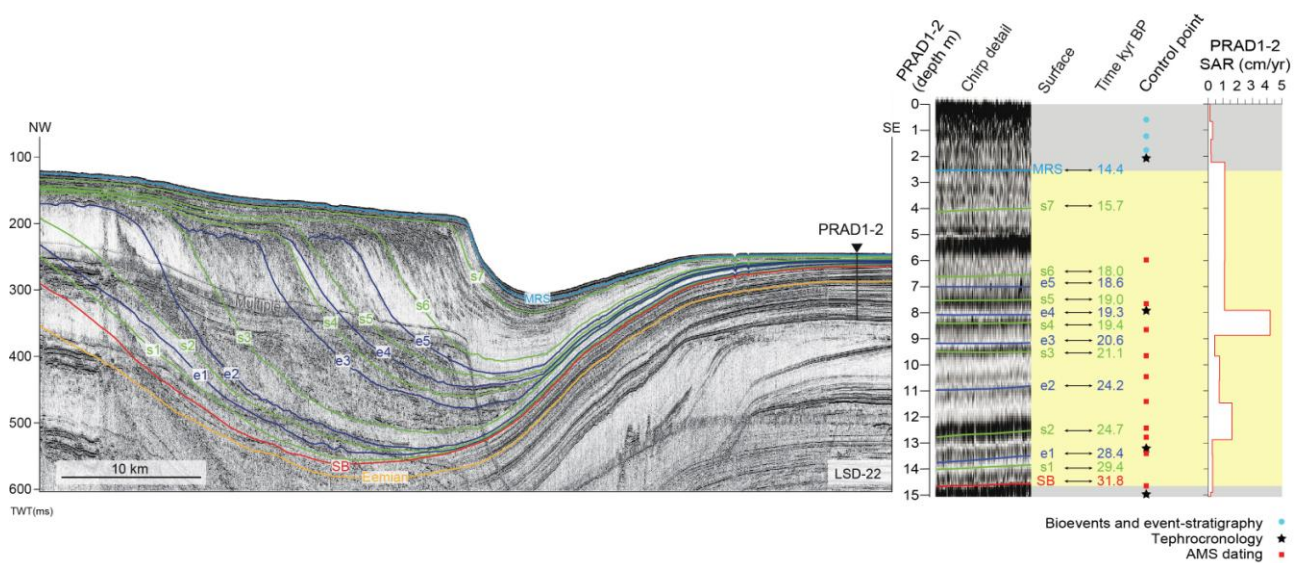


Fig. 5. Downdip multichannel seismic profile LSD-22 illustrates clinothem geometry along the main direction of progradation. The 16 control points and the name and age of seismic horizons are reported along the 15 m succession. SAR (sediment accumulation rate) is given in cm/yr.

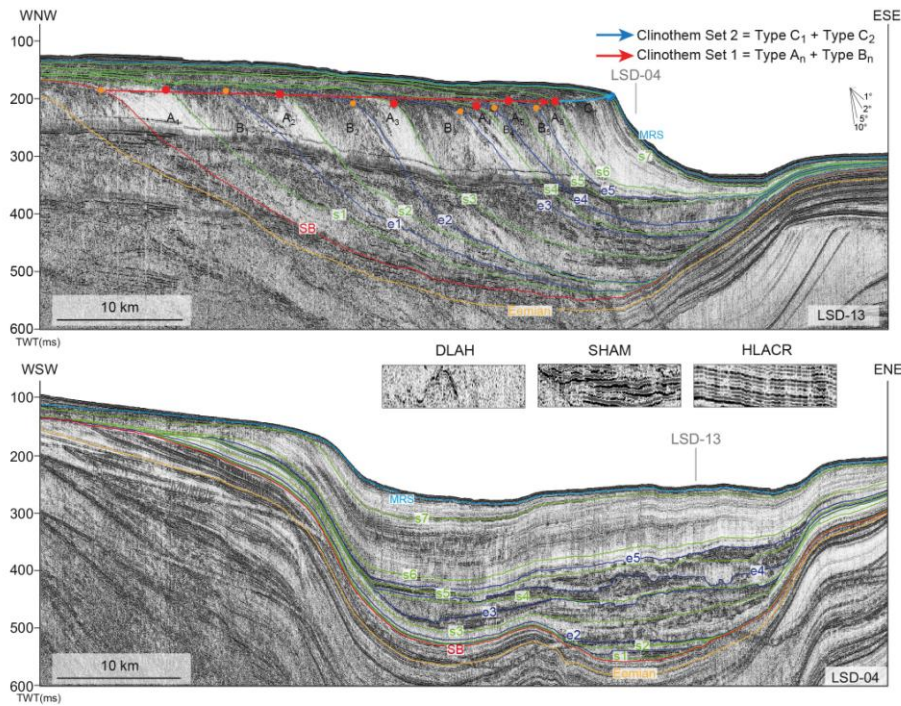


Fig. 6. Top: Down-dip multichannel seismic profile LSD-13 illustrating clinothem geometries along the main direction of progradation. Bottom: Along-strike profile LSD-04 highlighting the seismic facies of basinal deposits (see figure 1 for seismic lines location). Orange horizon marks top of Eemian (ca. 125 ky BP); red horizon is sequence boundary (SB) at base of Po River Lowstand Wedge (PRLW); green horizons (*s*) mark surfaces on top of Type A and Type C clinothems whereas blue horizons (*e*) are on top of Type B clinothems; light blue horizon is the maximum regression surface (MRS) on top of youngest Type C<sub>2</sub> clinothem (clinothems are numbered from older to younger). Red, orange, and blue dots mark shelf-edge of Type A, B, and C clinothems, respectively. Surface *s*<sub>6</sub> marks transition from progradational clinothem Set 1 (comprising stacked Type A and B clinothems) to aggradational clinothem Set 2 (constituted by stacked Type C clinothems). Insets illustrate distal basin seismic facies associated with Type A (Discontinuous and Low-Amplitude reflections with internal Hyperbolic diffractions, DLAH), Type B (Semi-continuous, High-Amplitude and Mounded reflections, SHAM) and Type C clinothems (High- and Low-Amplitude Continuous reflections, HLAC) in basin.

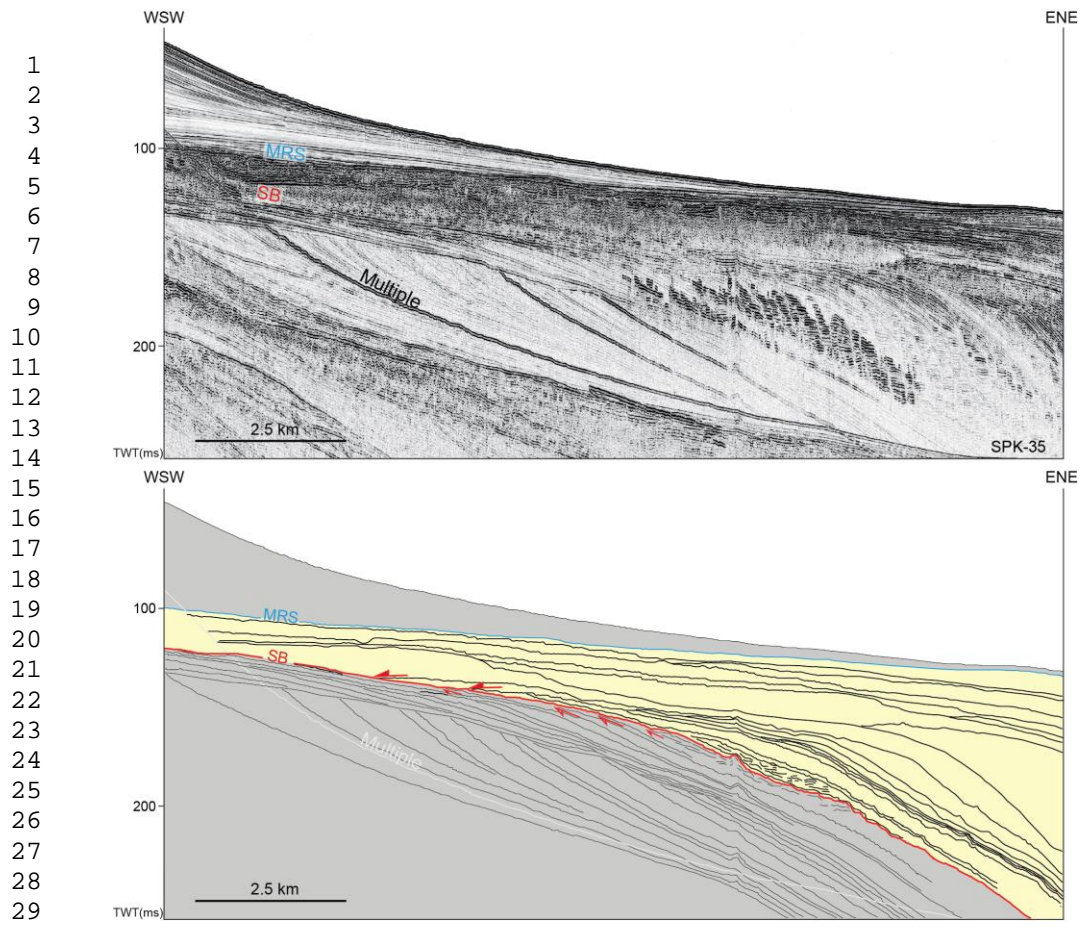


Fig. 7. Detail of the line drawing of SPK-35 sparker profile (along-strike orientation). Seismic terminations highlight the SB at base of the PRLW (yellow interval) with coastal onlap docked close to the shelf-edge.

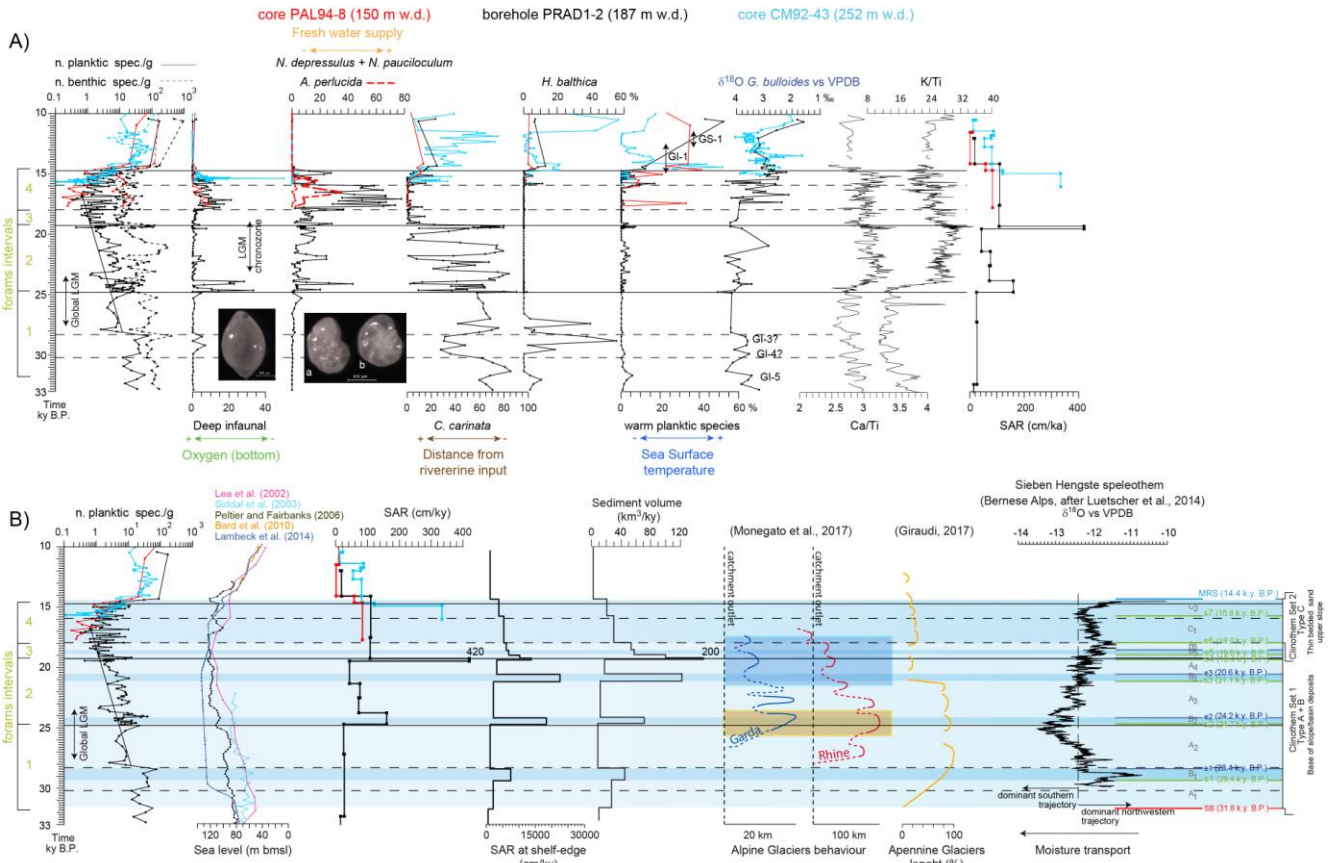


Fig. 8. A) Planktic and benthic foraminifera records of the cores CM92-43 (blue curves) and Pal94-8 (red curves) and of the borehole PRAD1-2 (black curves) plotted vs age. Note that the foraminifera concentration is plotted in logarithmic scale. The intervals corresponding to the Global LGM and to the LGM Chronozone are also reported. GI-1= Greenland Interstadial 1 (Bolling/Allerod), GS-1= Greenland Stadial 1 (Younger Dryas); B) Planktic and benthic foraminifera records along with eustatic curves, Sediment Accumulation Rate (SAR) from PRAD1-2 borehole and measured at the shelf-edge, clinothem volumes, curves of advance/retreat (yellow banner represents major culminations and pale-blue banner ice decay) of the Garda and Rhine glaciers relative to the catchment outlet (dashed line; from Monegato et al., 2017), and of the Apennine glaciers (from Giraudi, 2017), and Bernese Alps speleothem record. Time span by foraminifera intervals and type of clinothems are outlined for comparison.

1  
2  
3  
4  
5  
6  
7  
8  
9  
10  
11  
12  
13  
14  
15  
16  
17  
18  
19  
20  
21  
22  
23  
24  
25  
26  
27  
28  
29  
30  
31  
32  
33  
34  
35  
36  
37  
38  
39  
40  
41  
42  
43  
44  
45  
46  
47  
48  
49  
50  
51  
52  
53  
54  
55  
56  
57  
58  
59  
60  
61  
62  
63  
64  
65

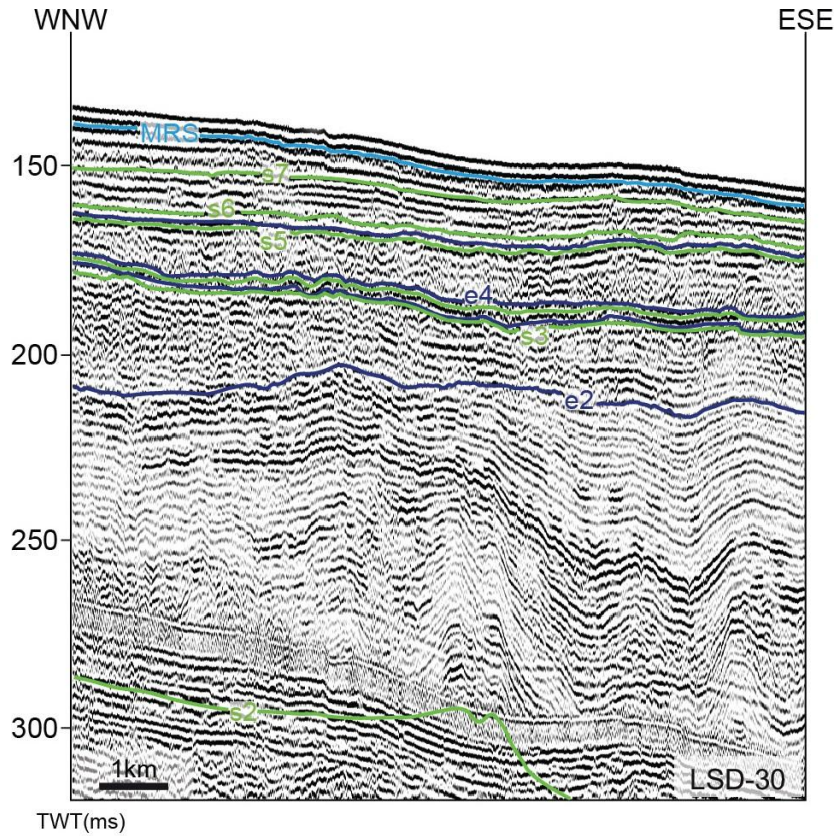


Fig. 9. Detail of LSD-30 multichannel profile with along strike orientation. Note the decreasing in dimensions of feeder systems and valley-related features and seismic unit thickness from the bottom to the top of the succession. Between s2 and e2 surfaces sediment strata up to several ten of meters thick show parallel to wedge-shaped high-amplitude reflection packages that pass laterally to low-amplitude reflections reminiscent of turbidite channel-levee complexes in the foreset.

1  
2  
3  
4  
5  
6  
7  
8  
9  
10  
11  
12  
13  
14  
15  
16  
17  
18  
19  
20  
21  
22  
23  
24  
25  
26  
27  
28  
29  
30  
31  
32  
33  
34  
35  
36  
37  
38  
39  
40  
41  
42  
43  
44  
45  
46  
47  
48  
49  
50  
51  
52  
53  
54  
55  
56  
57  
58  
59  
60  
61  
62  
63  
64  
65

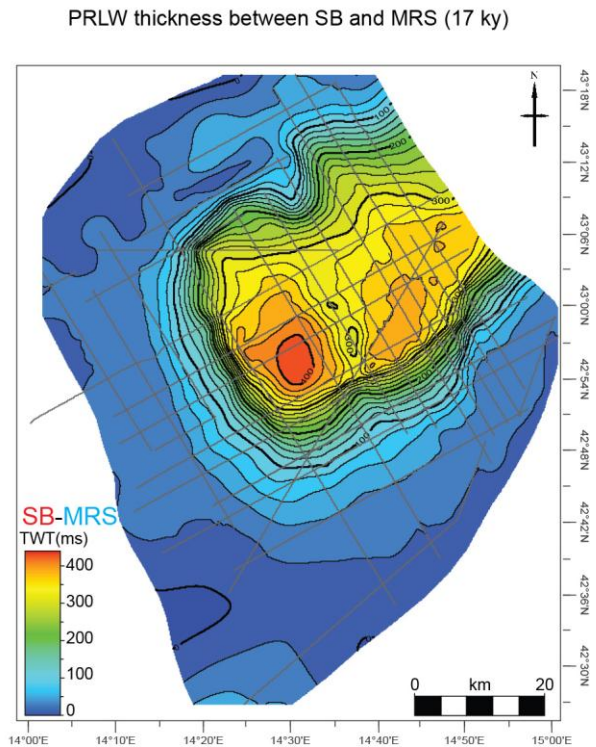
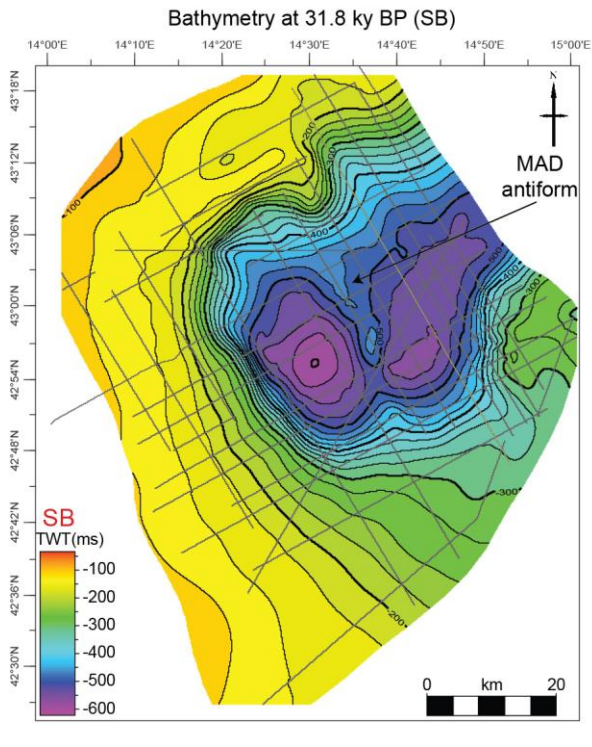


Fig. 10. Structural map of SB surface at 31.8 ky BP and the thickness map of the PRLW. Darkest color represents the deepest and thinner sector.

1  
2  
3  
4  
5  
6  
7  
8  
9  
10  
11  
12  
13  
14  
15  
16  
17  
18  
19  
20  
21  
22  
23  
24  
25  
26  
27  
28  
29  
30  
31  
32  
33  
34  
35  
36  
37  
38  
39  
40  
41  
42  
43  
44  
45  
46  
47  
48  
49  
50  
51  
52  
53  
54  
55  
56  
57  
58  
59  
60  
61  
62  
63  
64  
65

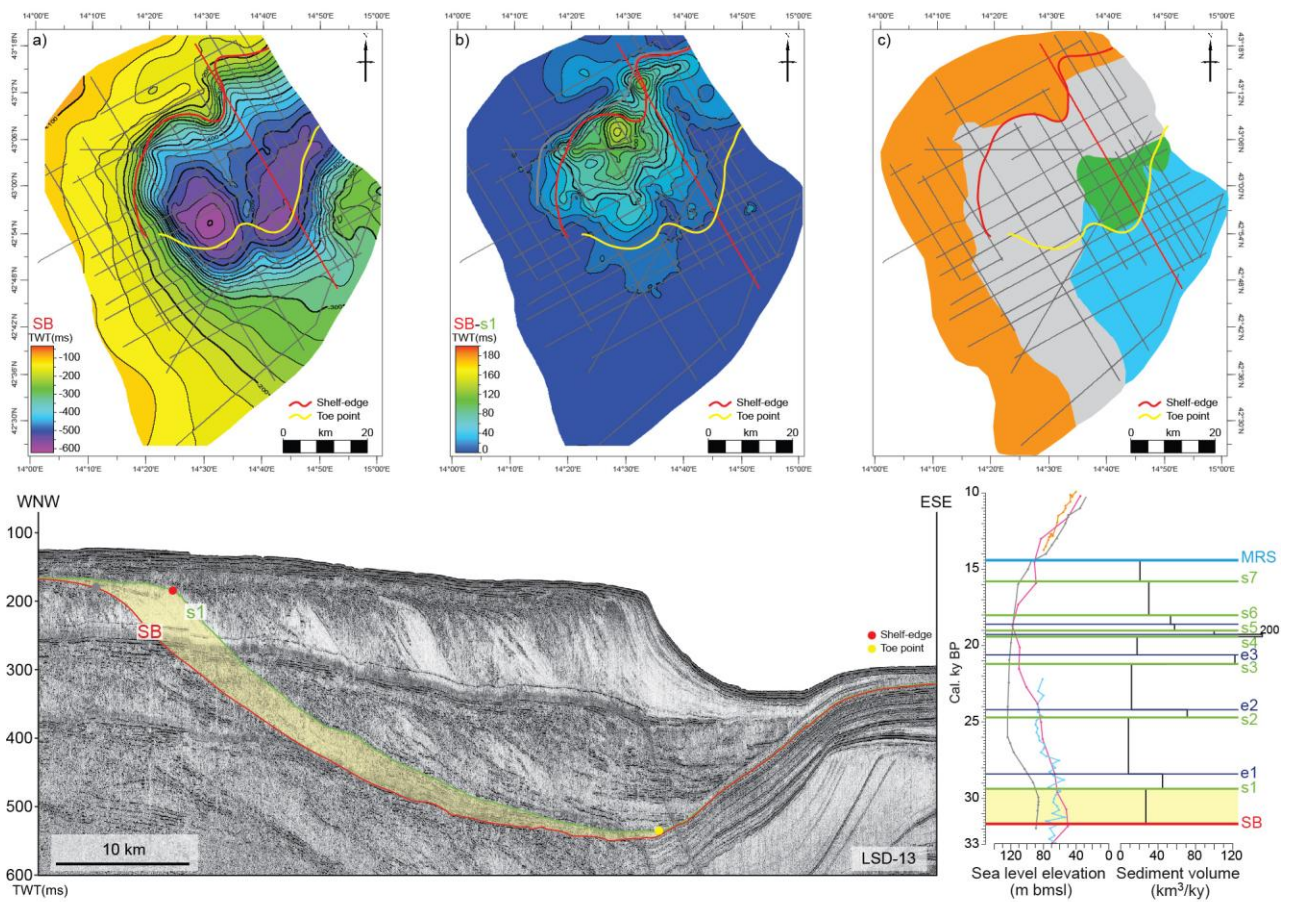


Fig. 11. Clinotherm A<sub>1</sub>. Top: a) structural map; b) thickness map; c) seismic facies map (see table 2 for the legend). Bottom: LSD-13 multichannel profile, eustatic curves (purple curve: Lea et al., 2002; light blue: Siddal et al., 2003; black curve: Peltier and Fairbanks, 2006; yellow curve: Bard et al., 2010; blue curve: Lambeck et al., 2014) and sediment volume (km<sup>3</sup>/ky) are given for each clinotherm that constitute the PRLW.

1  
2  
3  
4  
5  
6  
7  
8  
9  
10  
11  
12  
13  
14  
15  
16  
17  
18  
19  
20  
21  
22  
23  
24  
25  
26  
27  
28  
29  
30  
31  
32  
33  
34  
35  
36  
37  
38  
39  
40  
41  
42  
43  
44  
45  
46  
47  
48  
49  
50  
51  
52  
53  
54  
55  
56  
57  
58  
59  
60  
61  
62  
63  
64  
65

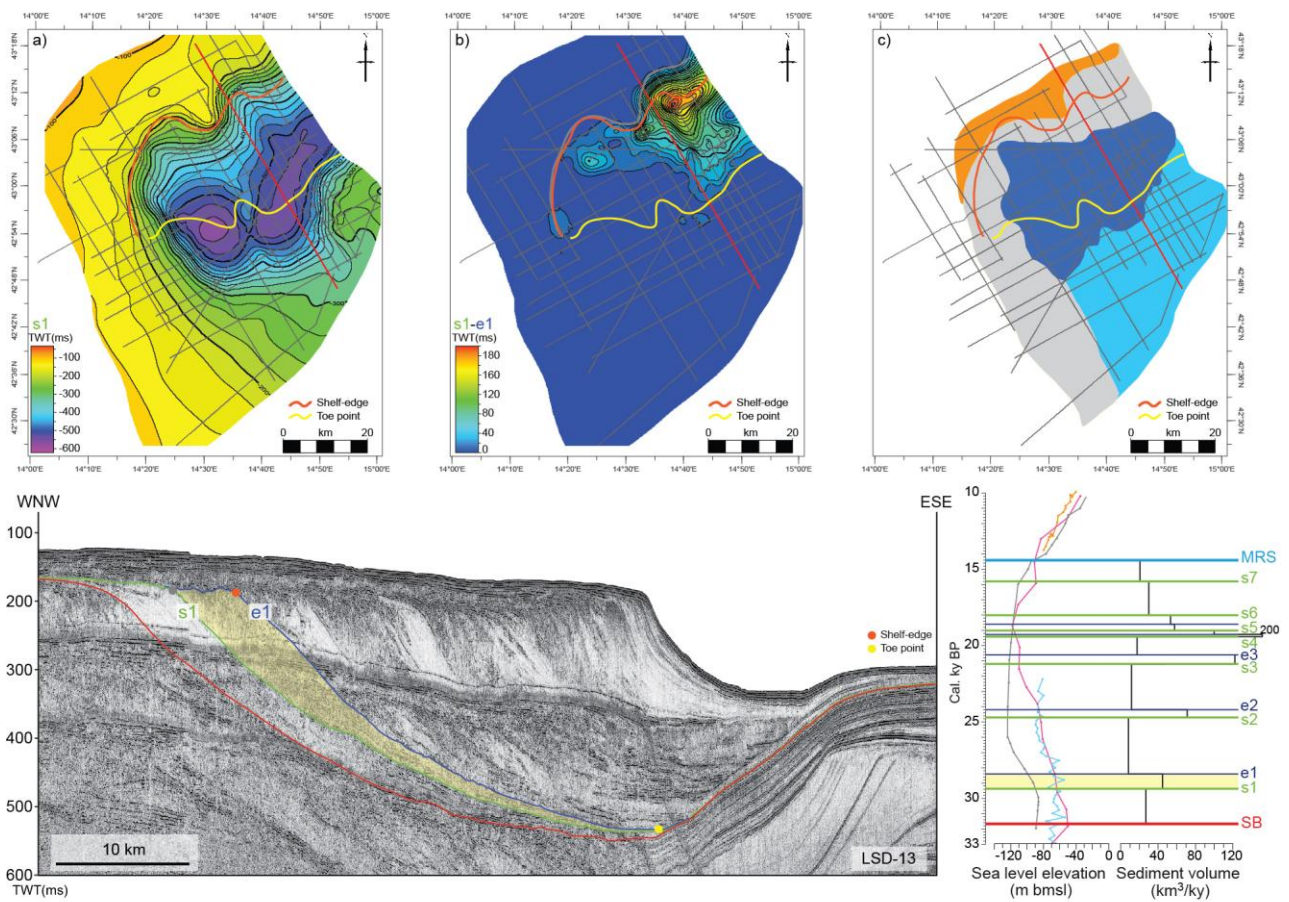


Fig. 12. Clinothem B<sub>1</sub>. Top: a) structural map; b) thickness map; c) seismic facies map (see table 2 for the legend). Bottom: LSD-13 multichannel profile, eustatic curves (purple curve: Lea et al., 2002; light blue: Siddal et al., 2003; black curve: Peltier and Fairbanks, 2006; yellow curve: Bard et al., 2010; blue curve: Lambeck et al., 2014) and sediment volume (km<sup>3</sup>/ky) are given for each clinothem that constitute the PRLW.

1  
2  
3  
4  
5  
6  
7  
8  
9  
10  
11  
12  
13  
14  
15  
16  
17  
18  
19  
20  
21  
22  
23  
24  
25  
26  
27  
28  
29  
30  
31  
32  
33  
34  
35  
36  
37  
38  
39  
40  
41  
42  
43  
44  
45  
46  
47  
48  
49  
50  
51  
52  
53  
54  
55  
56  
57  
58  
59  
60  
61  
62  
63  
64  
65

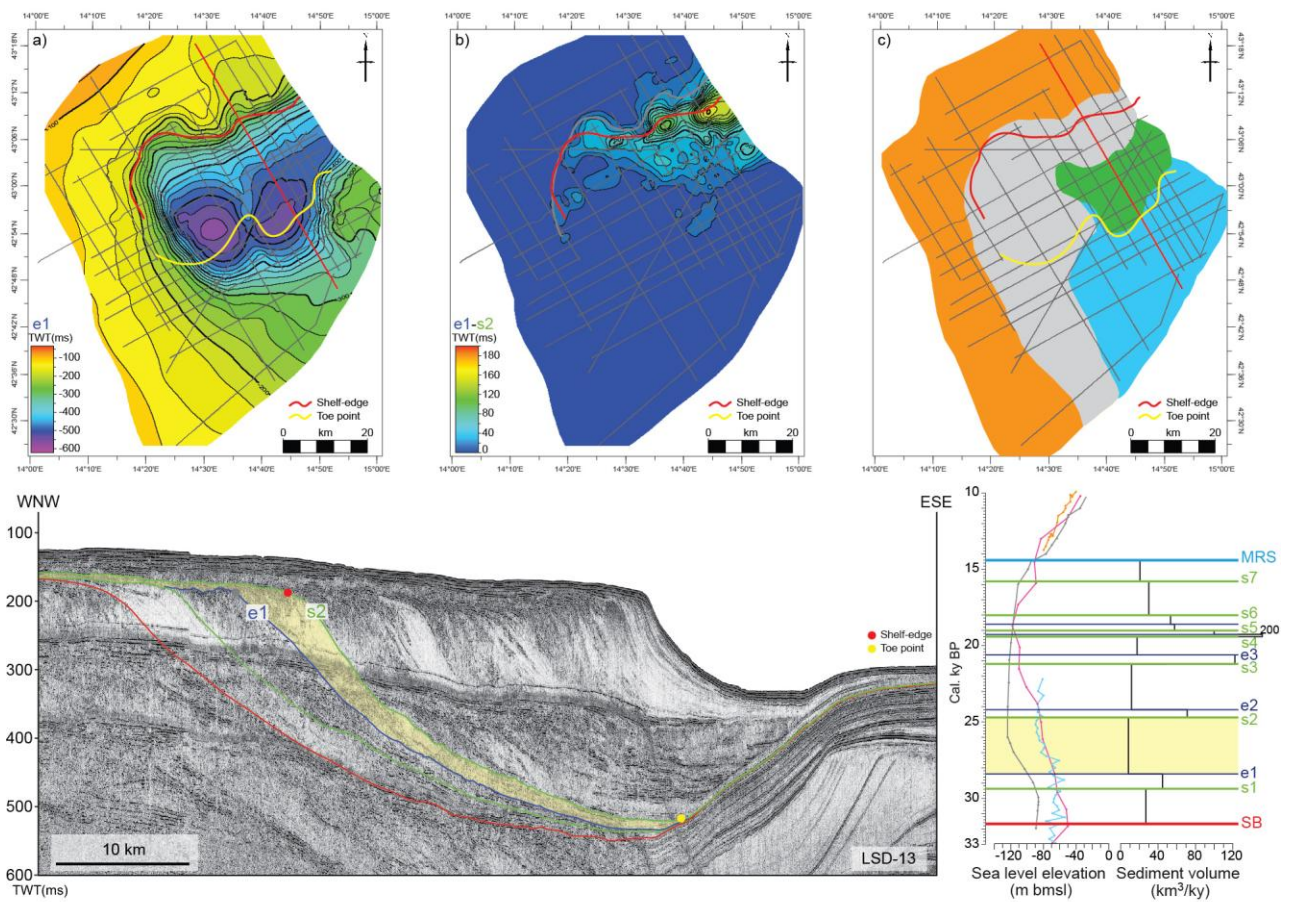


Fig. 13. Clinothem A<sub>2</sub>. Top: a) structural map; b) thickness map; c) seismic facies map (see table 2 for the legend). Bottom: LSD-13 multichannel profile, eustatic curves (purple curve: Lea et al., 2002; light blue: Siddal et al., 2003; black curve: Peltier and Fairbanks, 2006; yellow curve: Bard et al., 2010; blue curve: Lambeck et al., 2014) and sediment volume (km<sup>3</sup>/ky) are given for each clinothem that constitute the PRLW.

1  
2  
3  
4  
5  
6  
7  
8  
9  
10  
11  
12  
13  
14  
15  
16  
17  
18  
19  
20  
21  
22  
23  
24  
25  
26  
27  
28  
29  
30  
31  
32  
33  
34  
35  
36  
37  
38  
39  
40  
41  
42  
43  
44  
45  
46  
47  
48  
49  
50  
51  
52  
53  
54  
55  
56  
57  
58  
59  
60  
61  
62  
63  
64  
65

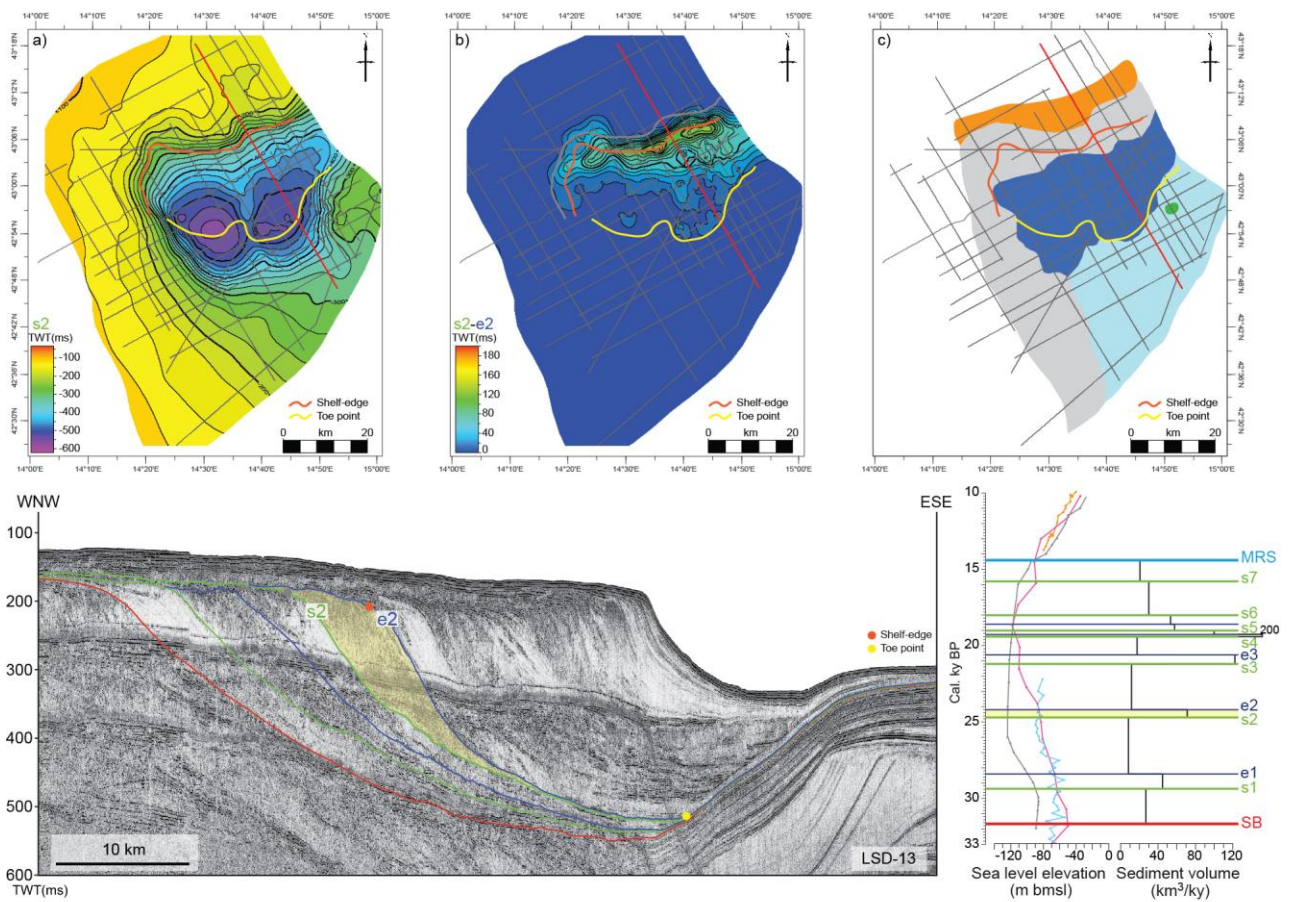


Fig. 14. Clinotherm B<sub>2</sub>. Top: a) structural map; b) thickness map; c) seismic facies map (see table 2 for the legend). Bottom: LSD-13 multichannel profile, eustatic curves (purple curve: Lea et al., 2002; light blue: Siddal et al., 2003; black curve: Peltier and Fairbanks, 2006; yellow curve: Bard et al., 2010; blue curve: Lambeck et al., 2014) and sediment volume (km<sup>3</sup>/ky) are given for each clinotherm that constitute the PRLW.

1  
2  
3  
4  
5  
6  
7  
8  
9  
10  
11  
12  
13  
14  
15  
16  
17  
18  
19  
20  
21  
22  
23  
24  
25  
26  
27  
28  
29  
30  
31  
32  
33  
34  
35  
36  
37  
38  
39  
40  
41  
42  
43  
44  
45  
46  
47  
48  
49  
50  
51  
52  
53  
54  
55  
56  
57  
58  
59  
60  
61  
62  
63  
64  
65

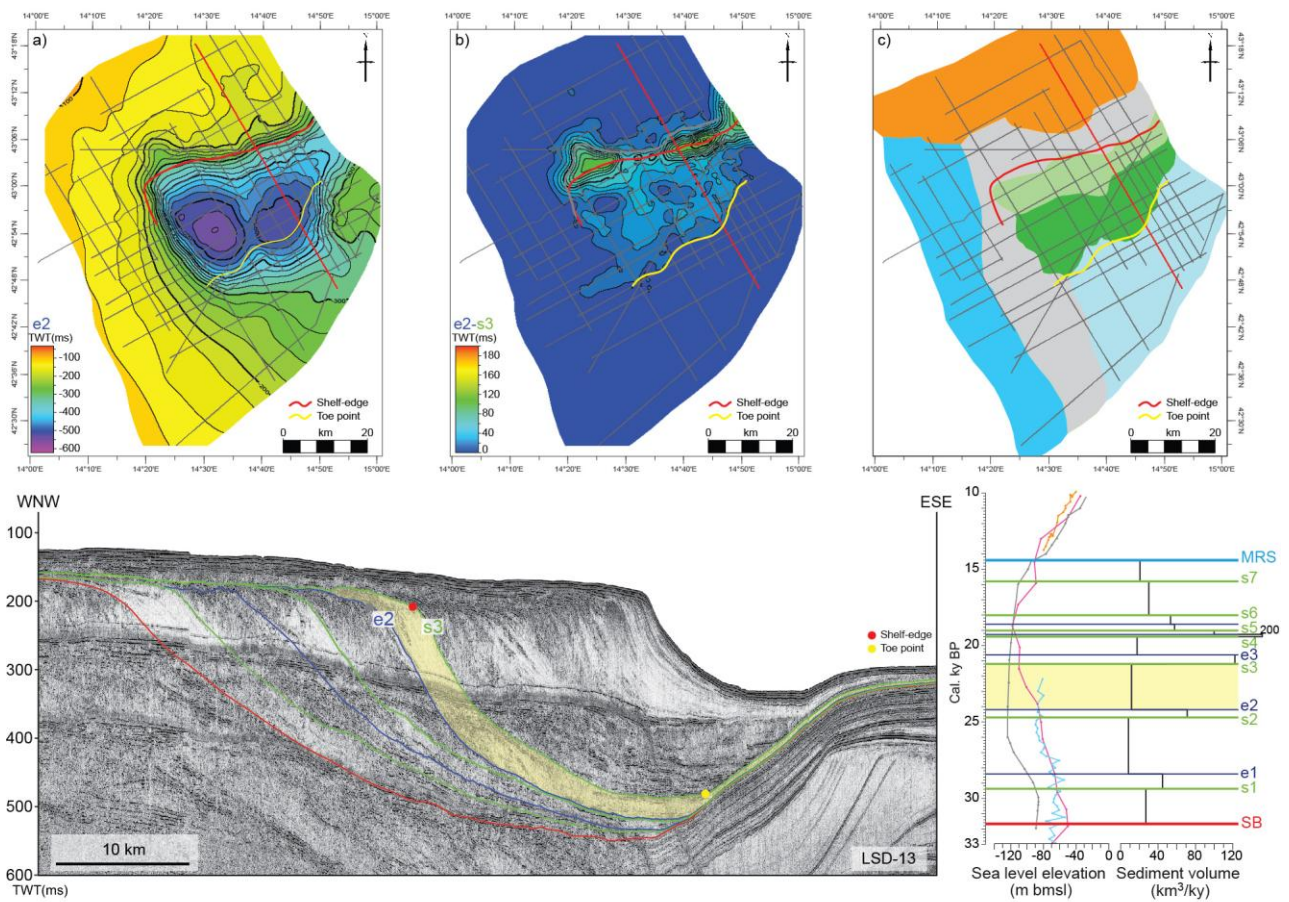


Fig. 15. Clinotherm A<sub>3</sub>. Top: a) structural map; b) thickness map; c) seismic facies map (see table 2 for the legend). Bottom: LSD-13 multichannel profile, eustatic curves (purple curve: Lea et al., 2002; light blue: Siddal et al., 2003; black curve: Peltier and Fairbanks, 2006; yellow curve: Bard et al., 2010; blue curve: Lambeck et al., 2014) and sediment volume (km<sup>3</sup>/ky) are given for each clinotherm that constitute the PRLW.

1  
2  
3  
4  
5  
6  
7  
8  
9  
10  
11  
12  
13  
14  
15  
16  
17  
18  
19  
20  
21  
22  
23  
24  
25  
26  
27  
28  
29  
30  
31  
32  
33  
34  
35  
36  
37  
38  
39  
40  
41  
42  
43  
44  
45  
46  
47  
48  
49  
50  
51  
52  
53  
54  
55  
56  
57  
58  
59  
60  
61  
62  
63  
64  
65

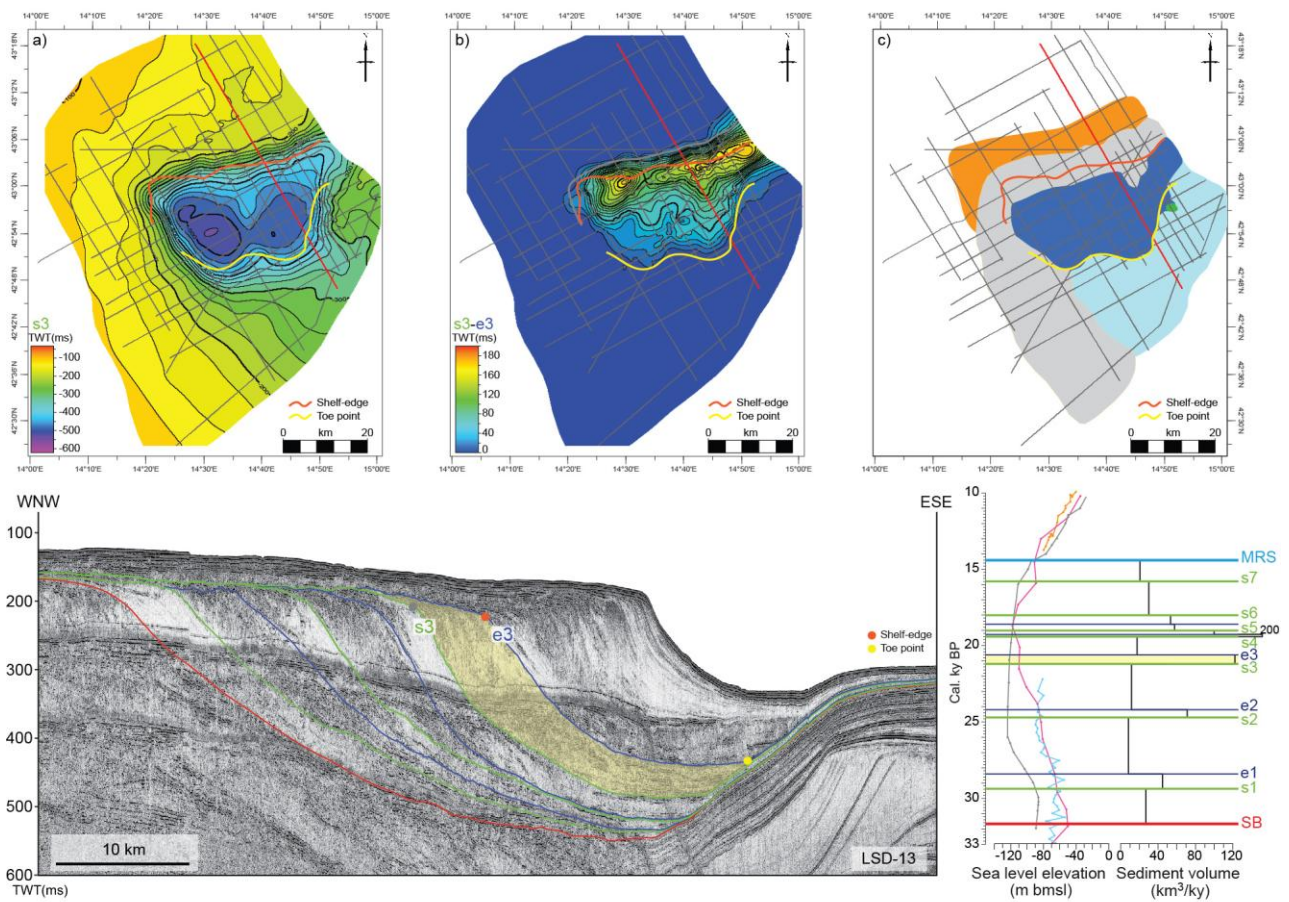


Fig. 16. Clinotherm B<sub>3</sub>. Top: a) structural map; b) thickness map; c) seismic facies map (see table 2 for the legend). Bottom: LSD-13 multichannel profile, eustatic curves (purple curve: Lea et al., 2002; light blue: Siddal et al., 2003; black curve: Peltier and Fairbanks, 2006; yellow curve: Bard et al., 2010; blue curve: Lambeck et al., 2014) and sediment volume (km<sup>3</sup>/ky) are given for each clinotherm that constitute the PRLW.

1  
2  
3  
4  
5  
6  
7  
8  
9  
10  
11  
12  
13  
14  
15  
16  
17  
18  
19  
20  
21  
22  
23  
24  
25  
26  
27  
28  
29  
30  
31  
32  
33  
34  
35  
36  
37  
38  
39  
40  
41  
42  
43  
44  
45  
46  
47  
48  
49  
50  
51  
52  
53  
54  
55  
56  
57  
58  
59  
60  
61  
62  
63  
64  
65

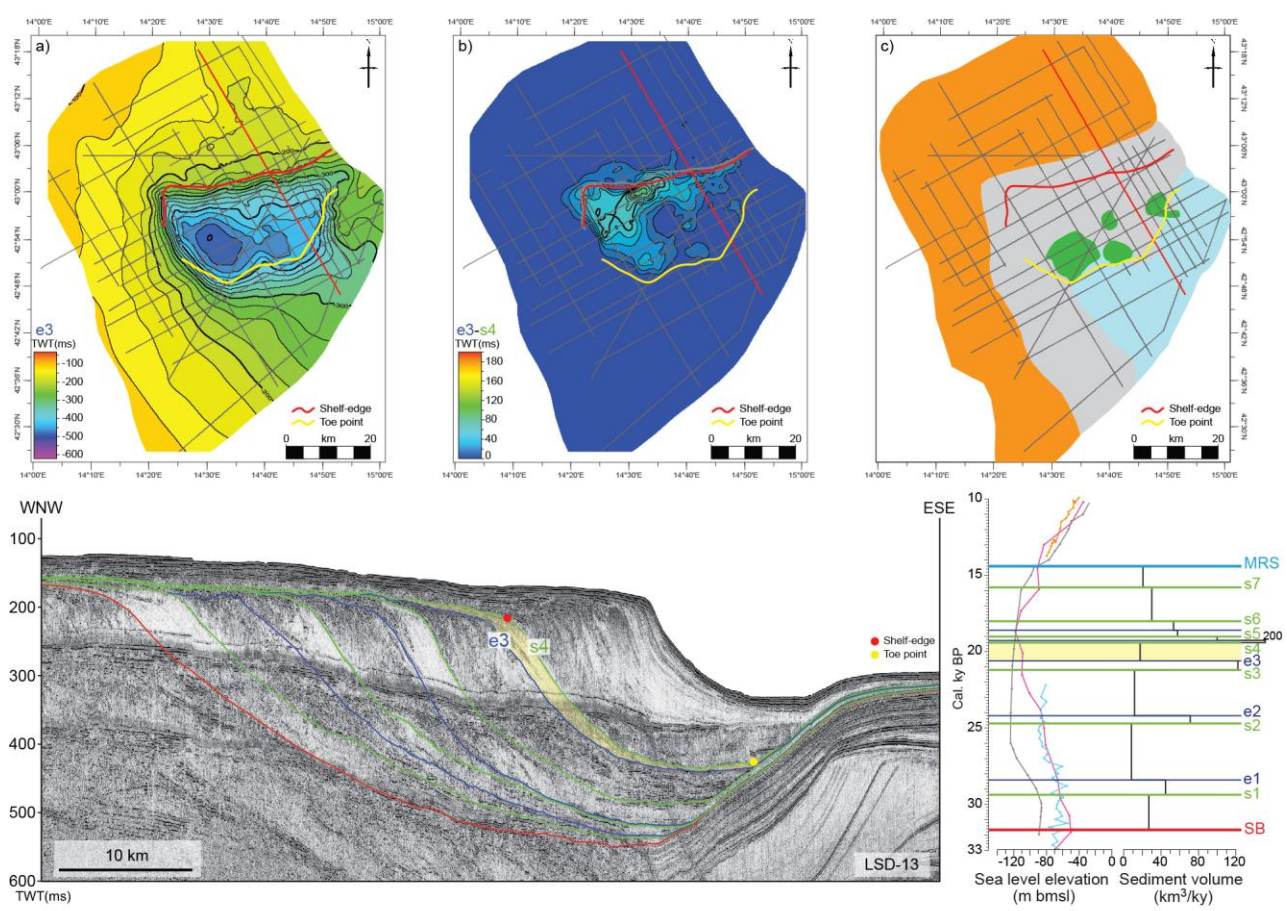


Fig. 17. Clinotherm A<sub>4</sub>. Top: a) structural map; b) thickness map; c) seismic facies map (see table 2 for the legend). Bottom: LSD-13 multichannel profile, eustatic curves (purple curve: Lea et al., 2002; light blue: Siddal et al., 2003; black curve: Peltier and Fairbanks, 2006; yellow curve: Bard et al., 2010; blue curve: Lambeck et al., 2014) and sediment volume (km<sup>3</sup>/ky) are given for each clinotherm that constitute the PRLW.

1  
2  
3  
4  
5  
6  
7  
8  
9  
10  
11  
12  
13  
14  
15  
16  
17  
18  
19  
20  
21  
22  
23  
24  
25  
26  
27  
28  
29  
30  
31  
32  
33  
34  
35  
36  
37  
38  
39  
40  
41  
42  
43  
44  
45  
46  
47  
48  
49  
50  
51  
52  
53  
54  
55  
56  
57  
58  
59  
60  
61  
62  
63  
64  
65

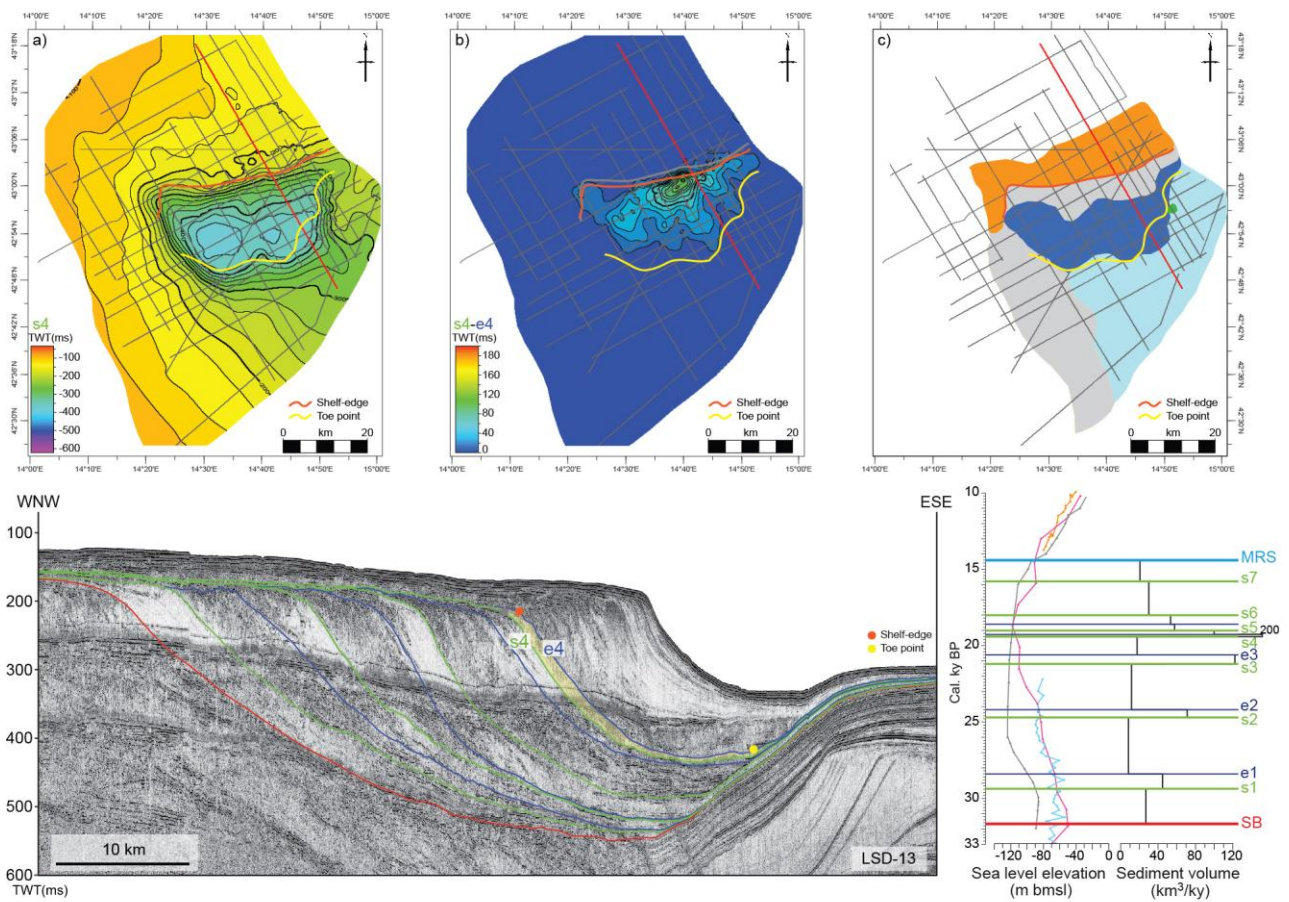


Fig. 18. Clinothem B<sub>4</sub>. Top: a) structural map; b) thickness map; c) seismic facies map (see table 2 for the legend). Bottom: LSD-13 multichannel profile, eustatic curves (purple curve: Lea et al., 2002; light blue: Siddal et al., 2003; black curve: Peltier and Fairbanks, 2006; yellow curve: Bard et al., 2010; blue curve: Lambeck et al., 2014) and sediment volume (km<sup>3</sup>/ky) are given for each clinothem that constitute the PRLW.

1  
2  
3  
4  
5  
6  
7  
8  
9  
10  
11  
12  
13  
14  
15  
16  
17  
18  
19  
20  
21  
22  
23  
24  
25  
26  
27  
28  
29  
30  
31  
32  
33  
34  
35  
36  
37  
38  
39  
40  
41  
42  
43  
44  
45  
46  
47  
48  
49  
50  
51  
52  
53  
54  
55  
56  
57  
58  
59  
60  
61  
62  
63  
64  
65

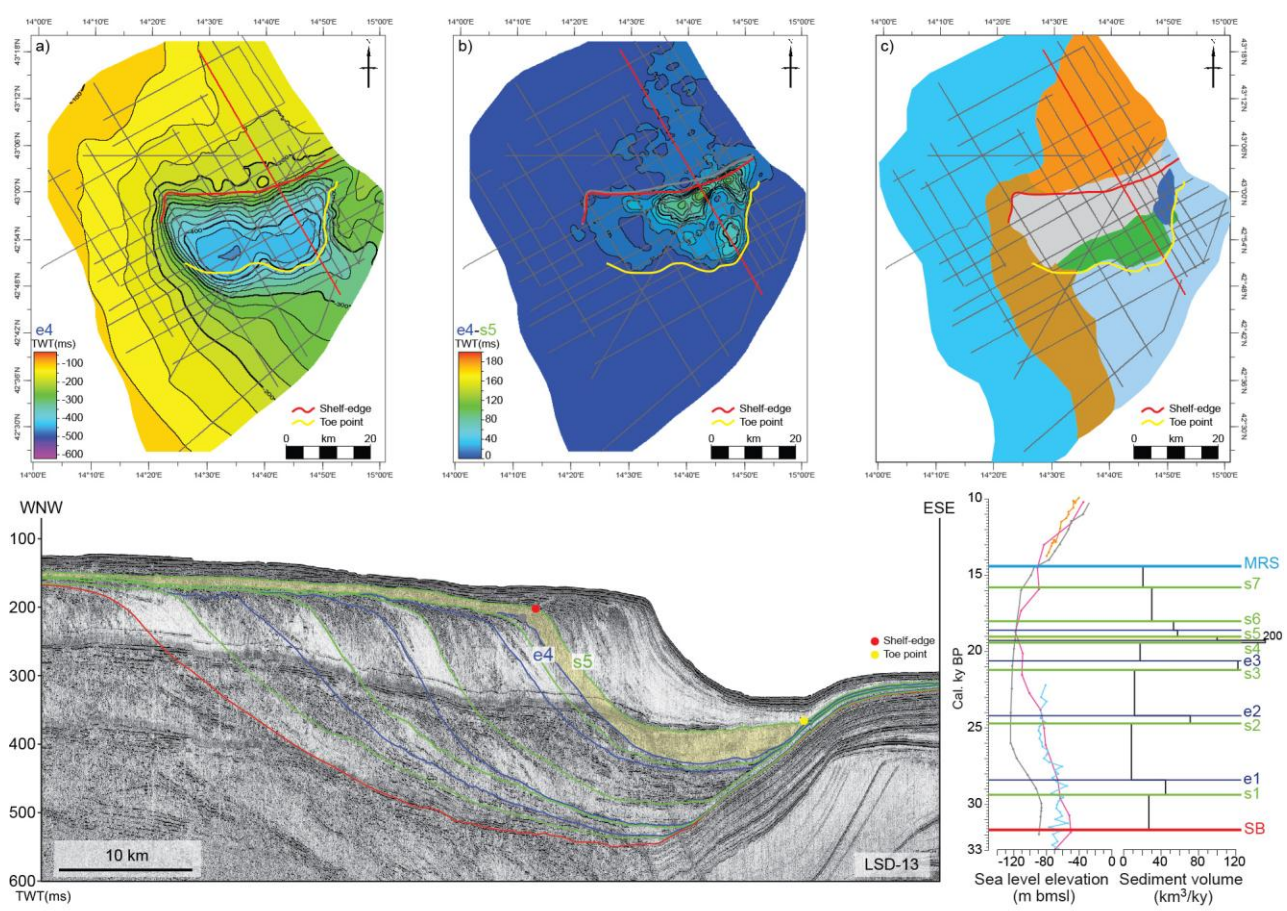


Fig. 19. Clinotherm A<sub>5</sub>. Top: a) structural map; b) thickness map; c) seismic facies map (see table 2 for the legend). Bottom: LSD-13 multichannel profile, eustatic curves (purple curve: Lea et al., 2002; light blue: Siddal et al., 2003; black curve: Peltier and Fairbanks, 2006; yellow curve: Bard et al., 2010; blue curve: Lambeck et al., 2014) and sediment volume (km<sup>3</sup>/ky) are given for each clinotherm that constitute the PRLW.

1  
2  
3  
4  
5  
6  
7  
8  
9  
10  
11  
12  
13  
14  
15  
16  
17  
18  
19  
20  
21  
22  
23  
24  
25  
26  
27  
28  
29  
30  
31  
32  
33  
34  
35  
36  
37  
38  
39  
40  
41  
42  
43  
44  
45  
46  
47  
48  
49  
50  
51  
52  
53  
54  
55  
56  
57  
58  
59  
60  
61  
62  
63  
64  
65

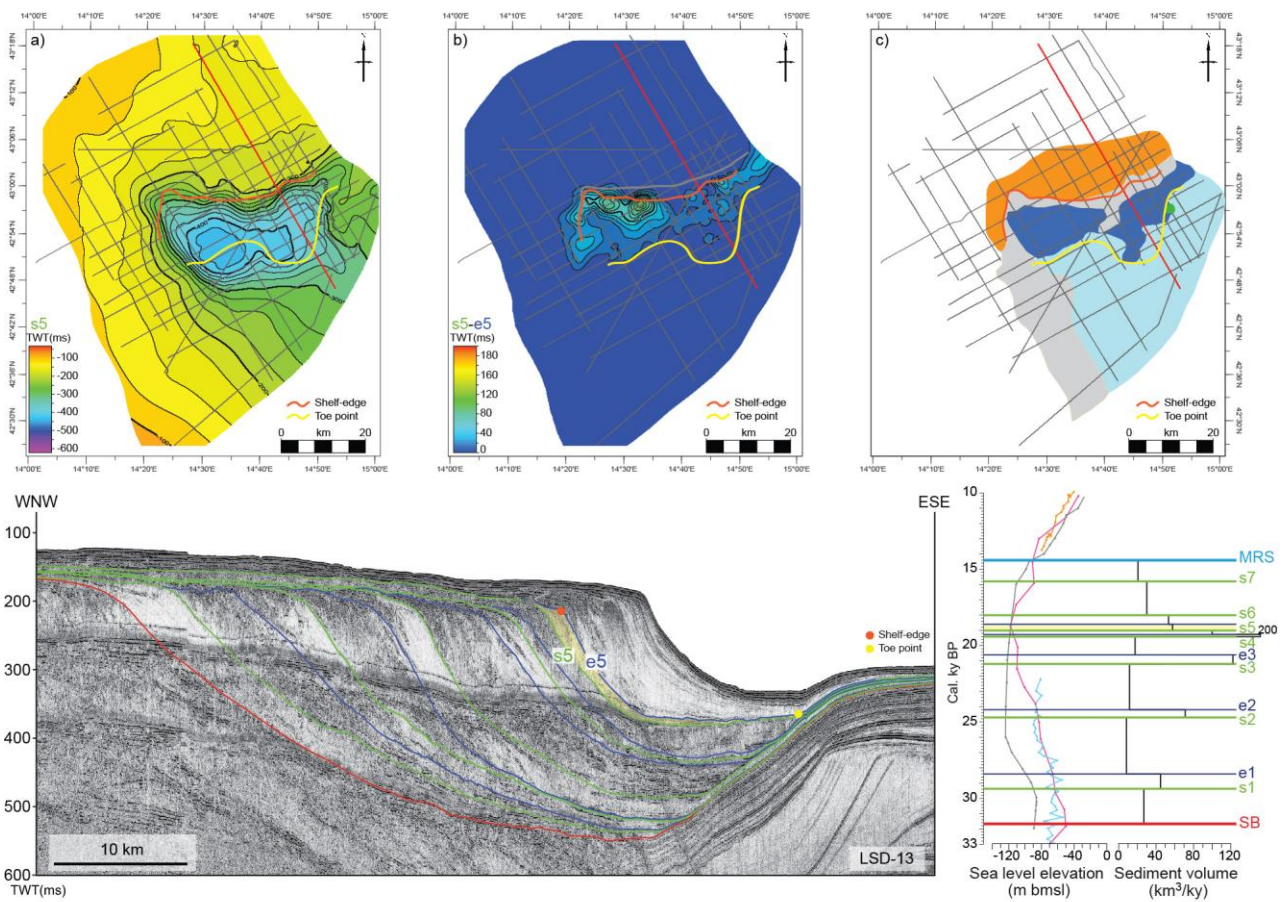


Fig. 20. Clinotherm B<sub>5</sub>. Top: a) structural map; b) thickness map; c) seismic facies map (see table 2 for the legend). Bottom: LSD-13 multichannel profile, eustatic curves (purple curve: Lea et al., 2002; light blue: Siddal et al., 2003; black curve: Peltier and Fairbanks, 2006; yellow curve: Bard et al., 2010; blue curve: Lambeck et al., 2014) and sediment volume (km<sup>3</sup>/ky) are given for each clinotherm that constitute the PRLW.

1  
2  
3  
4  
5  
6  
7  
8  
9  
10  
11  
12  
13  
14  
15  
16  
17  
18  
19  
20  
21  
22  
23  
24  
25  
26  
27  
28  
29  
30  
31  
32  
33  
34  
35  
36  
37  
38  
39  
40  
41  
42  
43  
44  
45  
46  
47  
48  
49  
50  
51  
52  
53  
54  
55  
56  
57  
58  
59  
60  
61  
62  
63  
64  
65

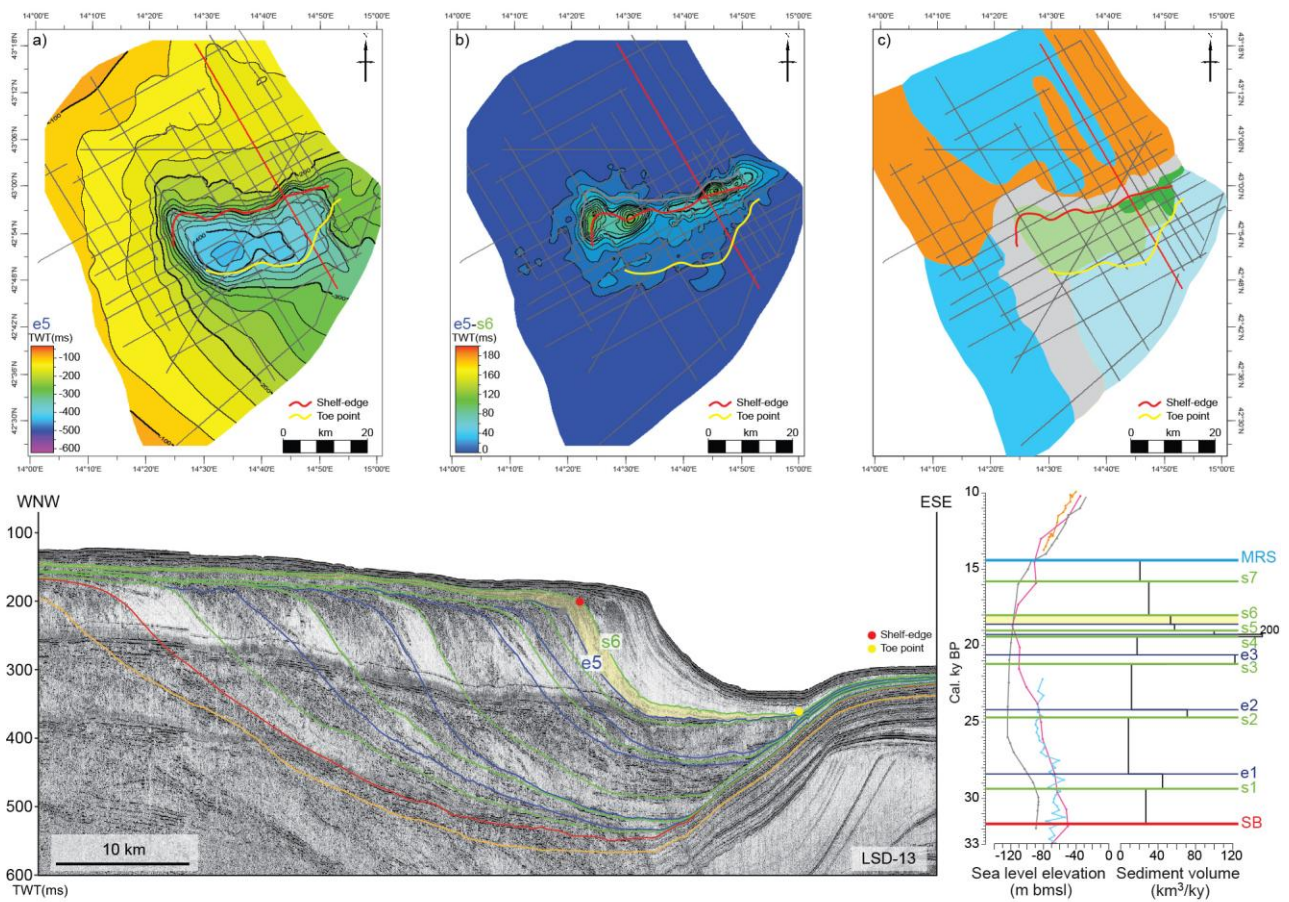


Fig. 21. Clinotherm A<sub>6</sub>. Top: a) structural map; b) thickness map; c) seismic facies map (see table 2 for the legend). Bottom: LSD-13 multichannel profile, eustatic curves (purple curve: Lea et al., 2002; light blue: Siddal et al., 2003; black curve: Peltier and Fairbanks, 2006; yellow curve: Bard et al., 2010; blue curve: Lambeck et al., 2014) and sediment volume (km<sup>3</sup>/ky) are given for each clinotherm that constitute the PRLW.

1  
2  
3  
4  
5  
6  
7  
8  
9  
10  
11  
12  
13  
14  
15  
16  
17  
18  
19  
20  
21  
22  
23  
24  
25  
26  
27  
28  
29  
30  
31  
32  
33  
34  
35  
36  
37  
38  
39  
40  
41  
42  
43  
44  
45  
46  
47  
48  
49  
50  
51  
52  
53  
54  
55  
56  
57  
58  
59  
60  
61  
62  
63  
64  
65

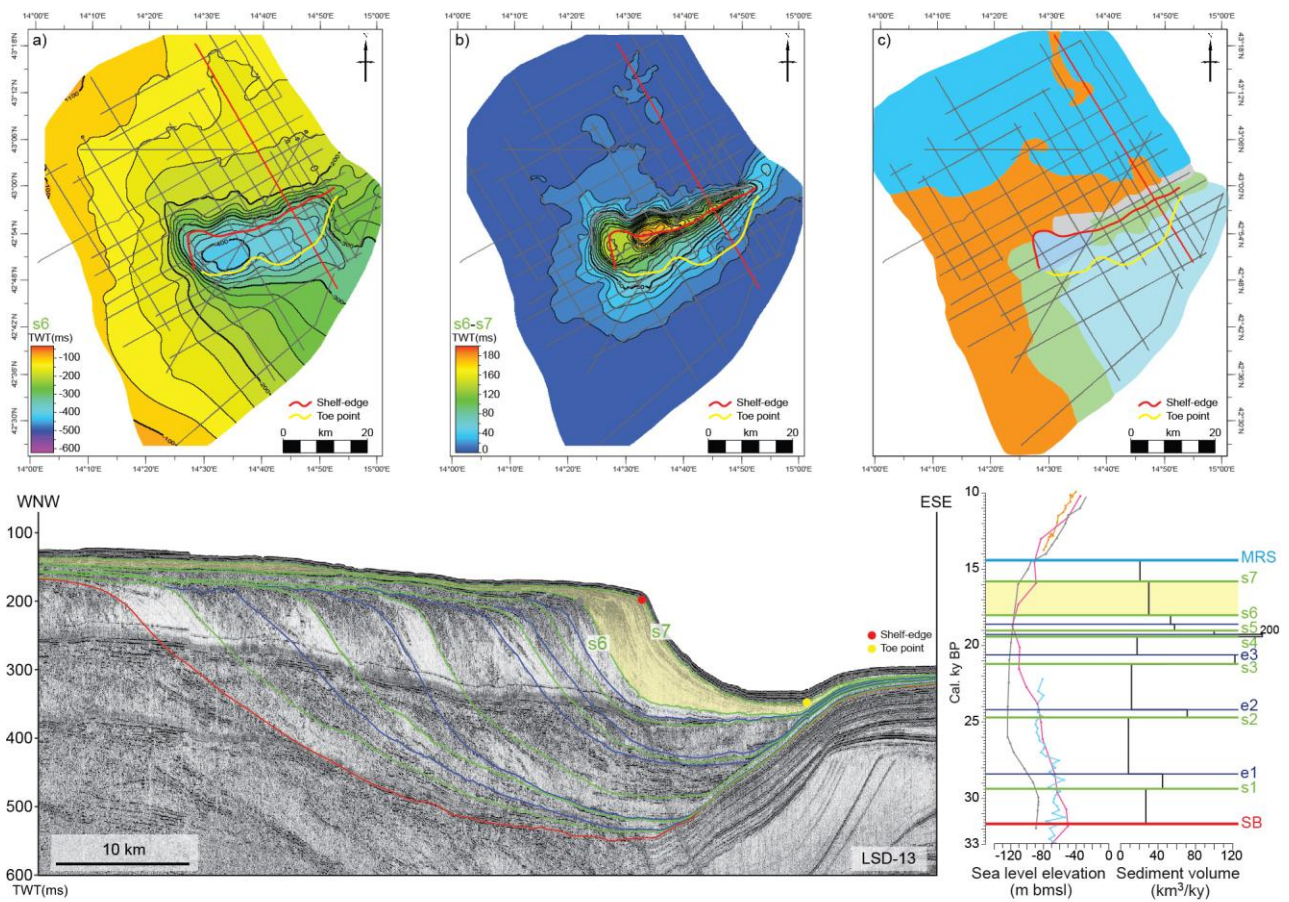


Fig. 22. Clinotherm C<sub>1</sub>. Top: a) structural map; b) thickness map; c) seismic facies map (see table 2 for the legend). Bottom: LSD-13 multichannel profile, eustatic curves (purple curve: Lea et al., 2002; light blue: Siddal et al., 2003; black curve: Peltier and Fairbanks, 2006; yellow curve: Bard et al., 2010; blue curve: Lambeck et al., 2014) and sediment volume (km<sup>3</sup>/ky) are given for each clinotherm that constitute the PRLW.

1  
2  
3  
4  
5  
6  
7  
8  
9  
10  
11  
12  
13  
14  
15  
16  
17  
18  
19  
20  
21  
22  
23  
24  
25  
26  
27  
28  
29  
30  
31  
32  
33  
34  
35  
36  
37  
38  
39  
40  
41  
42  
43  
44  
45  
46  
47  
48  
49  
50  
51  
52  
53  
54  
55  
56  
57  
58  
59  
60  
61  
62  
63  
64  
65

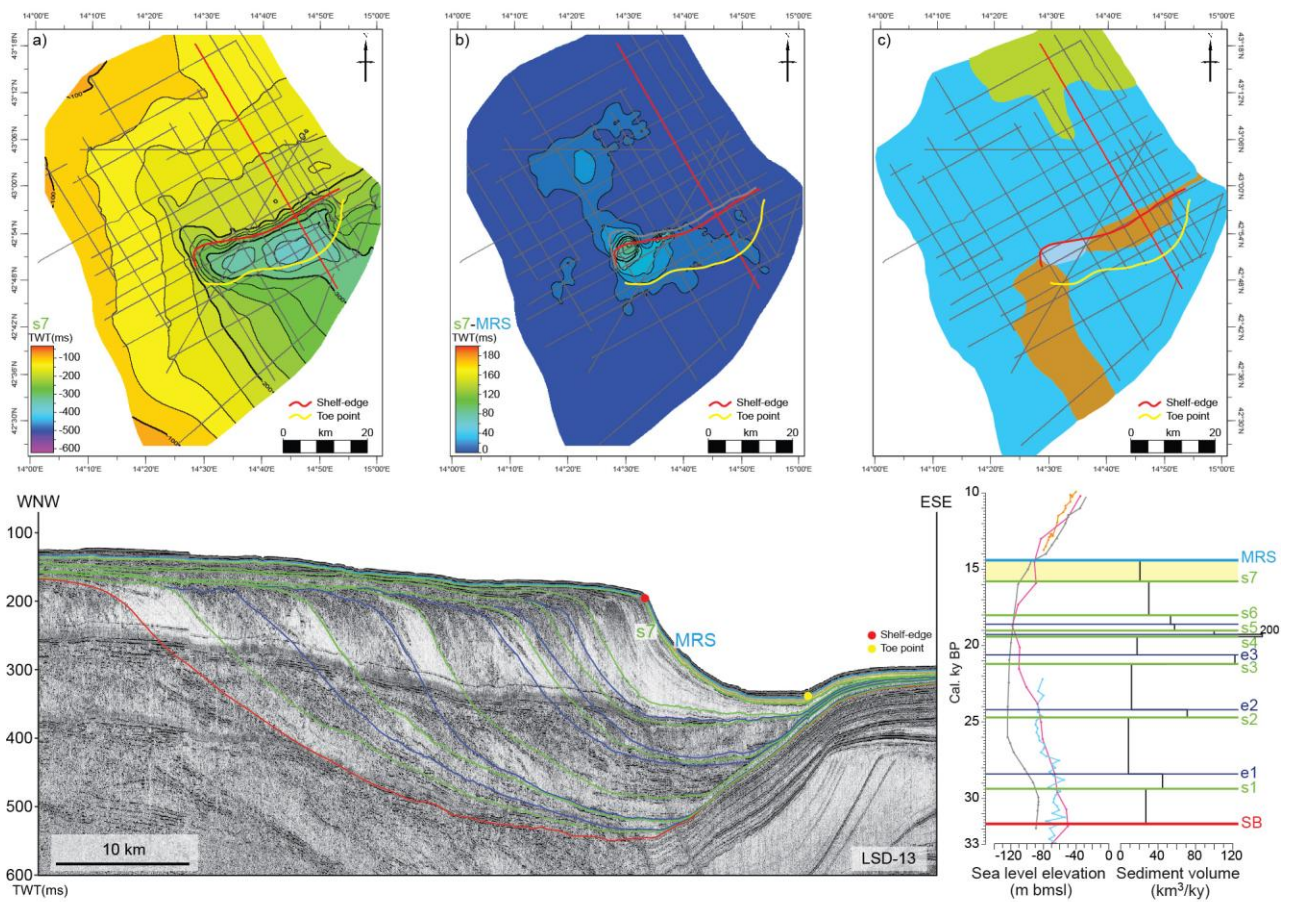


Fig. 23. Clinothem C<sub>2</sub>. Top: a) structural map; b) thickness map; c) seismic facies map (see table 2 for the legend). Bottom: LSD-13 multichannel profile, eustatic curves (purple curve: Lea et al., 2002; light blue: Siddal et al., 2003; black curve: Peltier and Fairbanks, 2006; yellow curve: Bard et al., 2010; blue curve: Lambeck et al., 2014) and sediment volume (km<sup>3</sup>/ky) are given for each clinothem that constitute the PRLW.

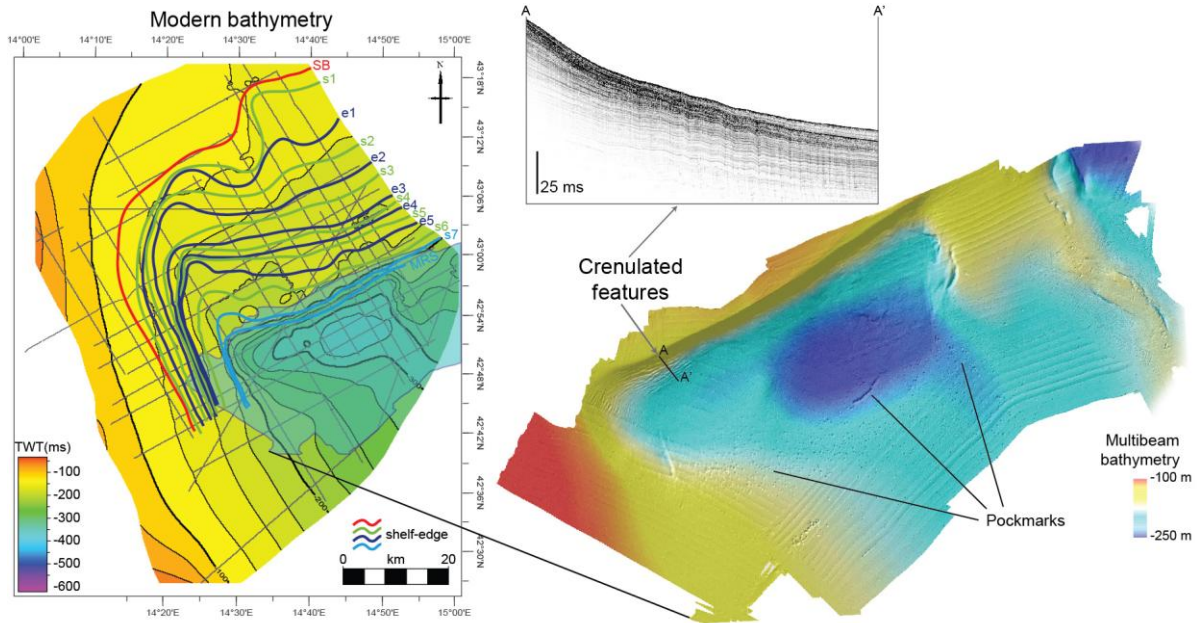


Fig. 24. The modern MAD bathymetry from seismic horizon interpolation with type of clinothems shelf-edge position during the PRLW progradation. The progradation produced a 40 km southward shift of the shelf-edge along with the burial of MAD antiform. Detail of the modern multibeam bathymetry shows slope-parallel bedforms (crenulation features) and a widespread field of seabed pockmarks.

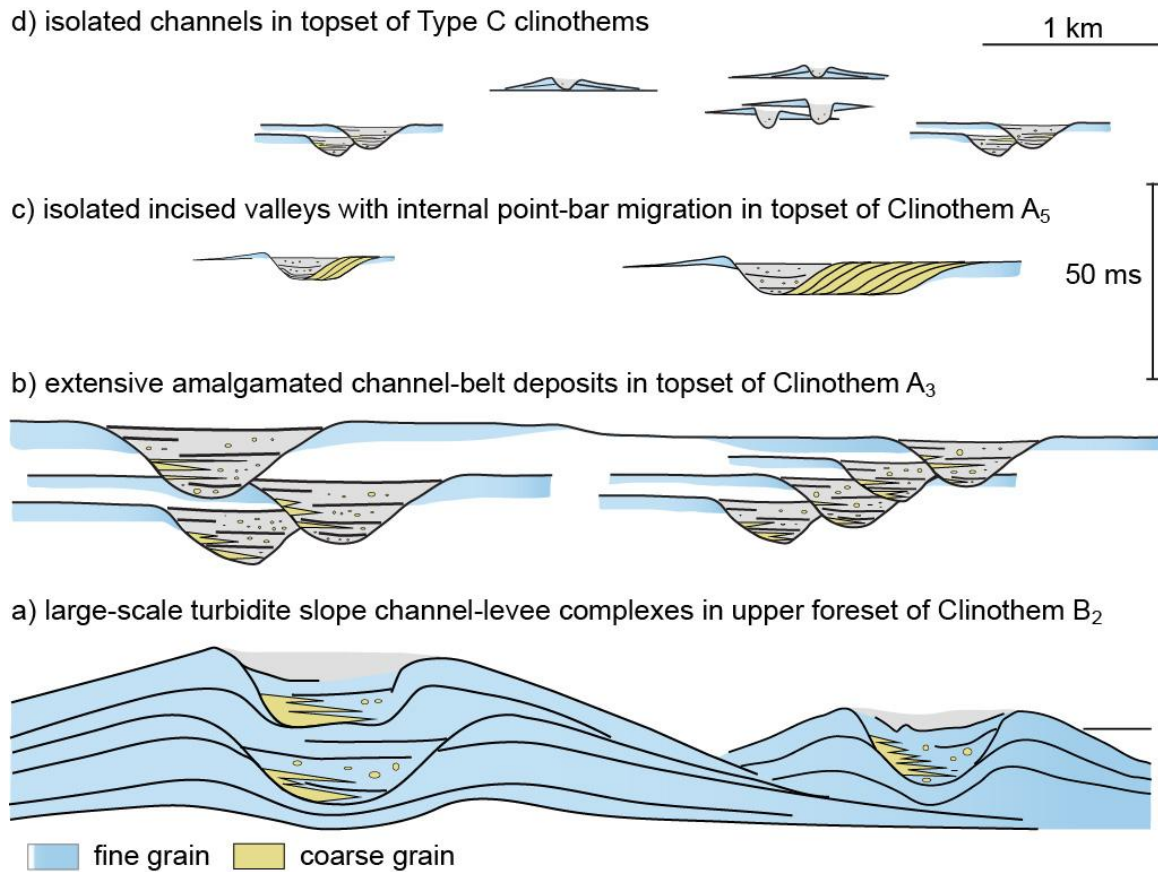


Fig. 25. Cartoon with idealized feeder systems from seismic lines. Note the decreasing in size of the feeder from bottom to the top of the succession and the deepening upward trend showing large-scale turbidite channel-levee complexes on the foreset (Clinothem B<sub>2</sub>); extensive acoustically transparent to chaotic units reminiscent of amalgamated channel-belt deposits up to 15 m thick (Clinothem A<sub>3</sub>); isolated incised valleys with a fill geometry characterized by oblique reflectors that denote point-bar migration (Clinothem A<sub>5</sub>); minor isolated channels, locally accompanied by subdued levees (Clinothem C<sub>2</sub>). During the progradation of the PRLW the main link between shelf and basin is preserved within Type B<sub>2</sub> clinothem formed during the eustatic fall, while the most extensive fluvial unit is preserved in the topset of Clinothem A<sub>5</sub>, deposited at the maximum eustatic lowstand of the last glacial.

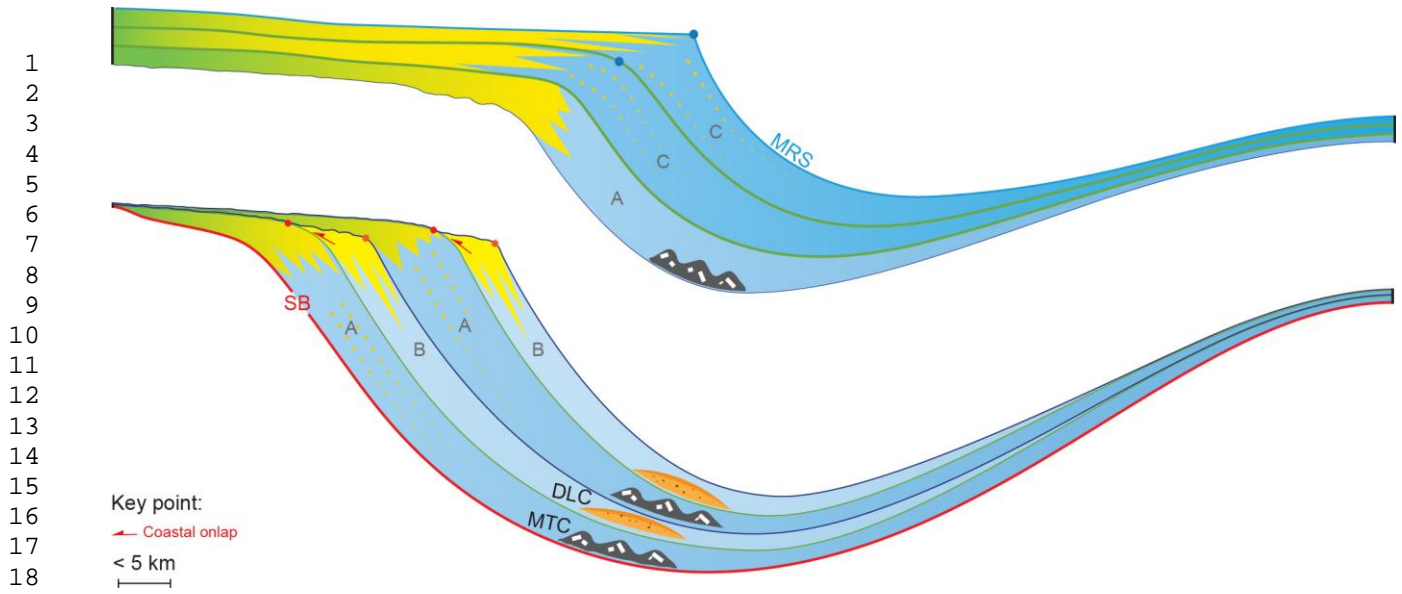


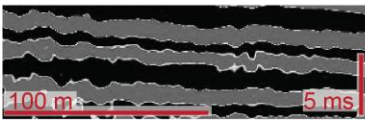

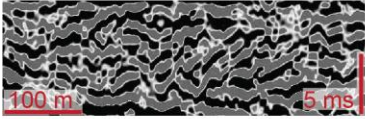

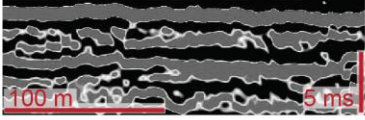

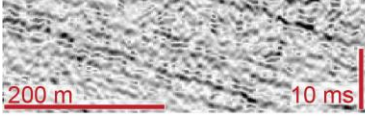



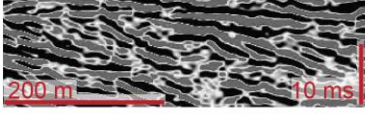
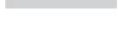
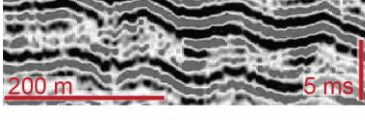



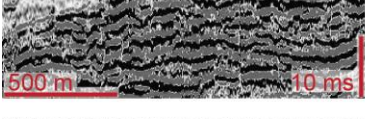

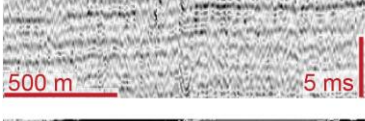

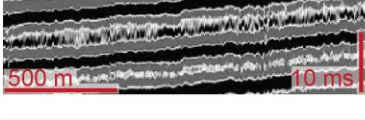

Fig. 26. Conceptual sketch of the type of clinoforms: in Type A clinothem the shoreline is within 10 km from the shelf-edge, the topset aggrades in the order of 10 m and margin destabilization is highlighted by MTCs in the basin; in Type B clinothem the shoreline is closer to the shelf-edge (< 5 km) and the topset degradation coupled with directly high amount of sediment bypass to the basin promote the formation of DLCs; in Type C clinothem the shoreline is more than 10 km from the shelf-edge, and no significant volume of coarse sediment reach the basin floor.



Sample top (m)	Control points	Source	Reference	Status
<b>PRAD1-2</b>				
0	0	modern time	Pellegrini et al. (2017)	
0.6	6000	LO <i>G. inflata</i>	Pellegrini et al. (2017)	
1.288	8500	Sapropel equivalent 1	Pellegrini et al. (2017)	
1.8	12000	Top GS-1	Pellegrini et al. (2017)	
2.18	14110	Neapolitan Yellow Tuff	Pellegrini et al. (2017)	
5.976	17540	<sup>14</sup> C	Pellegrini et al. (2017)	
7.82	19275	<sup>14</sup> C + Greenish/Verdoline	Pellegrini et al. (2017)	
8.8	19498	<sup>14</sup> C	Pellegrini et al. (2017)	
9.6	21350	<sup>14</sup> C	Pellegrini et al. (2017)	
10.50	22528	<sup>14</sup> C	Pellegrini et al. (2017)	
11.40	23780	<sup>14</sup> C	Pellegrini et al. (2017)	
12.78	24725	<sup>14</sup> C	Pellegrini et al. (2017)	
13.36	27200	VRa + <sup>14</sup> C	Pellegrini et al. (2017)	
14.8	32350	<sup>14</sup> C	Pellegrini et al. (2017)	
14.94	33300	Codola (base)	Pellegrini et al. (2017)	
16.53	39500	Campanian Ignimbrite	Pellegrini et al. (2017)	
<b>PAL94-8</b>				
1.78-1.82	8631 - 9074	<sup>14</sup> C	Asioli (1996)	accepted
2.05	11500	Top GS	Asioli et al. (2001)	accepted
2.08	14110	Neapolitan Yellow Tuff	Calanchi et al. (2008)	rejected
2.28-2.32	13350 - 13742	<sup>14</sup> C	Asioli (1996)	rejected
2.40-2.41	14653	Abrupt increase of <i>G. ruber</i> at base of GI-1	Asioli (1996); Asioli et al. (2001)	accepted
3.53-3.54	16002 (interpolated)	Y1 tephra	Calanchi et al. (2008)	accepted
4.64-4.68	17169 - 17695	<sup>14</sup> C	Asioli (1996)	accepted
<b>CM92-43</b>				
3.90	10480	<sup>14</sup> C	Asioli et al. (2001)	accepted
3.98	11390	<sup>14</sup> C	Asioli et al. (2001)	accepted
4.33	11750	<sup>14</sup> C	Asioli et al. (2001)	accepted
4.53	12005	<sup>14</sup> C	Asioli et al. (2001)	accepted
4.93	12700	<sup>14</sup> C	Asioli et al. (2001)	accepted
6.05	14110	Neapolitan Yellow Tuff	(Bourne et al., 2010)	accepted
6.50	14653	Abrupt increase of <i>G. ruber</i> at base of GI-1	Asioli et al. (2001)	accepted
6.80	14900	$\delta^{18}\text{O}$ stratigraphy TI A	Asioli et al. (2001)	accepted
10.48	16002	(from core Pal94-8)	this study	accepted

Tab. 1. The age model for the PRLW succession based on PRAD1-2 borehole, PAL94-8 and CM92-43 sediment cores (see supplemental material) and encompassing <sup>14</sup>C dates, tephra layers, bio and stratigraphic events.

1  
2  
3  
4  
5  
6  
7  
8  
9  
10  
11  
12  
13  
14  
15  
16  
17  
18  
19  
20  
21  
22  
23  
24  
25  
26  
27  
28  
29  
30  
31  
32  
33  
34  
35  
36  
37  
38  
39  
40  
41  
42  
43  
44  
45  
46  
47  
48  
49  
50  
51  
52  
53  
54  
55  
56  
57  
58  
59  
60  
61  
62  
63  
64  
65

Seismic facies	Acronym and color in seismic facies map	Internal Reflections	Clinoform sector	Depositional Environment
	HAC 	High Amplitude Continuous	Topset	Delta plain
	HACCh 	High Amplitude Chaotic	Topset/ Foreset	Delta/Coastal plain
	HAD 	High Amplitude Discontinuous	Topset	Lagoon
	LACDip 	Low Amplitude Continuous Dipping	Foreset	Prodelta
	HACDip 	High Amplitude Continuous Dipping	Foreset	Prodelta
	HACChDip 	High Amplitude Chaotic Dipping	Foreset	Prodelta
	HACWDip 	High Amplitude Continuous Wavy Dipping	Foreset	Prodelta
	DLAH 	Discontinuous Low Amplitude Hyperbolic	Foreset/ Bottomset	Mass-Transport Complexes
	SHAM 	Semi-continuous High Amplitude Mounded	Foreset/ Bottomset	Channel-levee Complexes
	LAC 	Low Amplitude Continuous	Bottomset	Distal Basin
	HAC 	High Amplitude Continuous	Bottomset	Distal Basin

Tab. 2. Seismic facies template for the PRLW encompassing the acronym and the color legend used in the main text and in the seismic facies maps. A summarized seismic facies description and interpretation is also reported.

1  
2  
3  
4  
5  
6  
7  
8  
9  
10  
11  
12  
13  
14  
15  
16  
17  
18  
19  
20  
21  
22  
23  
24  
25  
26  
27  
28  
29  
30  
31  
32  
33  
34  
35  
36  
37  
38  
39  
40  
41  
42  
43  
44  
45  
46  
47  
48  
49  
50  
51  
52  
53  
54  
55  
56  
57  
58  
59  
60  
61  
62  
63  
64  
65

Clinothem	Interval span (cal.ky)	Maximum Thickness (m)	Volume (km <sup>3</sup> )	Maximum Accummulation Rates (km <sup>3</sup> /yr)	Average shelf-edge progradation (km)	Foreset inclination (°)	Depocenter
C <sub>2</sub>	1.4	64	30	21.5	1.1	2	Elliptical, restricted on the western slope
C <sub>1</sub>	2.2	150	67	30.5	5.5	1.9	E-W elongated, convey the structural confinement in the western sub-basin
A <sub>6</sub>	0.6	85	33.5	56	3	1.9	Elliptical in western sub-basin and elongated in the eastern one
B <sub>5</sub>	0.4	78	23	57.5	4	2	On the western upper slope, compensation compared to A <sub>5</sub>
A <sub>5</sub>	0.3	80	30	100	0.5	1.8	Coalescent depocenters on the slope
B <sub>4</sub>	0.1	82	20	200	1.5	1.8	Elongated on the central slope, digitated external geometry, compensation compare to A <sub>4</sub>
A <sub>4</sub>	1.2	75	21	17.5	1.5	1.6	On the western slope, reflecting the structural confinement at the toe
B <sub>3</sub>	0.5	136	61	122	6.5	1.8	Coalescing depocenters E-W elongated and with digitated external geometry
A <sub>3</sub>	3.1	90	40	13	3	2.1	Two main depocenters on the slope, digitated external geometry
B <sub>2</sub>	0.5	95	36	72	4.5	1.8	Three main depocenters on the slope
A <sub>2</sub>	3.7	120	33	9	2.6	1.5	Restricted on the eastern slope
B <sub>1</sub>	1.0	160	44	44	3.2	1	Radial, compensation compare to A <sub>1</sub>
A <sub>1</sub>	2.4	110	66	27.5	3.8	0.9	Radial, restricted on the central outer shelf

Tab. 3. Summary of the characteristics of single type of clinothems.

Clinothem	Pre-existing bathymetry	Depositional Patterns	Topset character; <i>Interpretation</i>	Foreset character; <i>Interpretation</i>	Proximal Bottomset character; <i>Interpretation</i>	Distal Bottomset Character; <i>Interpretation</i>	Shelf-Edge Trajectory
							Retrogradational
C2	MAD antiform almost buried; two sub-basins with similar depth	Circular depocenter is in the western sub-basin and a widespread area of topset aggradation on the north-western shelf	HAC seismic facies; <i>delta plain deposits</i> . HAD seismic facies confined to the East;	HACDip seismic facies; <i>muddy prodelta</i> . HACWDip seismic facies; heterolithic prodelta deposits locally characterized by crenulation features	LAC seismic facies; <i>fine-grained basin-floor setting</i>	LAC seismic facies; <i>fine-grained basin-floor setting</i>	Aggradational
C1	MAD antiform expressed mainly in bottomset region. Deeper sub-basin in the western sector	E-W elongated, distal area confined by structure on southern rim	HAC seismic facies mainly in the northern area and HACH seismic facies in the western area; <i>Narrow (few tens of m wide) isolated channels, with local subdued levees (bayhead deltas in sheltered lagoon/estuary)</i>	LACDip to HACWDip reflections; <i>muddy to sandy prodelta deposits locally characterized by crenulation features</i>	LAC seismic facies; <i>fine-grained basin-floor setting</i>	LAC seismic facies; <i>fine-grained basin-floor setting</i>	Aggradational
A6	MAD antiform expressed mainly in bottomset region. Prominent bulge at the shelf-edge and an indentation is presents in the eastern sub-basin	Circular and elongated depocenters in the western and in the eastern sub-basin, respectively	HAC seismic facies; <i>delta plain</i> . HACH seismic facies; <i>amalgamated channel-belts</i> .	HACDip seismic facies; muddy prodelta	HACDip seismic facies; <i>muddy prodelta</i> . DLAH seismic facies in the eastern sub-basin; <i>Mass Transport Complexes (MTC)</i> .	LAC seismic facies; <i>fine-grained basin-floor setting</i>	Progradational
B5	MAD antiform expressed mainly in bottomset region prominent bulge at the shelf-edge	Two main coalescing depocenters in the western sub-basin extending to the upper slope; compensation compensational to A5		HACH seismic facies; <i>Amalgamated channels</i> . HACHDip seismic facies; <i>sandy prodelta</i> .	SHAM seismic facies; <i>Distributary Lobe Complexes (DLC)</i>	LAC seismic facies; <i>fine-grained basin-floor setting</i>	Degradational
A5	MAD antiform expressed mainly in bottomset region	Coalescent depocenters on slope, thickest in foreset-bottomset area	HAC seismic facies in western area; <i>delta plain</i> . HACH seismic facies; <i>amalgamated channel-belts</i> . Isolated incised valleys with oblique reflections ( <i>point-bars in meandering streams</i> )	HACDip seismic facies in western area; <i>heterolithic prodelta</i> . HACHDip seismic facies in eastern area; <i>sandy prodelta</i> .	DLAH seismic facies; <i>Mass Transport Complexes (MTC)</i> . SHAM in a restricted area; <i>Distributary Lobe Complexes (DLC)</i>	HAC seismic facies; <i>fine-grained basin-floor setting</i>	Progradational
B4	MAD antiform expressed mainly in bottomset region	Elongated on central slope, compensational to A4, digitate map pattern		HACH, HACHDip seismic facies; <i>amalgamated channels on foreset</i> ; SHAM seismic facies; <i>Distributary Lobe Complexes (DLC)</i>	SHAM seismic facies; <i>Distributary Lobe Complexes (DLC)</i>	LAC seismic facies; <i>fine-grained basin-floor setting</i>	Degradational
A4	Western sub-basin deeper than eastern sub-basin	Confined to western slope, due to structural confinement; linear progradation pattern; structural confinement at toe of clinothem	HACH seismic facies; <i>amalgamated channel-belt deposits</i>	HACHDip seismic facies; <i>sandy prodelta</i>	DLAH seismic facies; <i>MTCs with scattered distribution</i>	LAC seismic facies; <i>fine-grained basin-floor setting</i>	Progradational
B3	Western sub-basin deeper than eastern sub-basin	Coalescing depocenters elongated E-W with digitate map pattern; distal area confined by structure on southern rim		HACHDip seismic facies; <i>sandy prodelta</i>	SHAM seismic facies; <i>Distributary Lobe Complexes (DLC)</i>	LAC seismic facies; <i>fine-grained basin-floor setting</i>	Degradational
A3	Western sub-basin deeper than eastern sub-basin	Two main depocenters; digitate map pattern; distal area confined by structure on southern rim	HACH in northern area; extensive acoustically transparent to chaotic units up to 15 m thick ( <i>amalgamated channel-belt deposits</i> ); HACH in eastern area; <i>delta plain sandy-silty deposits</i>	HACHDip seismic facies; <i>sandy prodelta</i>	LACDip seismic facies; <i>muddy prodelta</i> . DLAH seismic facies; <i>Mass Transport Complexes (MTC)</i>	LAC seismic facies; <i>fine-grained basin-floor setting</i>	Progradational
B2	MAD antiforms still subtly expressed	Elongated WSW-ENE on the slope area		HACHDip seismic facies; <i>sandy prodelta</i> ; Locally parallel to wedge-shaped high-amplitude reflection packages pass laterally to low-amplitude reflections <i>Large-scale turbidite slope channel-levee complexes covered by mud wedges with no evidence of channelization</i>	SHAM seismic facies; <i>Distributary Lobe Complexes (DLC)</i>	HAC seismic facies; <i>fine-grained basin-floor setting</i>	Degradational
A2	MAD antiform expressed as area of minimum depth on structural map	Linear progradation, restricted to eastern slope area	HACH seismic facies; <i>amalgamated channels on broad coastal plain</i>	HACHDip seismic facies; <i>sandy prodelta</i>	DLAH seismic facies; <i>Mass Transport Complexes (MTC)</i>	HAC seismic facies; <i>fine-grained basin-floor setting</i>	Progradational
B1	MAD antiform still expressed in seafloor morphology	Radial, compensational to A1 (east of A1 depocenter)		HACHDip seismic facies; <i>sandy prodelta</i>	SHAM seismic facies; <i>Distributary Lobe Complexes (DLC)</i>	HAC seismic facies; <i>fine-grained basin-floor setting</i>	Degradational
A1	MAD antiform strikes NNW-SSE from coeval shelf-edge, forming two sub-basins	Radial, restricted on the central outer shelf	HACH seismic facies; <i>amalgamated channels; broad coastal plain NW (Po River) and WSW (Apennine rivers) of MAD</i>	HACHDip seismic facies; <i>channelized prodelta</i>	DLAH seismic facies confined to area east of MAD antiform, lap onto southern margin of basin; <i>Mass Transport Complexes (MTC)</i>	HAC seismic facies; <i>fine-grained basin-floor setting</i>	Progradational
APD							

Tab. 4a. Summary of characteristics of clinothems and shelf-edge trajectories.

Global Events	Eustasy	Sediment Supply	Surface-water Character	Bottom-water Character	Water Depth Changes	Regional Climate	Interval Age Span (cal. ky)	Surface Age (cal. ky)	SAR (km <sup>3</sup> /ky)
Meltwater pulse 1A (MWP 1A)	Fast rise	Substantial decrease: abandonment of the system	Warmer water		Abrupt Increase			v 14.4 v	
Onset of Termination IA (T-1A)	Fast Rise		Onset of warm. Abrupt increase in freshwater discharge: salinity drops	Century-scale, oscillations in fresh water input into the basin. Abrupt increase in freshwater discharge: salinity drops. Increase and continuous stressed condition		Glaciers retreating	1.4	v 15.8 v	21.5
	Fast Rise	Culmination of century-scale oscillations in fresh water input into the basin	Abrupt increase in freshwater discharge: salinity drops	Century-scale, oscillations in fresh water input into the basin. Abrupt increase in freshwater discharge: salinity drops. Increase and continuous stressed condition		Glaciers retreating	2.2	v 18.0 v	30.5
	Fast Rise	Decrease in sediment supply	Abrupt increase in freshwater discharge: salinity drops	Century-scale, oscillations in fresh water input into the basin. Abrupt increase in freshwater discharge: salinity drops. Increase and continuous stressed condition	Progressively Increase	Alpine waxing and waning, and Apennine glaciers retreating	0.6	v 18.8 v	56
Partial collapse of the Northern Hemisphere ice sheets. First meltwater pulse	Rise begins (eustatic jump of 15 m)	Increase in sediment supply	Abrupt increase in freshwater discharge: salinity drops	Century-scale, oscillations in fresh water input into the basin. Abrupt increase in freshwater discharge: salinity drops. Increase and continuous stressed condition	Increase	Alpine and Apennine glaciers retreating	0.4	v 19.0 v	57.5
	Fall slows to stillstand	Decrease in sediment supply	Cold	Century-scale, oscillations in fresh water input into the basin. Increase and continuous stressed condition		Alpine and Apennine glaciers advancing	0.3	v 19.3 v	100
First meltwater pulse; partial collapse of N. Hemisphere ice sheets	Fall slows to stillstand	Increase in sediment supply; Onset of century-scale, oscillations in fresh water input into the basin	Cold	Onset of century-scale, oscillations in fresh water input into the basin. Increase and continuous stressed condition		Alpine and Apennine glaciers advancing	0.1	v 19.4 v	200
LGM Chronozone	Fall slows to stillstand	Decrease in sediment supply	Cold	Millennial oscillations in riverine input. Minor ventilation of the bottom		Alpine and Apennine glaciers advancing	1.2	v 20.6 v	17.5
LGM Chronozone	Slower fall to 135 m below present sea level	Increase in sediment supply	Cold	Millennial oscillations in riverine input. Minor ventilation of the bottom		Alpine and Apennine glaciers retreating	0.5	v 21.1 v	122
End of Global LGM	Slower fall to 135 m below present sea level	Decrease in sediment supply	Cold	Millennial oscillations in riverine input. Minor ventilation of the bottom		Waxing and waning of Alpine and Apennine glaciers	3.1	v 24.2 v	13
Enhanced moisture source over southern Europe and Mediterranean: Global LGM	Slower fall to 135 m below present sea level	Increase in sediment supply; Composition changes: increased Ca/Ti, K/Ti due to change in weathering intensity or locaotin of sediment provenance	Cold	Onset of millennial oscillations in riverine input. Minor ventilation of the bottom		Alpine and Apennine glaciers advancing	0.5	v 24.7 v	72
Greenland Stadial 3	Slower fall to 135 m below present sea level	Decrease in sediment supply	Relatively far from direct riverine input	Relatively well oxygenated; decreasing quality of organic matter	Progressively decreasing	Alpine and Apennine glaciers advancing	3.7	v 28.4 v	9
Further increase in Laurentide and Scandanavian ice-sheet volumes	Slower fall to 135 m below present sea level	Increase in sediment supply	Cold and productive			Apennine glaciers advancing	1	v 29.4 v	44
Dansgaard-Oeschger Interstadial 5; Rapid growth phase of Laurentide and European ice sheets.	Fall from 80 to 125 m below present sea level.	Overall increase in sediment supply to the basin compare to the underlying APD succession	Cold and productive		Abrupt decreasing	Apennine glaciers advancing	2.4	v 31.8 v	27.5

Table 4b. Summary of global events, eustacy, sediment supply, water character and regional climate regime during clinotherms progradation.

## SUPPLEMENTAL MATERIAL

### Chronology of sediment cores

Seismic stratigraphic correlation for the upper part of the study area are corroborated by the stratigraphy of two sediment cores acquired in the bottom and in the upper slope of the Mid Adriatic Dip (MAD). The chronology of sediment cores (PAL94-8 and CM92-43), already published by Asioli (1996) and Asioli et al. (2001), is here partially revised for the interval older than 15 ky BP (Tab. 1). For core Pal94-8 the radiocarbon dates available in literature (Asioli, 1996) were re-calibrated online with the updated software Calib 7.1. (Stuiver, et al., 2017) after a correction of  $136 \pm 41$   $^{14}\text{C}$ -years regional reservoir effect ( $\delta\text{R}$ ) for planktic foraminifera (from the dataset Marine Reservoir Correction Database <http://calib.qub.ac.uk/marine/>) and an extra 200 years for benthic foraminifera according to the offset reported by Piva et al. (2008a, b). Because of the presence of reworked microfauna along with shell debris and silty-sandy mud between cm 230-210, the  $^{14}\text{C}$  date at 2.28-2.32 m and the Neapolitan Yellow Tuff tephra (NYT, C2) at 2.08 m (Calanchi et al., 2008) were not considered in our age model (Tab. 1).

The age model by Asioli et al. (2001) has been adopted for the core CM92-43, in addition to the age of 14.1 ky BP for the NYT at 6.05 m (Calanchi, 2008; Bourne et al., 2010), while the age of the base of the core has been approximated by the physical correlation of a seismic reflection corresponding to a tephra layer detected in core Pal94-8 at 3.53 m (Y1-ET1-TM11 according to Calanchi et al., 2008). However, the origin of this and of other geochemically similar distal tephras in central Adriatic cores (Calanchi et al., 2008) has been recently revised by Albert et al. (2013), who related them to an “undefined eruptive phase” of the Mount Etna occurred between 17.640-18.324 yr BP (age interpolated from Monticchio varves for the correlative tephra TM-11), that is ca. 700 years older than the Biancavilla ignimbrite (Y1). The interpolated age of this undefined tephra calculated in core PAL94-8 is ca. 16 ky BP, quite younger than the age estimated by Albert et al. (2013). If the Albert et alii tephra age is adopted in Pal94-8 chronology, the  $^{14}\text{C}$  dating at 4.64-4.68 m should be rejected, as an age inversion would occur. If it is relatively easy to reject an age older

1  
2  
3  
4  
5  
6  
7  
8  
9  
10  
11  
12  
13  
14  
15  
16  
17  
18  
19  
20  
21  
22  
23  
24  
25  
26  
27  
28  
29  
30  
31  
32  
33  
34  
35  
36  
37  
38  
39  
40  
41  
42  
43  
44  
45  
46  
47  
48  
49  
50  
51  
52  
53  
54  
55  
56  
57  
58  
59  
60  
61  
62  
63  
64  
65

than expected (because of reworking, bioturbation), it is more difficult to find a reason for rejecting an age younger than expected, therefore we retained the <sup>14</sup>C date at 4.64-4.68 m waiting for an improved definition of this undefined tephra, using this later as “guide line/reflection”. Accordingly, the “tephra-bearing” seismic reflection has been tied from Pal94-8 to CM92-43 site, where it lies approximately 80 cm below the maximum core penetration (10.7 m). In Table 1 a summary of the discussed control points is reported.

#### REFERENCES FOR SUPPLEMENTAL MATERIAL

- Albert, P.G., Tomlinson, E.L., Lane, C.S., Wulf, S., Smith, V.C., Coltelli, M., Keller, J., Lo Castro, D., Manning, C.J., Müller, W., and Menzies, M.A., 2013, Late glacial explosive activity on Mount Etna: Implications for proximal–distal tephra correlations and the synchronisation of Mediterranean archives. *Journal of Volcanology and Geothermal Research*, v. 265, p. 9–26.
- Asioli, A., 1996, High resolution foraminifera biostratigraphy in the Central Adriatic basin during the last deglaciation: a contribution to the PALICLAS Project. *Memorie-Istituto Italiano di Idrobiologia*, v. 55, p. 197-218.
- Asioli, A., Trincardi, F., Lowe, J.J., Ariztegui, D., Langone, L., and Oldfield, F., 2001, Sub-millennial scale climatic oscillations in the central Adriatic during the Late glacial: palaeoceanographic implications: *Quaternary Science Reviews*, v. 20(11), p. 1201-1221.
- Bourne, A.J., Lowe, J.J., Trincardi, F., Asioli, A., Blockley, S.P.E., Wulf, S. Matthews, I.P. Piva, A., and Vigliotti, L., 2010, Distal tephra record for the last ca 105,000 years from core PRAD 1-2 in the central Adriatic Sea: implications for marine tephrostratigraphy: *Quaternary Science Reviews* v. 29, p. 3079-3094.
- Calanchi, N., Cattaneo, A., Dinelli, E., Gasparotto, G., Lucchini, F., 1998, Tephra layers in Late Quaternary sediments of the central Adriatic Sea. *Marine Geology*, v. 149, p. 191–209.

1 Piva, A., Asioli, A., Schneider, R. R., Trincardi, F., Andersen, N., Colmenero-Hidalgo, E.,  
2 Dennielou, B., Flores, J.A., and Vigliotti L., 2008a, Climatic cycles as expressed in sediments  
3 of the PROMESS1 borehole PRAD1-2, Central Adriatic, for the last 370 ka, 1: integrated  
4 stratigraphy. *Geochemistry, Geophysics, Geosystems*, v. 9 (1), Q01R01, doi:  
5 10.1029/2007GC001713.  
6  
7  
8  
9

10  
11 Piva, A., Asioli, A., Andersen, N., Grimalt, J. O., Schneider, R. R., and Trincardi, F., 2008, Climatic  
12 cycles as expressed in sediments of the PROMESS1 borehole PRAD1-2, central Adriatic, for  
13 the last 370 ka: 2. Paleoenvironmental evolution. *Geochemistry, Geophysics, Geosystems*,  
14 9(3).  
15  
16  
17  
18  
19  
20

21 Stuiver, M., Reimer, P. J., and Reimer, R. W., 2017, CALIB 7.1 [WWW program] at [http://calib.](http://calib.org)  
22  
23  
24  
25  
26  
27  
28  
29  
30  
31  
32  
33  
34  
35  
36  
37  
38  
39  
40  
41  
42  
43  
44  
45  
46  
47  
48  
49  
50  
51  
52  
53  
54  
55  
56  
57  
58  
59  
60  
61  
62  
63  
64  
65